

https://dspace.org/

Micro-cracking and crack growth in notched concrete and mortar beams

Gill, Laurence Mark

2015-02-05
http://hdl.handle.net/10539/16873

Downloaded from a DSpace repository. https://dspace.org/

MICRO-CRACKING AND CRACK GROWTH IN NOTCHED CONCRETE AND MORTAR BEAMS

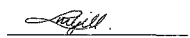
Laurence Mark Gill

A dissertation submitted to the Faculty of Engineering, University of the Witwatersrand, Johannesburg, in fulfilment of the degree of Master of Science in Engineering.

Johannesburg, 1988

DECLARATION

I declare that this dissertation is my own, unaided work. It is being submitted for the degree of Master of Science in Engineering in the University of Witwatersrand, Johannesburg. It has not been submitted before for any degree or examination in any other University.



TWENTY SECOND day of NOVEMBER 1988.

ABSTRACT

This dissertation addresses the question of the fracture behaviour of notched concrete and mortar beams. The major purpose of the work was to study the development of the micro-cracked zone and identify the point at which main crack growth began, and thus to characterise concrete and mortar at the start of main crack growth.

Notched concrete and mortar beams of width 100 mm, depth either 200 mm or 300 mm, and with a span/depth ratio of three, were tested. Measurements of midspan deflection, midspan load, surface displacements across the fracturing section and ultrasonic pulse transit time were made. Ordinary Portland cement and mineral aggregates were used for the concrete and mortar beams.

The J-integral, surface displacements across the fracturing section and ultrasonic pulse transit time measurements were used to detect the onset of main crack growth. It was found that a reduction in the load carrying capacity of concrete and mortar is possible due to micro-cracking only. The value of the J-integral at the start of main crack growth was found to be essentially the same for concrete and mortar. The value of the J-integral at the start of micro-cracking was

found to be essentially the same for concrete and mortar, and about 40% of the value of the J-integral at the start of main crack growth. The value of the J-integral at the start of micro-cracking and at the start of main crack growth was found, on average, to increase for an increase in beam depth.

Surface displacements across the fracturing section showed the tension zone at the start of main crack growth to be approximately twice the size of the compression zone for both concrete and mortar. The size of the micro-cracked zone, as determined from surface displacements across the fracturing section, was found to be 42% of the residual ligament depth for concrete, and 41% of the residual ligament depth for mortar.

Scatter in the results was found to be considerable, thus meaning that only general trends could be identified.

ACKNOWLEDGEMENTS

I acknowledge with gratitude the help of the following people, whose support and assistance made the completion of this dissertation possible.

Dr M.G. Alexander, my supervisor, who provided guidance and advice throughout; Dr R.B. Tait, my co-supervisor, who gave valuable comment on interpretation of my results; Mr Bob van der Merwe and Mr Andries Mtlabine, laboratory staff in the Construction Materials Laboratory of the Civil Engineering Department, University of the Witwatersrand, who helped with the technical work; Mr Andrew Simons, a friend and fellow student, who gave valuable assistance with the casting and testing of specimens.

CONTENTS Page

DECLARATION		ii
ABSTRACT		iii
ACKNOWLEDGEMENTS		v
CONTENTS		vi
LIST OF FIGURES		xii
LIST OF TABLES		xx
LIST OF SYMBOLS		xxiii
1.	INTRODUCTION	1
1.1	FRACTURE MECHANICS OF CONCRETE AND CEMENTITIOUS MATERIALS	1
1.2	DEFINITIONS	2
1.2.1	CEMENTED MATERIAL	2
1.2.2	CONCRETE	2
1.2.3	MORTAR	3
1.2.4	LINEAR ELASTIC FRACTURE MECHANICS (LEFM)	3
1.2.5	NON-LINEAR FRACTURE MECHANICS (NLFM)	3
1.2.6	STRESS-FREE CRACK	3
1.2.7	MICRO-CRACKED ZONE	3
1.3	OBJECTIVES OF THE INVESTIGATION	4
1.4	ORGANISATION OF THE DISSERTATION	5

PART I

FRACTURE MECHANICS AND CONCRETE - A REVIEW

2.	THE FRACTURE MECHANICS APPROACH TO THE FAILURE OF CEMENTED MATERIALS	8
2.1	HISTORICAL BACKGROUND TO FRACTURE MECHANICS	8
2.1.1	GRIFFITH'S CONTRIBUTION	8
2.1.2	CONDITIONS FOR FRACTURE	11
2.1.3	THE STRESS AT A CRACK TIP	15
2.1.4	THE EFFECTIVE FRACTURE SURFACE ENERGY CONCEPT	17
2.2	FRACTURE MECHANICS AND CEMENTED MATERIALS	18
2.2.1	INTRODUCTION	18
2.2.2	A REVIEW OF SOME PAST EXPERIMENTAL WORK	20
	2.2.2.1 INTRODUCTION	20
	2.2.2.2 EXPERIMENTAL WORK	21
2.2.3	FRACTURE MODELS	30
	2.2.3.1 INTRODUCTION	30
	2.2.3.2 THE GLUCKLICH MODEL	33
2.2.4	APPLICATIONS OF LINEAR ELASTIC FRACTURE MECHANICS	37
	2.2.4.1 LINEAR ELASTIC FRACTURE MECHANICS PARAMETERS	39
2.2.5	NON-LINEAR FRACTURE MECHANICS PARAMETERS	42
	2.2.5.1 CRACK OPENING DISPLACEMENT (COD)	43
	2.2.5.2 THE PRINCIPLE OF THE J-INTEGRAL	45
	2.2.5.3 R-CURVE ANALYSIS	50

2.2.6	SUMMARY OF THE FRACTURE MECHANICS APPROACH TO CEMENTED MATERIALS	53
2.2.7	CONCLUDING REMARKS	54

PART II

EXPERIMENTAL FRACTURE STUDIES

3.	EXPERIMENTAL WORK	57
3.1	INTRODUCTION AND OBJECTIVES	57
3.2	DETAILS OF SPECIMENS	58
3.3	CONCRETE AND MORTAR MIXES	63
3.4	MATERIALS CONTROL TESTS	65
3.4.1	CUBE COMPRESSION TESTS	65
3.4.2	PRISM TESTS FOR ELASTIC MODULUS	65
3.4.3	RESULTS OF MATERIALS CONTROL TESTS	66
3.5	EXPERIMENTAL APPARATUS	71
3.5.1	DEFLECTION MEASURING RIG	71
3.5.2	ELECTRONIC TRANSDUCERS	73
3.5.3	RECORDING EQUIPMENT	74
3.5.4	TESTING MACHINE	78
3.6	TEST PROCEDURE	80
3.6.1	SPECIMEN PREPARATION PRIOR TO TESTING	80
3.6.2	LOADING	81
3.7	SUMMARY	83

4.	FRACTURE TEST RESULTS	86
4.1	Introduction	86
4.2	Load-Deflection Records	86
4.3	SURFACE DISPLACEMENTS ACROSS THE FRACTURING SECTION	90
4.4	ULTRASONIC TEST RECORDS	93

PART III

ANALYSIS AND INTERPRETATION OF DATA FROM FRACTURE TESTS

5.	IDENTIFICATION OF THE POINT OF INITIATION OF MAIN CRACK GROWTH IN NOTCHED CONCRETE AND MORTAR BEAMS	97
5.1	INTRODUCTION	97
5.2	SURFACE DISPLACEMENT PROFILES	97
5.3	THE J-INTEGRAL	107
5.4	IDENTIFICATION OF THE CHANGEOVER FROM MICRO-CRACKING TO MAIN CRACK GROWTH USING THE J-INTEGRAL	108
5.5	COMPARISON OF THE MAXIMUM LOAD CYCLE AND THE CYCLE DURING WHICH MAIN CRACK GROWTH BEGAN	117
5.6	COMPARISON OF THE J-VALUES AT THE START OF MAIN CRACK GROWTH	123

5.7	THE VALUE OF J AT THE START OF MICRO-CRACKING (J_i)	126
5.8	DEPENDANCE OF J_i AND J_c ON SPECIMEN GEOMETRY	137
5.9	NOTCH TIP DISPLACEMENT (COD) AT INITIATION OF MAIN CRACK GROWTH	141
5.10	THE USE OF ULTRASONICS TECHNIQUES	145
5.10.1	INTRODUCTION	145
5.10.2	IDENTIFICATION OF THE START OF MAIN CRACK GROWTH USING ULTRASONICS	146
	5.10.2.1 PULSE TRANSIT TIME AND FRACTURE ENERGY	146
	5.10.2.2 PULSE TRANSIT TIME AND THE CONCEPT OF PERMANENT DAMAGE	154
5.11	CONCLUDING DISCUSSION	1[illegible]
6.	MATERIAL CHARACTERISATION FROM FRACTURE ZONE SIZE MEASUREMENTS DURING FRACTURE	173
6.1	INTRODUCTION	173
6.2	TENSION AND COMPRES[illegible]N ZONE SIZES	175
6.3	THE POSITION OF THE NEUTRAL AXIS DURING FRACTURE	182
6.4	DETERMINING THE MICRO-CRACKED ZONE SIZE FRO[illegible] THE DISPLACEMENT PROFILES	186
6.5	CONCLUDING DISCUSSION	197

7. CONCLUSIONS AND RECOMMENDATIONS FOR FUTURE WORK 200

7.1 THE OBJECTIVES OF THIS WORK 200

7.2 SUMMARY OF EXPERIMENTAL WORK 200

7.3 SUMMARY OF RESULTS 201

7.3.1 IDENTIFICATION OF THE POINT OF INITIATION OF MAIN CRACK GROWTH 201

7.3.2 MATERIAL CHARACTERISATION FROM FRACTURE ZONE SIZE MEASUREMENTS 204

7.4 MAJOR CONCLUSIONS 205

7.5 OVERALL EVALUATION AND DISCUSSION 208

7.6 RECOMMENDATIONS FOR FUTURE RESEARCH 209

APPENDIX A DETAILS OF CONCRETE MIXES AND PRODUCTION PROCEDURES FOR FRACTURE TESTS 210

APPENDIX B DETAILS OF EXPERIMENTAL APPARATUS 214

APPENDIX C RECORDS OF TEST RESULTS 219

REFERENCES 262

BIBLIOGRAPHY 274

LIST OF FIGURES

Figure		Page
2.1	Griffith case for (a) surface crack and (b) internal crack (from ref 4)	12
2.2	Crack propagation for the ideal Griffith case (from ref 4)	16
2.3	Stress-strain diagrams for hardened cement paste, aggregate and concrete (from ref 8)	32
2.4	Crack propagating in a non-homogeneous brittle material under monotonically increasing stress (from ref 4)	36
2.5	Energy rate curve corresponding to FIG 2.4 (from ref 4)	36
2.6	Crack progressing in a bi-phase material (from ref 4)	38
2.7	Variation of fracture toughness with crack growth of cement paste, mortar and concrete (from ref 66)	44
2.8	Fundamental expression of the J-integral (from ref 4)	46
2.9	Definition of the area 'A' for determining J_c	49
2.10	The energy concept in plane stress (from ref 34)	52

3.1	Typical fracture beam	61
3.2	View of a fracture beam resting on its support rollers	62
3.3	View of a cracked fracture beam after testing	62
3.4	View of the dial gauge compressometer used for the elastic modulus tests	67
3.5	View of the deflection measuring rig	72
3.6	View of a fracture beam ready for testing	72
3.7	View of the LVDT clamps and blocks prior to gluing to the beam	75
3.8	View of the LVDT clamps and blocks glued in position on a beam	75
3.9	Detail of ultrasonic transducer probe positions on a typical fracture beam	77
3.10	View of the rollers greased and ready to be placed between the half-round beam support and the machined steel plate	79
3.11	View of the rollers positioned between the half-round beam support and the machined steel plate	79

3.12	Typical Load vs Deflection record	84
4.1	Typical area 'A' described in section 4.2, together with the eight equidistant spaces used to calculate the area 'A' by Simpson's rule	89
4.2	Typical traces obtained from LVDTs on the crack face of a fracturing beam	94
5.1	Surface displacement profile for beam 12A	102
5.2	Surface displacement profile for beam 18A	103
5.3	Surface displacement profile for beam 10B	104
5.4	Surface displacement profile for beam 12B	105
5.5	Atypical surface displacement profile-beam 5A	106
5.6	J-integral plotted against surface displacement of notch tip for beam 7A	111
5.7	J-integral plotted against surface displacement of notch tip for beam 11A	112
5.8	J-integral plotted against surface displacement of notch tip for beam 3B	113

5.9	J-integral plotted against surface displacement of notch tip for beam 6B	114
5.10	Linear regression fit of J-in.egral data ASTM-813[72] method	128
5.11	Evaluation of J_i using the ASTM-813 method on a graph of the J-integral versus the surface displacement at the notch tip. BEAM 17A	131
5.12	Evaluation of J_i using the ASTM-813 method on a graph of the J-integral versus the cumulative difference in peak ultrasonic pulse transit time. BEAM 17A	132
5.13	Evaluation of J_i using the ASTM-813 method on a graph of the J-integral versus the surface displacement at the notch tip. BEAM 1B	133
5.14	Evaluation of J_i using the ASTM-813 method on a graph of the J-integral versus the cumulative difference in peak ultrasonic pulse transit time. BEAM 1B	134
5.15	J-integral plotted against cumulative difference in peak ultrasonic pulse transit time for beam 9A	148

5.16 J-integral plotted against cumulative difference in peak ultrasonic pulse transit time for beam 17A 149

5.17 J-integral plotted against cumulative difference in peak ultrasonic pulse transit time for beam 2B 150

5.18 J-integral plotted against cumulative difference in peak ultrasonic pulse transit time for beam 12B 151

5.19 Crack patterns obtained from mortars loaded within the sample chamber of an SEM: (a), (b) compact tension specimens; (c), (d) compression specimens (from ref 74) 156

5.20 (a) & (b) Plots of change in trough pulse transit time for beams 15A & 16A 157

5.21 (a) & (b) Plots of change in trough pulse transit time vs change in peak pulse transit time for beams 17A & 18A 158

5.22 (a) & (b) Plots of change in trough pulse transit time vs change in peak pulse transit time for beams 1B & 2B 159

5.23 (a) & (b) Plots of change in trough pulse transit time vs change in peak pulse transit for beams 3B & 4B 160

5.24 (a) & (b) Plots of change in trough pulse transit time vs change in peak pulse transit time for beams 5B & 8B 161

5.25 (a) & (b) Plots of change in trough pulse transit time vs change in peak pulse transit time for beams 9B & 10B 162

5.26 (a) & (b) Plots of change in trough pulse transit time vs change in peak pulse transit time for beams 11B & 12B 163

6.1 Definition of stress zones in a concrete or mortar beam during fracture (from ref 4) 176

6.2 Plot of compression zone depth $(d-d_{na})$ vs tension zone depth $(d_{na}-c)$ for the concrete beams 180

6.3 Plot of compression zone depth $(d-d_{na})$ vs tension zone depth $(d_{na}-c)$ for the mortar beams 181

6.4 Plot of compression vs tension zone sizes during progressive micro-cracking up to the start of main crack growth (concrete beams) 183

6.5	Plot of compression vs tension zone sizes during progressive micro-cracking up to the start of main crack growth (mortar beams)	184
6.6	Position of the neutral axis at the start of main crack growth (concrete beams)	187
6.7	Position of the neutral axis at the start of main crack growth (mortar beams)	188
6.8	Schematic surface strain profile used to determine the size of the micro-cracked zone at the start of main crack growth (from ref 4)	191
6.9	Size of the micro-cracked zone at the start of main crack growth (concrete beams)	194
6.10	Size of the micro-cracked zone at the start of main crack growth (mortar beams)	195
B.1	Deflection measuring rig set for a 900 mm long beam	215
C.1	Plots of the J-integral versus surface displacement at the notch tip for the concrete beams, and linear regression according to the ASTM-813 method.	240

C.2	Plots of the J-integral versus surface displacement at the notch tip for the mortar beams, and linear regression according to the ASTM-813 method.	247 -252
C.3	Plots of the J-integral versus the cumulative difference in peak ultrasonic pulse transit time for the concrete beams, and linear regression according to the ASTM-813 method.	253 -255
C.4	Plots of the J-integral versus the cumulative difference in peak ultrasonic pulse transit time for the mortar beams, and linear regression according to the ASTM-813 method.	256 -261

LIST OF TABLES

Table		Page
3.1	*SUMMARY OF FRACTURE BEAMS, SERIES A AND B*	60
3.2	CONCRETE MIX PROPORTIONS	64
3.3	MORTAR MIX PROPORTIONS	64
3.4	*RESULTS FOR CUBE COMPRESSION TESTS ON* CONCRETE	68
3.5	RESULTS FOR CUBE COMPRESSION TESTS ON MORTAR	69
3.6	RESULTS FOR ELASTIC MODULUS TESTS ON CONCRETE	70
3.7	RESULTS FOR ELASTIC MODULUS TESTS ON MORTAR	70
4.1	*TYPICAL EXAMPLE OF* LOAD VS DEFLECTION DATA	87
4.2	EXAMPLE OF DISPLACEMENTS ACROSS A FRACTURING SECTION	91
4.3	*TYPICAL EXAMPLE OF ULTRASONIC RECORD*	93
5.1	CRITICAL CYCLE FOR THE CONCRETE BEAMS	116
5.2	CRITICAL CYCLE FOR THE MORTAR BEAMS	117
5.3	COMPARISON OF CRITICAL CYCLE (START OF MAIN CRACK GROWTH) AND MAXIMUM LOAD IN CONCRETE BEAMS	119
5.4	COMPARISON OF CRITICAL CYCLE (START OF *MAIN CRACK GROWTH*) AND MAXIMUM LOAD IN MORTAR BEAMS	120
5.5	REDUCTION IN THE LOAD CARRYING CAPACITY OF THE CONCRETE BEAMS DUE TO *MICRO-CRACKING*	121

5.6	REDUCTION IN THE LOAD CARRYING CAPACITY OF THE MORTAR BEAMS DUE TO MICRO-CRACKING	122
5.7	J_c VALUES FOR CONCRETE	124
5.8	J_c VALUES FOR MORTAR	125
5.9	J_i FOR THE CONCRETE BEAMS	135
5.10	J_i FOR THE MORTAR BEAMS	136
5.11	AVERAGE J_i VALUES FOR CONCRETE BEAMS OF DIFFERENT GEOMETRY	139
5.12	AVERAGE J_i VALUES FOR MORTAR BEAMS OF DIFFERENT GEOMETRY	140
5.13	AVERAGE J_c VALUES FOR CONCRETE BEAMS OF DIFFERENT GEOMETRY	140
5.14	AVERAGE J_c VALUES FOR MORTAR BEAMS OF DIFFERENT GEOMETRY	141
5.15	COD AT START OF MAIN CRACK GROWTH FOR THE CONCRETE BEAMS	143
5.16	COD AT START OF MAIN CRACK GROWTH FOR THE MORTAR BEAMS	144
5.17	IDENTIFICATION OF THE CYCLE DURING WHICH MAIN CRACK GROWTH BEGAN FOR CONCRETE BEAMS USING AN ULTRASONIC TECHNIQUE	153
5.18	IDENTIFICATION OF THE CYCLE DURING WHICH MAIN CRACK GROWTH BEGAN FOR MORTAR BEAMS USING AN ULTRASONIC TECHNIQUE	154
5.19	IDENTIFICATION OF THE ONSET OF MAIN CRACK GROWTH (CRITICAL CYCLE) FOR CONCRETE BEAMS FOR CONCRETE BEAMS USING AN ULTRASONIC TECHNIQUE TO RECORD PERMANENT DAMAGE	167

5.20	IDENTIFICATION OF THE ONSET OF MAIN CRACK GROWTH (CRITICAL CYCLE) FOR MORTAR BEAMS FOR CONCRETE BEAMS USING AN ULTRASONIC TECHNIQUE TO RECORD PERMANENT DAMAGE	168
6.1	GENERAL FIGURE LEGEND	173
6.2	SIZE OF THE MICRO-CRACKED ZONE IN CONCRETE BEAMS	196
6.3	SIZE OF THE MICRO-CRACKED ZONE IN MORTAR BEAMS	197
C.1	RESULTS OF ALL THE TESTS FOR MAXIMUM FORCE ON EACH CYCLE, J-INTEGRAL FOR EACH CYCLE, ULTRASONIC PULSE TRANSIT TIME FOR EACH CYCLE AND EXACT BEAM DIMENSIONS	220 -230
C.2	RESULTS OF ALL THE TESTS FOR SURFACE DISPLACEMENTS ACROSS THE FRACTURING SECTION FOR EACH CYCLE	231 -239

LIST OF SYMBOLS

The symbols below are those most commonly used in the text. Less common symbols a defined where they occur in the text.

mcz	Micro-cracked zone
γ	Surface energy
E	Young's modulus
σ	Stress
R	Crack growth resistance
c	Crack depth / Crack length
c_o	Initial notch depth
d	Overall beam depth
J	J-Integral
J_c	Critical J-integral value (J-integral value at start of main crack growth)
G	Strain energy release rate
G_c	Critical strain energy release rate
K	Stress intensity factor
K_c	Critical stress intensity factor
L	Overall beam length
S	Loading span
b	Beam width (breadth)
b_o	Initial residual ligament depth
h	Residual ligament depth (d-c)
na	Neutral axis
COD	Crack opening displacement
d_{na}	Depth of neutral axis (from compressive face)
K_t	Stress concentration factor
J_i	J-integral value at the start of micro-cracking
J_{cycle}	Cyclic J-integral value for the cycle during which main crack growth began
γ'	Surface energy

1. INTRODUCTION

1.1 FRACTURE OF CONCRETE AND CEMENTED MATERIALS

Concrete is used for applications which cover a tremendous range of complexity and sophistication. Methods for control of material performance are necessary at all stages of design and construction to ensure behaviour consistent with the function and importance of the structure. Standard testing procedures are used to give an idea of the bulk performance of the material, but as yet no reliable methods for specific properties such as durability and cracking resistance have been developed.

The principles of linear-elastic fracture mechanics (LEFM) and, more recently, non-linear fracture mechanics (NLFM) have been applied to concrete[1,2,3], but only with limited success. Concrete and mortar are very difficult to model due to their complex heterogeneity, and for this reason a considerable amount of work is still necessary to ensure the development of design related parameters in fracture. One of the most difficult aspects of fracture tests on cemented materials is the identification of the various types of cracking during loading, for example micro-cracking

or main crack growth. Many fracture mechanics parameters rely on accurate determination of crack lengths, and other parameters relate to identification of the exact instant of crack initiation within a specimen. This dissertation represents an attempt to identify the point of main crack initiation during the fracture process and deals with characterisation of the fracture behaviour of concrete and mortar specimens at this point.

1.2 DEFINITIONS

The materials examined in this investigation were concrete and mortar. The following definitions apply.

1.2.1 CEMENTITIOUS MATERIALS

A material based on Portland cement as binder, generally comprising an intimate mixture of binder water and mineral aggregates.

1.2.2 CONCRETE

A cemented material comprising an intimate mixture of hardened cement paste and fine and coarse aggregates, where the size of the coarse aggregate particles exceeds 4,75 mm. The material may be regarded as coarse aggregate particles embedded in a mortar matrix.

1.2.3 MORTAR

A cemented material comprising an intimate mixture of hardened cement paste and fine aggregate particles of maximum size 4,75 mm.

1.2.4 LINEAR ELASTIC FRACTURE MECHANICS (LEFM)

This refers to fracture mechanics formulations based on the assumption that the material is a homogeneous, perfectly linear elastic, isotropic continuum.

1.2.5 NON-LINEAR FRACTURE MECHANICS (NLFM)

This refers to fracture mechanics formulations based on the assumption that the material exhibits non-linear, pseudo-plastic behaviour. (e.g. a material such as concrete).

1.2.6 STRESS-FREE CRACK (ALSO CALLED MAIN CRACK)

A physical cleavage in the material extending from a notch (in the case of notched beams as tested in this work) or some other stress raiser and which has no stress transfer between the crack faces.

1.2.7 MICRO-CRACKED ZONE

A zone which includes a zone of aggregate pull-out and

extends immediately ahead of the stress-free (main) crack tip. Tensile stress transfer may occur in this zone due to aggregate interlock and remaining matrix ligaments.

1.3 OBJECTIVES OF THE INVESTIGATION

The programme of testing in this work arose mainly from points brought to notice in the work of Alexander[4]. These points, summarised below, include the following work:

1. A detailed study of the early development of the micro-cracked zone (mcz) with a view to investigating a fracture parameter at the initiation of main crack growth.

   NOTE:
   Alexander's research produced parameters relating to both the linear elastic conditions at the start of micro-cracking and to main crack growth at the peak of mcz development. However the conditions described in 1. above remained unclear and therefore prompted further research in this investigation.

2. A detailed study of the behaviour of the mcz at the start of main crack growth.

3. Characterisation of the fracture behaviour of concrete as well as a coarse-grained mortar.

4. Investigation of the use of ultrasonic pulse velocity techniques for the detection of cracking.

5. Development of an experimental technique to reduce specimen support friction.

1.4 ORGANIZATION OF THE DISSERTATION

The dissertation is divided into three parts as follows: -

PART I FRACTURE MECHANICS AND CONCRETE - A REVIEW

This part forms Chapter 2 and consists of a summary of the highlights of past experimental work on fracture mechanics. Basic concepts are discussed and the application of these concepts to cemented materials is dealt with.

PART II EXPERIMENTAL WORK

This part forms Chapters 3 and 4. Details of materials, mixing and casting procedures, test equipment, test procedures, data collection and processing, and materials control tests are given. Examples of various data records are also presented.

PART III ANALYSIS AND INTERPRETATION OF DATA FROM FRACTURE TESTS

This part forms chapters 5, 6 and 7. It deals with fracture zone measurements and identification of various types of cracking using displacement profile measurements and ultrasonic pulse techniques. These results are used to characterise the fracture of concrete and mortar beams especially at the point of changeover from micro-cracking to main crack growth. The closing Chapter 7 summarises the results and offers suggestions for further research.

PART 1

FRACTURE MECHANICS AND CONCRETE - A REVIEW

2. THE FRACTURE MECHANICS APPROACH TO THE FAILURE OF CEMENTED MATERIALS

2.1 HISTORICAL BACKGROUND TO FRACTURE MECHANICS

Because of their complex structure and heterogeneity, cement-bonded materials pose very real problems for the researcher. Analysis must start at a microscopic structural level and extend to the more challenging area of engineering application.

Fracture mechanics, an approach first developed earlier this century, has been applied as a principle to cemented materials, but this area of research is still in its early stages. It does, however, hold promise in helping to explain the mechanisms of fracture and possibly may eventually provide the engineer with usable and reliable design parameters.

2.1.1 GRIFFITH'S CONTRIBUTION

The discrepancy between predicted failure stresses and actual failure stresses of materials has long been recognised by the scientific world.

In addition to the question of stress at failure or strength, the mode of failure of many materials is difficult to predict. There is no definite method of determination of a failure mode based purely on microstructural analysis. Materials which are essentially

brittle can exhibit ductile failure under certain conditions, and vice versa. These factors have led to the search for alternative ways of explaining material behaviour.

The first significant fracture development research came from Griffith[5]. He used the concept of energy conservation to relate the stored strain energy of a loaded elastic brittle material to the surface energy of the cracks produced during cracking. He also reasoned that structural flaws played a major role in determining the effective service strengths of various materials.

Griffith proposed that for a crack to propagate the release of stored strain energy of an elastic material during fracture was just sufficient to overcome the surface energy requirement of the new crack surfaces of the material when it fails. He showed that the stress σ_t required to just separate two layers of atoms x mm apart was

$$\sigma_t = \sqrt{\frac{E\gamma}{x}} \qquad (2.1)$$

where:

E = Young's Modulus.

γ = Surface Energy. (or elastic work term)

Using this equation, the intrinsic failure strength of ordinary materials was predicted to be about ten to one hundred times greater than their actual bulk strength. Griffith , during his work on the tensile strength of thin glass fibres, found that the thinner the fibre he tested, the greater was its strength. The extrapolated strengths of near zero diameter fibres in fact very closely approximated the theoretical strength predicted by his tensile strength equation.

Orowan[6] reported that for certain materials the more important flaws in a material appear on the surface rather than in the interior. These flaws cause large stress concentrations which in turn break local bonds by overstressing, long before the bulk stress of the material reaches critical values. A crack initiates in this way and travels in a continuous manner of stress transfer until failure occurs, at a stress well below the theoretical value. However, not all materials fail by the spread of a crack from a local defect and this model is only applicable to homogeneous materials in the elastic regime. Another method of failure is that of plastic flow where failure occurs by shearing or ductile microvoid coalescence. Materials that are brittle at normal temperatures require a very high stress to initiate plastic flow and hence fail in a brittle manner. Conversely, materials that are ductile at normal temperatures require a relatively lower stress for plastic flow to occur and therefore usually fail in a ductile manner.

Orowan accomodates this by extending Griffith's original equation 2.1 and including a so called plastic work term p which is discussed in more detail in section 2.1.4.

2.1.2 CONDITIONS FOR FRACTURE

Two conditions must be fulfilled for a crack to propagate in a material. Firstly, it must be energetically feasible, and secondly there must be a molecular mechanism by which the energy transformation can occur.

(i) The Griffith criterion

The Griffith criterion of energetic feasibility, as has already been mentioned, states that crack propagation will only occur if the strain energy released upon crack growth is sufficient to provide the surface energy that is required for the new crack surfaces.

Therefore the condition for crack growth is:

$$\frac{dU}{dc} \geq \frac{dW}{dc}$$

where U is the elastic strain energy, W the surface energy required for crack growth, and dc the increment of crack extension.

Referring to FIG 2.1, Griffith calculated $\frac{dU}{dc}$ as :

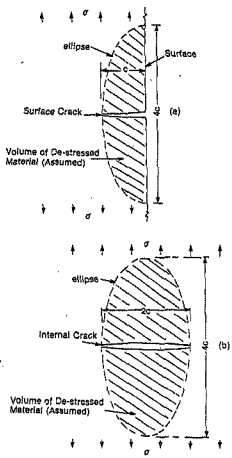


FIG 2.1 Griffith case for (a) surface crack and (b) internal crack (from ref 4)

$$\frac{dU}{dc} = \frac{2\pi\sigma^2 c}{E}$$

Usually $\frac{dU}{dc}$ is replaced by G to give

$$G = \frac{2\pi\sigma^2 c}{E}$$

Where E is Youngs modulus and where G is known as the "elastic strain energy release rate". Note that the term "rate" here refers to increment of crack advance and has nothing to do with time.

The energy consumed in crack propagation is denoted by

$$R = \frac{dW}{dc}$$

and is known as the crack resistance. In an ideally brittle material R is assumed constant since the energy required to produce a crack is the same for each increment dc, but in most practical situations R varies non-linearly but monotonically with crack length.

Hence crack growth occurs when a critical elastic strain energy release rate is achieved, ie when the strain energy release during crack growth equals or exceeds the energy requirement of the fracture surfaces.

Now $W = 4\gamma c$ where γ is the unit surface energy of the crack and $R = \frac{dW}{dc} = 4\gamma$

Therefore at crack instability:

$$\sigma = \sqrt{\frac{2\gamma E}{\pi c}} \qquad (2.2)$$

(Griffith's equation)

Griffiths's assumptions for the derivation of this formula were:-

1. The material is perfectly linearly elastic up to the point of brittle fracture.

2. The volume of destressed material due to the presence of the crack is equal to half the volume of an ellipse of major axis 4c.

3. The crack resistance R is a linear function of crack depth c and is therefore constant for an increment dc.

In more practical terms, Griffith's equation 2.2 can be explained as follows:-

1. The release of strain energy is proportional to the square of the crack depth, while the surface

energy increases in direct proportion to the crack depth. Therefore the rate of release of strain energy increases with increasing crack depth while the rate of demand of surface energy is constant.

2. A shallow crack consumes more surface energy than it releases strain energy until a critical depth c_c is reached, called the point of instability, where the propagating crack begins to release more stored strain energy than it consumes. Stable crack growth occurs for $c < c_c$, and spontaneous unstable crack growth occurs for $c > c_c$.

The above is best illustrated by FIG. 2.2 which plots the surface energy requirement and the elastic strain energy release as functions of c.

2.1.3 THE STRESS AT A CRACK TIP

The Griffith criterion represents a condition that is necessary for a crack to propagate in an elastic brittle material but is not always sufficient for this to occur.

A material must be able to have molecular bonds at a crack tip broken before any further cracking will take

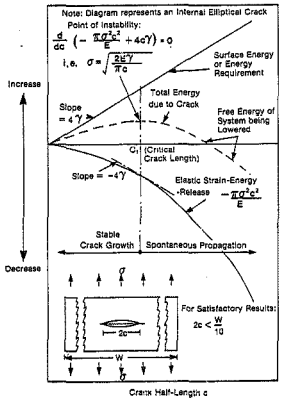


FIG 2.2 Crack propagation for the ideal Griffith case (from ref 4)

place. The molecular mechanism for crack propagation is facilitated by the stress concentration concept.

At a crack tip, the ratio between the maximum local stress σ_{max} and the bulk stress σ is given by K_t, the stress concentration factor:

$$K_t = 2\sqrt{\frac{c}{r}} \qquad (2.3)$$

Where r is the crack tip radius and c is the crack length for a surface crack and half the crack length for an internal crack. In a brittle material, r remains approximately constant while c increases as crack growth takes place. Therefore K steadily increases and the energy balance becomes more favourable for crack propagation. This leads to rapid failure.

2.1.4 THE EFFECTIVE FRACTURE SURFACE ENERGY CONCEPT

The surface energy γ_s as proposed by Griffith and appearing in equation 2.2 has often proved numerically elusive for researchers. Griffith envisaged γ_s being the pure free surface energy resulting from the creation of new fracture surfaces. The material is assumed to be homogeneous and linear elastic right up to fracture (i.e. perfectly brittle). This is not true since most materials exhibit some ductility (plastic or pseudo-plastic deformation) before failure.

The energy balance then actually exists between the elastic energy release and the total work done in propagating the crack, as pointed out by Blight[7]. This work includes the free surface energy of the fracture surfaces, as well as the plastic work consumed at the crack tip during propagation, and any other energy-absorbing mechanisms linked with fracture. Mathematically :-

$$\gamma' = \gamma_s + \gamma_p \qquad (2.4)$$

where

γ' represents the total work of fracture, and is called the effective fracture surface energy.

γ_s represents the free surface energy.

γ_p represents the plastic work plus any other work required for fracture. In practice usually $\gamma_p >> \gamma_s$ particularly for metals. This substantiates the inadequacy of considering the pure free surface energy only.

2.2 FRACTURE MECHANICS AND CEMENTED MATERIALS

2.2.1 INTRODUCTION

This chapter has dealt so far with the fundamental approach to fracture mechanics. It is clear that the models proposed by Griffith are not a sufficiently good representation of the fracture process for cemen-

ted materials since they greatly simplify the mechanism of cracking and assume the existence of a perfectly homogeneous linear elastic material.

The experimental work covered by this dissertation does not cover all the aspects of fracture mechanics developed to date. Instead, certain important areas were selected and applied to the results. These areas had to do with mainly NON LINEAR FRACTURE MECHANICS (NLFM) theory.
For the sake of completeness, many of the important parameters both from LINEAR ELASTIC FRACTURE MECHANICS (LEFM) and NLFM are presented in this section in condensed form. The area covered is, however, restricted to cemented materials.

The fracture resistance of concrete has been the subject of many past investigations (ref 1, pg 2). There has been, however, a tendency to borrow fracture mechanics technology developed for metals and alloys and apply it directly to concrete. Parameters such as the critical strain energy release rate G_c or critical stress intensity factor K_c are often measured and documented. Their usefulness is suspect, however, since they generally apply to the instability of a single crack. In concrete, fracture of the aggregates, cracking of mortar and debonding of mortar and aggregate can occur before global instability of the whole system. The theory of LEFM utilising G_c or

K_c or even non-linear fracture toughness parameters which depend on a single crack are basically inapplicable because of their inability to take into account the intervening stage of micro-cracking.

The main concern is therefore to understand the behaviour of micro-cracked concrete systems and the mechanics of damage accumulation. The most serious obstacle in this area at present may not necessarily be the complexities of stress analysis, but rather determining the influence of local micro-cracking on global material behaviour.

2.2.2 A REVIEW OF SOME PAST EXPERIMENTAL WORK

2.2.2.1 INTRODUCTION

This section deals with previous experimental applications of both LEFM and NLFM to concrete and other cemented materials.

Areas addressed include: The determination of the fracture parameter G; studies of fracture energy; affects of aggregate types and volumes on fracture parameters; the study of the fracture parameter K; the effects of notches on prismatic beams; the usefulness of the J-integral as a fracture parameter; and the differentiation between micro-cracking and main crack growth.

2.2.2.2 THE EXPERIMENTAL WORK

The first experimental application of fracture mechanics to concrete was carried out by M.F. Kaplan in 1961[8]. He tested three different mixes using beams of 76 x 76 x 406 mm and 152 x 152 x 510 mm with varying notch depths. He found that G was approximately constant for different notch depths, although G for the smaller beams was roughly 38% less than for the larger beams. Four-point loading gave G_c values about 15% lower than those for three-point loading. G_c was, in general, about 12 times as large as that estimated from the surface energy of concrete. Kaplan concluded that LEFM provided an appropriate fracture criterion for concrete.

Glucklich[9] carried out static and fatigue tests on 1000 x 100 x 50 mm mortar beams in flexure. He found G to be about 7,5% lower in fatigue than in static tests and concluded that the strain energy release rate was applicable for both types of loading. He found G to be independent of notch depth.

Moavenzadeh and Kuguel[10] applied the Griffith Theory to several different concretes, mortars and cement pastes tested as beams (25 x 25 x 305 mm) in 3- point bending. A microscopic technique was used to estimate the true fracture area and it was found that the fracture energy obtained was about ten times that calcula-

ted from theory. This suggested a zone of micro-cracking ahead of the main crack. Koyanagi and Sakai[11] investigated the crack arrest mechanism discussed earlier by measuring K and G , using beams 47 x 100 x 388 mm and a 10 mm notch, tested in three-point bending. They found that both bulk strength and E increased with increasing aggregate volumes and reasoned that aggregates must play a significant role in crack arrest during fracture. Also, G and K showed an increase with increasing aggregate volume except for lightweight aggregates where G_c and K_c decreased for increasing aggregate volume.

Brown[12] measured the K (fracture toughness) of hardened cement paste and mortar using a compliance technique to determine crack growth. He found that for the paste, K was independent of crack growth while for mortar K increased with increasing crack growth. For both the paste and the mortar, crack growth initiated at a lower K value than was required to sustain it.

Blight[13] made use of fracture energy in his approach to design of cemented materials using the effective fracture surface energy . His work was based on two principles:-

- There is a simple equivalence between work done on the structure or member in applying the ulti-

mate load and the equivalent energy of the resulting fracture surface.

- In the absence of geometrical stress-raisers, the strength of the material will be governed by the presence of inherent starter flaws in the material.

Blight[13] reasoned that direct application of the Griffith energy equation 2.2 yielded a critical natural flaw size of about 10 mm for concrete and pavement materials such as cement treated bases. He based this on laboratory values for δ'. This flaw size compares well with those found in cemented materials laid under normal working conditions. Blight then applied his theory to a number of practical problems associated with the cracking of roads with cement treated bases. He was able to predict typical crack spacings and flexural failure loads of unreinforced slabs subjected to line loads or heavy moving wheel loads.

Cooper and Pigg[14] conducted slow bend tests on hardened cement paste beams with sawn triangular notches. The work of fracture and surface energy were estimated from the area under the load deflection curves. From the Griffith equation, the critical flaw size was then calculated to be about 7 mm for dry specimens and 6 mm for wet specimens. This compares well with Blight's work as described above.

In an effort to determine the applicability of LEFM to concrete, Walsh[15] tested beams ranging from 76 to 380 mm deep and 255 to 1270 mm long. She calculated K_{Ic} for each case and concluded that the minimum beam depth for LEFM to be valid is 228 mm. Smaller members, she found, may be notch insensitive and failure loads can be related to the modulus of rupture of the fracture section. This phenomenon was explained by reasoning that specimens must be large enough so that the zone of disturbance near a crack tip is small compared to the specimen dimensions.

Mindess and Nadeau[16] carried out tests on mortar and concrete to determine whether K_{Ic} depends on the length of the crack front. Notched beams with a constant length of 203,2 mm and depth of 50,8 mm but with the width (crack front length) varying from 45 to 254 mm were cast and tested in 3-point bending. No dependence of fracture toughness on crack front length was found thus implying a plane strain condition.

In a similar study, Morita and Kato[17] attempted to determine the relationship between the fracture strength and fracture toughness of concrete using an acoustic emission technique. 100 x 100 x 420 mm beams with varying notch widths and notch depths were tested in 3-point bending. It was found that K_{Ic} was independent of notch width and notch depth, and that

concrete is notch-insensitive for notch/depth ratios less than about 0,64.

The concept of N. .inear Fracture Mechanics was used by Halvorsen[18] to measure the toughness of, amongst ther things, different hardened cement paste and concrete mixes. He used the J-integral for this purpose and found that it dependent on specimen dimensions, especially depth. Following further analysis, it was concluded that the J-integral might be useful in characterising fracture in cemented materials.

Use of the J-integral was also investigated by Rokugo[19]. He used notched beams of mortar, concrete and fibre reinforced concrete, tested in bending. Different methods of evaluating the J-integral were examined. Various beam sizes, aggregate sizes and notch depths were studied. Rokugo concluded that the J-integral is a suitable criterion for fracture mechanics in cemented materials.

To further reinforce the concept of the J-integral in fracture mechanics, Carrato[20] studied notched mortar, concrete and fibre-reinforced concrete beams in bending. He found J_c to be independent of notch type, notch tip sharpness, or notch thickness. Notch depth became important only when the maximum aggregate size approached that of the uncracked ligament. Also, within the limited range of sizes tested, J_c was

independent of specimen size and did not vary between 3-point and 4-point loading. Carrato concluded that the J-integral is very useful as a fracture criterion for both plain and fibre-reinforced concrete.

Kim et al[21] carried out studies on mortar beams of varying size and notch/depth ratios. Their results were in conflict with many obtained so far and may be listed as follows:

- For all beam sizes the nominal flexural strengths of notched beams were about 75% of those of the unnotched beams.
- K showed a high scatter but seemed to be independent of notch/depth ratio.
- The initial K value was higher for deeper beams.
- After slow crack growth during loading was estimated using compliance techniques, the recalculated K values showed a larger scatter than the K values based on the initial crack depth.

The authors therefore concluded that:

- The compliance method for estimating slow crack growth is not accurate.
- Notch effects can be measured, even in shallow beams.
- The existence of a true K for concrete is uncertain.

The fracture toughness parameter G and its methods of determination for concrete specimens have been well researched by Petersson[22]. His conclusions are as follows:

- The determination of G indirectly from 3-point bending tests is too dependent on specimen size to be of practical use.
- A stable 3-point bending test can be used to directly calculate G based on the area under the load vs deflection curve.
- LEFM cannot be used unless the beam length is at least ten times greater than its depth. This ensures that the effect of the micro-cracked zone ahead of the main crack tip is minor.

In further studies, Petersson[23] used the fictitious crack model to analyse the results of a series of G tests on concrete. The experiments were conducted on 50 x 50 x 600 mm specimens in 3-point bending, with a 25 mm sawn central notch. He concluded that;

- G is strongly dependent on aggregate quality with higher G values for stronger aggregates. G also increases with age and with decreasing water/cement ratio.
- For normal concrete G varies between 60 and 100 N/m.
- G is not affected by maximum aggregate size.

- G_f increases to some extent with increasing volume fraction of aggregates.
- Wide scatter in the data can make conclusions uncertain.

Nallathambi et al[24] tested beams in 3-point bending to determine the effects of specimen size and mix parameters on G_f. It was found, amongst other things, that;

- G_f decreased with increasing notch/depth ratio.
- G_f increased with increasing aggregate size.
- G_f increased slightly with increasing specimen depth.
- G_f decreased with increasing specimen span.

Alexander[4] tested notched concrete beams of width 100 mm and with depths ranging from 100 mm to 800 mm. *Notch depth ratios ranged from 0,2 to 0,5.* The beams were loaded at midspan and simply supported with a span/depth ratio of four. It was found, amongst other things, that:-

- The 100 mm deep beams were notch-insensitive. For the larger beams, notch-sensitivity increased with increasing depth.

- Support roller friction could adversely affect the results.

- Compliance relationships, based on LEFM theory, were not entirely valid for concrete beams. Therefore slow crack growth cannot be ignored in fracture calculations.

- Concrete departed considerably from ideal elastic-brittle behaviour during fracture. The tension zone size was roughly twice the compression zone size.

- The micro-cracked zone reached a maximum size after which main crack growth began and the relative micro-cracked zone size remained constant.

Alexander[4] highlighted required areas of future work with some of the most important being:-

- further studies of the micro-cracked zone using notched fracture beams:- in particular, confirmation of existing relationships for (a) the size of the zone in beams of different depth, (b) zone stresses relative to zone sizes, and (c) variation of zone sizes and zone stresses during crack growth.

Other researchers have also presented techniques and parameters for characterising fracture in cemented materials. Mention should be made of Bazant[25], and

Hillerborg and colleagues[26]. Also the work of Shah and colleagues[27] should be noted.

To close this section, the following conclusion, drawn by Mindess[28], is presented.

After reviewing the applications of fracture mechanics to concrete with particular attention to the questions of notch sensitivity, the applicability of LEFM and the specimen size required for valid tests, Mindess says:-

- There is still no agreement on how best to characterise the fracture of concrete.
- There is probably almost no truly valid fracture data on concrete in the literature reviewed.

2.2.3 FRACTURE MODELS

2.2.3.1 INTRODUCTION

In the simplest case, concrete and mortar may be modelled as composite materials consisting of two phases, hardened cement paste and aggregates. This, however, fails to describe the fracture behaviour of concrete. Both the aggregate and the paste exhibit brittle failure characteristics while the stress-strain curve of concrete deviates from linearity even at low levels,

and has a descending slope after maximum load,[29] (FIG 2.3).

On a microscopic scale it has been observed that the deviation of the stress-strain diagram from linearity is linked to the growth of pre-existing bond cracks[29]. At higher loads continuous cracks - i.e. cracks combining bond cracks and mortar cracks - are formed.

Crack propagation in concrete can be linked to the heterogeneity of the material on different levels. It has been postulated that cracks may follow very complex paths[30] and furthermore numerous cracks are formed in the vicinity of an initial crack, rather than one single crack. In addition, propagating cracks may be arrested by aggregate particles resulting in multiple branching. Thus, the true crack surface in concrete is considerably larger than the apparent nominal crack surface[31].

The fracture energy term described earlier (section 2.1.4) must apply to the composite material rather than to discrete phases. The aggregates in concrete modify the stress field and impose an arresting action on the cracks, causing the fracture resistance of concrete to be greater than that of an equivalent paste. The crack-arresting function of the aggregates and mechanisms of micro-cracking give concrete a non-

and has a descending slope after maximum load,[29] (FIG 2.3).

On a microscopic scale it has been observed that the deviation of the stress-strain diagram from linearity is linked to the growth of pre-existing bond cracks[29]. At higher loads continuous cracks - i.e. cracks combining bond cracks and mortar cracks - are formed.

Crack propagation in concrete can be linked to t terogeneity of the material on different levels. has been postulated that cracks may follow very complex paths[30] and furthermore numerous cracks are formed in the vicinity of an initial crack, rather than one single crack. In addition, propagating cracks may be arrested by aggregate particles resulting in multiple branching. Thus, the true crack surface in concrete is considerably larger than the apparent nominal crack surface[31].

The fracture energy term described earlier (section 2.1.4) must apply to the composite material rather than to discrete phases. The aggregates in concrete modify the stress field and impose an arresting action on the cracks, causing the fracture resistance of concrete to be greater than that of an equivalent paste. The crack-arresting function of the aggregates and mechanisms of micro-cracking give concrete a non-

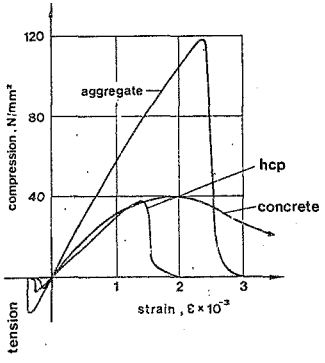


FIG 2.3 Stress-strain diagrams for hardened cement paste, aggregate and concrete (from ref 29).

linear or pseudo-plastic nature, since these phenomena increase the energy demand for crack propagation[32].

This phenomenon of apparent non-linear plasticity in concrete is best illustrated by reference to Glucklich's model for the fracture of a non-homogeneous material[33]. It should be mentioned that there are many fracture models in existence. For example: The Microplane Model[34] describes tensile strain softening due to micro-cracking, the Damage Model (ref 1, pg 50) describes a decrease in elastic modulus and load relaxation at the crack tip, and the Cohesive Force Model (ref 1, pg 220) describes a cohesive force distribution behind the crack tip. However, to describe all these approaches in detail would be beyond the scope of this dissertation. For this reason, one model, namely that due to Glucklich[33], was chosen since it helps with the understanding of the Griffith fracture concept (described earlier in this chapter) as applied to non-homogeneous materials.

2.2.3.2 THE GLUCKLICH MODEL

Firstly, it is necessary to point out the limitations of Griffith's ideal case. His equation 2.2 can be interpreted as a term for surface energy demand rate, 4γ and a term for strain energy release rate, $2\pi\sigma^2 c/E$ with these rates being expressed in terms of crack length c. This means that the energy demand is con-

stant at 4Y while the energy release increases linearly with crack length for a certain stress. So, a material with a certain crack length c, under increasing stress would remain stable until a critical stress was reached, when it would become possible for crack growth to occur and even to continue for subsequent decreasing stress. Since this case is ideal, it is probably never attained in a real situation and hence of a more complex model was proposed by Glucklich[33].

Glucklich's model applies Griffith's case to complex materials such as concrete and mortar and takes into account the question of effective surface energy as explained earlier in this chapter. FIG 2.4 shows a probable energy balance for crack propagation in a complex material. As the crack grows, so does the micro-cracked zone ahead of it. Therefore the energy requirement curve is no longer a straight line but an increasing function of crack depth c. This curve becomes linear at point A when the micro-cracked zone has reached its maximum size for a particular case.

Consider an initial flaw or crack of depth c_o, in a material under a global tensile stress σ_0. A growing crack is stopped at point c_2, because of an increase in energy demand. The stress must then rise to σ_1, before the crack continues to grow to c_2, where it is once again stopped due to energy demand. This process continues until point A is reached which

represents the critical energy level - a point of instability. At this stage both energy release and energy requirement are critical and unstable crack propagation follows. The dotted line drawn between the steps in FIG 2.4 represents the actual energy path followed. FIG 2.5 shows FIG 2.4 in terms of energy rates. The energy demand rate is shown by the bold black line and rapidly increases until point A is reached. It then remains at a constant maximum. At point A, spontaneous crack propagation is possible and can continue even for decreasing stress. This clearly explains the tensile failure of a concrete specimen under increasing load.

The Glucklich[33] model can be applied very well to a multiphase material such as concrete. Concrete consists of two or more distinct material phases with each phase having its own energy-requirement curve. This is shown in FIG 2.6 as curves of differing slope, with the toughest phase having the steepest slope. A crack of say depth c_o would progress until depth c_1. At this stage, upon entering a tougher phase, the crack would stop and the overall stress would have to rise so as to overcome the energy demand of the tough phase. The tough phase therefore increases the overall toughness of the material. The crack arresting mechanism need not necessarily be a discrete phase, but can also be an interface such as the aggregate-paste interface in concrete.

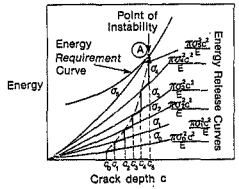


FIG 2.4 Crack propagating in a non-homogeneous brittle material under monotonically increasing stress (from ref 4).

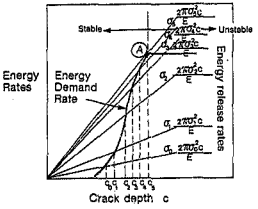


FIG 2.5 *Energy rate curve corresponding to FIG 2.4 (from ref 4).*

2.2.4 APPLICATIONS OF LINEAR ELASTIC FRACTURE MECHANICS

The behaviour of concrete and cement paste under load has a number of characteristics which suggest that a fracture mechanics approach can be used to explain these materials[35]:

1. Fracture when considered locally generally occurs in a brittle fashion.

2. The strengths of both concrete and mortar are dependent on loading rate; also, these materials are subject to static fatigue.

3. The ratio of tensile to compressive strength in these materials is about 1:10 which is very close to the Griffith prediction of 1:8.

4. Aggregate-matrix interfaces produce stress concentrations which could easily be of such a magnitude as to exceed the local theoretical strength in these regions.

5. Most investigations of notch-sensitivity show that these materials are notch-sensitive, particularly hardened cement paste. Ziegeldorf et al[36] showed that notch sensitivity is a necessary, though not sufficient, condition for the application of LEFM to cementitious materials.

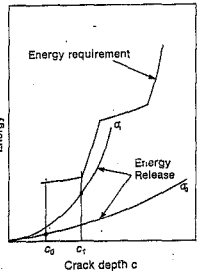


FIG 2.6 Crack progressing in a bi-phase material (from ref 4)

Application of LEFM theory to any material is based on the assumption that the material is homogeneous and elastic on a global scale, and that the elastic modulus E and Poisson's ratio ν are constant throughout the material. Concrete is, of course, both heterogeneous and discontinuous and therefore average values for the various properties are assumed.

It is apparent from the above that the application of fracture mechanics principles to cemented materials yields results which have a considerably lower confidence level than the results obtained from the application of fracture mechanics principles to metals and alloys. In view of the heterogeneity of cemented materials (when compared with metals) it is clear that considerable further research is required before valid fracture tests and parameters can be found, which will be useful for predicting structural performance at an engineering level.

2.2.4.1 LINEAR ELASTIC FRACTURE MECHANICS PARAMETERS

The two fracture parameters based on LEFM assumptions are the critical strain energy release rate G_c and the critical stress intensity factor K_c. For simple cases, G_c and K_c can be calculated analytically while in complex instances finite element methods or other numerical techniques are required.

(i) MEASUREMENT OF THE CRITICAL STRAIN ENERGY RELEASE RATE

The strain energy release rate G is given by

$$G = 2\pi cc'/E \quad (2.5)$$ (see section 2.1.1, FIG 2.1)

G depends on the material, the specimen geometry and the state of growth of the crack. It can be measured in a laboratory with notched test specimens. Only the applied force and the crack length need to be measured to compute G. The applied load at the point of instability can easily be obtained from an autographic load-displacement trace but the crack length is far more difficult to measure. This is because the critical crack length c must include the length of induced slow crack growth in addition to the original notch depth. This induced length can be found by using methods such as the compliance method[37], an ink staining technique or high speed photography.

It must be realised that the crack length at the exact point of instability (i.e. onset of unstable crack growth) need only be known if the value of G_c, the critical energy release rate, is required.

(ii) MEASUREMENT OF THE STRESS-INTENSITY FACTOR

The phenomena of surface energy and plastic work accompanying fracture are not yet fully understood (ref 66,

pg 425-429). For this reason, the strain energy approach described in the preceding section has distinct limitations. The stress-intensity approach, involving the parameters K or K_c is therefore now generally preferred to the energy approach. The K_c parameter is often a more useful representation of a material for engineering applications, while G_c is more useful when fracture mechanics is applied to material development.

K_c, the value of K at the point of instability of crack growth in a material may be regarded as a measure of a material's fracture toughness or resistance to brittle fracture. The higher the value of K, the larger the crack that can be tolerated, and when a critical value K_c is reached, the crack will extend.

K can be written as:

$$K = \alpha \sigma \sqrt{\pi c} \qquad (2.6)$$

Where α = geometric correction factor
σ = applied stress
c = crack length.

The largest source of error in K_c (and G_c) measurements is the uncertainty about the exact crack length at the point of instability for cementitious materials. Many techniques have been used to measure the

crack length, with ultrasonics showing good results more recently both for detecting the onset of main crack growth, and for continued monitoring of further crack growth (ref 66, pg 425-429).

The test methods to determine K include among others 3-point and 4-point bending of notched rectangular beams, plate specimens with a centre crack, double cantilever beams, compact tension specimens and double-edge-cracked tests.

From the reported test data (ref 66, pg 425-429) it seems that the two major factors affecting fracture toughness appear to be the matrix strength and the type and volume concentration of aggregate particles acting as crack arrestors. Addition of suitable aggregate can therefore increase fracture toughness, although volume fraction, rather than grading, seems to be more important. Also, higher volumes of aggregate can bring about a progressive increase in toughness with crack growth see FIG 2.7.

2.2.5 NON-LINEAR FRACTURE MECHANICS PARAMETERS

In cemented materials, considerable apparent plasticity and large amounts of inelastic deformation prior to final failure often invalidate the application of LEFM theory. In these materials it is likely that both crack opening and crack extension occur at approximate-

ly the same time. For this reason non-linear approaches have been developed. The main advantage of these non-linear methods is that they recognise energy dissipation other than the formation of fracture surfaces, and in that respect, they are superior to LEFM methods (ref 66, pg 414).

The most common techniques of non-linear fracture mechanics which have been applied to cemented materials are:

i) the critical crack opening displacement method (COD)[38,39,40]

ii) the J-integral approach[40,41]

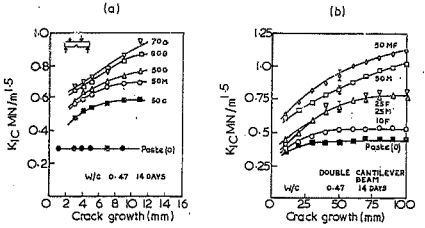
iii) the R-curve analysis[42,43,44]

iv) the fictitious crack model[45,46,47].

In this section, the COD, the J-integral and the R-curve approach will be dealt with.

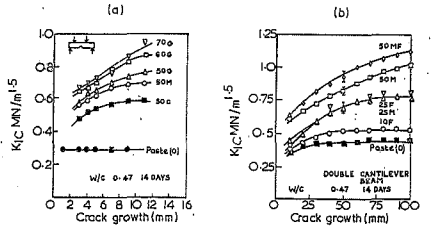
2.2.5.1 CRACK OPENING DISPLACEMENT (COD)

The COD can be used to characterise fracture behaviour in the vicinity of a sharp notch by considering the opening of the notch faces. This can be shown to be analogous to G_c, and thus COD values can be related



Variation of fracture toughness with crack growth of cement paste, mortar and concrete, (a) Notched beam, 4-point bending test. (b) Double cantilever beam test. Aggregate sizes: F = fine (52-100 mesh), M = medium (14-25 mesh), MF = mixture of equal proportions of M and F, C = coarse (10-5mm) and G = graded (10-100 mesh)

FIG 2.7 Variation of fracture toughness with crack growth in cement pastes, mortar and concrete (from ref 66)



Variation of fracture toughness with crack growth of cement paste, mortar and concrete, (a) Notched beam, 4-point bending test. (b) Double cantilever beam test. Aggregate sizes: F = fine (52-100 mesh), M = medium (14-25 mesh), MF = mixture of equal proportions of M and F, C = coarse (10-5mm) and G = graded (10-100 mesh)

FIG 2.7 Variation of fracture toughness with crack growth in cement paste, mortar and concrete (from ref 66)

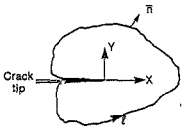
to K_c. The COD can even be measured when there is micro-cracking (or plastic flow in the case of ductile materials) ahead of the crack. It has been found, in general, that COD values depend to some extent on specimen geometry.

2.2.5.2 THE PRINCIPLE OF THE J-INTEGRAL

Once it was realised that crack tip plasticity in cemented materials is large enough to influence the energy release rate associated with LEFM, the need for a more meaningful fracture parameter was recognised.

For this reason the J-integral, first proposed by Rice[48], has been applied to cemented materials by several researchers in an effort to circumvent the problem of uncertainty in the crack stress field. In its basic mathematical form the expression for the J-integral is given together with a diagram in FIG 2.8. J is really a generalised relation for the energy release due to crack propagation, which may also be valid if there is appreciable crack tip plasticity. It is, in its fundamental form, a path *independent line integral of energy density* along a closed path around a crack.

From[49] a physical viewpoint J may be interpreted as the energy per unit area of crack advance (including non-linear behavior), or



$$J = \int_{\ell} W\, dy - \bar{T} \cdot \left(\frac{\partial \bar{U}}{\partial x}\right) ds$$

Where ℓ = *Path of integration*, taken counterclockwise around the crack tip;
W = Strain energy density;
$\bar{T}$ = Traction vector *defined by the outward* normal vector $\bar{n}$ on the path ℓ;
$\bar{U}$ = Displacement vector; and
s = Arc length along the path ℓ, $ds^2 = dx^2 + dy^2$.

FIG 2.8 Fundamental *expression of* the J-Integral (from ref 4)

$$J = \frac{-1}{B} \frac{dU}{dc} \qquad (2.7)$$

where B = Crack Width

U = work done

c = Crack Length

Considerable work on developing the J-integral as an analytical tool for elastic-plastic crack-tip field analysis has been carried out by Begley and Landes[50] using a compliance technique. However, both this method and another one developed by Bucci et al[51] require several different specimens which must then be compared.

Obviously, a method for measuring J from a single specimen design (i.e. same initial crack size) would be much more desirable. One such method, developed by Rice et al[52], appears to offer the simplest single specimen design technique for measuring J and was further developed by Landes and Begley[53].

In this technique, bend-type specimens or compact tension specimens with a deep crack are loaded and J is determined as a function of displacement from the expression:-

$$J = \frac{2.A}{W.h} \qquad (2.8)$$

Where:

A = Area under the load-displacement curve up to the point of maximum load

W = Specimen width

h = uncracked ligament depth (for a beam, d-c)

Note that the constant 2.0 applies to the bend specimen, and is different for other specimen types.

In measuring A, the area under the curve, the area due to elastic unloading is included using a vertical line as shown in FIG 2.9.

It should be noted that path-independence of the J-integral has been shown thus far only by using the deformation theory of plasticity[54] which does not allow for unloading. Therefore the J-integral fracture criterion is only valid up to the peak load; for concrete the point of peak load may not necessarily be the point of crack initiation. There is not yet a methodology to use the J-integral for stable crack growth[55].

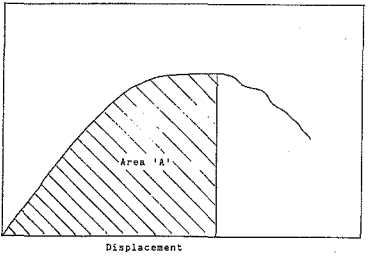


FIG 2.9 Definition of the area 'A' for determining J

As a final point, J_c is exactly equal to G_c for linear-elastic materials, and it is only for non-linear materials that the preceding methodology need be adopted.

2.2.5.3 R-CURVE ANALYSIS (CRACK GROWTH RESISTANCE CURVES)

The R-curve concept[56,57] was developed to incorporate slow crack growth as an essential part of plane stress behaviour. Originally, it was applied to metals but has recently been extended for use in cemented materials. R-curves characterise the resistance to fracture of materials during incremental slow stable crack extension. They provide a record of the *toughness development as a crack is driven stably* under increasing crack-driving forces.

An R-curve is a plot of crack growth resistance in a material as a function of actual or effective crack extension. Thus, the R-curve describes the variation in the crack growth resistance with crack length c.

During slow stable crack growth the energy release rate equals the energy consumption rate. Therefore:

$$G = R \quad (R = \text{energy consumption rate}) \qquad (2.9)$$

As can be seen in FIG 2.10 the instantaneous values of

G during crack growth will indicate how R depends on crack size. R in fact increases during slow crack growth, as can be seen in FIG 2.10. Also shown in FIG 2.10 are lines indicating how G depends on crack size and applied stress.

During slow crack growth both G and R follow the line ABC (since G = R as stated above). After a crack extension LM the crack has reached a length c . This is the point of fracture instability because from this point on G follows the line CD and remains larger than R. The fracture condition here is the point of tangency.

$$\frac{dG}{dc} = \frac{dR}{dc} \qquad (2.10)$$

The method of R curve analysis involves the continuous measurement of load and slow stable crack growth. The load values are converted to K values for the particular loading and structural configuration. These K values can also be thought of as crack growth resistance values or R values. The resulting plot of K (or R) versus crack growth at the K values is the R-curve.

The concept of an R-curve as shown in FIG 2.10 is very similar to the Glucklich model[33] dealt with in FIG's 2.4 and 2.5. The Glucklich model considers the increas-

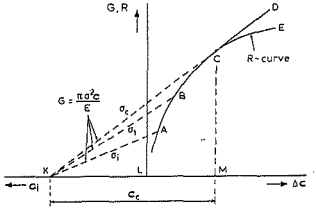


FIG 2.10 The energy concept in plane stress (from ref 55)

ing resistance to crack growth which occurs in a multi-phase material. The R-curve concept of increasing crack growth resistance fits in well with this model.

2.2.6 SUMMARY OF THE FRACTURE MECHANICS APPROACH TO CEMENTED MATERIALS

Fracture mechanics assumes the existence of a single flaw or crack that can, under increasing load, lead to complete fracture and failure of the material concerned. LEFM assumes that this crack propagates within a homogeneous continuum which behaves in a brittle manner with very little plastic deformation.

In cemented materials, especially "coarse grained" materials such as mortar and concrete, the constituents of the composite material are usually not small in comparison with the dimensions of a beam, a slab, or a column. Also, even in tension, concrete does not fail in a brittle manner. Concrete is a complex, heterogeneous material that contains inherent flaws and cracks and has the added complication of aggregate matrix interfaces. When concrete fractures, it develops a fracture zone (as compared with a single crack) in which micro-cracking occurs, and therefore LEFM can only be considered to be a rough approximation of the real material behaviour. NLFM has been developed to attempt to include material heterogeneity but still

assumes the existence of a single crack instead of a zone of cracking.

At this stage, fracture mechanics is far from providing a complete approach to the fracture of cemented materials. What is even more lacking is the direct applicability of fracture mechanics principles to design in cemented materials.

2.2.7 CONCLUDING REMARKS

The comment by Mindess at the end of section 2.2.2.2 illustrates the need for further work in the field of cemented materials.

Few researchers have attempted to explain or characterise the phenomenon of micro-cracking in cemented materials, the work of Alexander[4] being an attempt in this regard.

An understanding of the mechanism of fracture is essential for the development of more representative models in fracture mechanics and the key to understanding this mechanism lies in the identification of the various stages of cracking in heterogeneous materials such as concrete. Alexander's work brought to notice the role of micro-cracking in concrete, and this dissertation attempts to further the understanding of this process by attending to those aspects which posed

unanswered questions or required further investigation. From Alexander's work it was clear that there was considerable scope for further investigation of the process of micro-cracking as well as the necessity for reducing support roller friction, which he found could adversely affect the results of a fracture test. With the above in mind, the objectives of this dissertation were defined as:-

- a detailed study of the early development of the micro-cracked zone with a view to investigating a fracture parameter at the start of main crack growth.

- a detailed study of the behaviour of the micro-cracked zone at this point.

- characterisation of the fracture behaviour of concrete and mortar at the start of main crack growth.

- development of an experimental technique to reduce support friction.

PART II

EXPERIMENTAL FRACTURE STUDIES

3. EXPERIMENTAL WORK

3.1 INTRODUCTION AND OBJECTIVES

The work of Alexander[4], together with the background to concrete and mortar fracture testing given in the literature survey presented in the previous section, has drawn attention to those aspects of fracture that require further investigation. These include fracture processes in notched concrete and mortar beams, including the presence, extent, and influence of micro-cracking as outlined at the end of the previous section.

The effects of specimen depth and notch depth and their influence on the micro-cracked zone have also shown a need for further research. A series of tests was therefore carried out to investigate the above points. These tests were spread over a period of 7 months and were performed on notched concrete and mortar beams of various sections and depths. Test apparatus and instrumentation was designed and built to allow continuous, accurate monitoring of fracture processes. This chapter describes details of specimens, mixes and materials, test equipment and testing procedures. It also deals with results of materials control tests and certain aspects of the fracture test results.

The work carried out by Alexander[4] examined the problems of plane strain fracture testing of cemented materials. Seve~ questions were left unanswered and it was these qu...cions that prompted specific objectives to be defined for the present fracture testing programme. These objectives (which are outlined in more detail at the end of the previous section) were:

1. To investigate the processes of fracture by the study and analysis of load-deflection curves and continuous measurement of displacement profiles across a fracturing section obtained during fracture tests. Ultrasonic pulse velocity measurements were also used.

2. To make a detailed study of the early development of the micro-cracked zone with a view to determining a fracture parameter at the initiation of main crack growth, and also with the aim of studying the stresses associated with this process.

3. To develop an experimental technique to overcome the problem of support friction.

3.2 DETAILS OF SPECIMENS

A total of thirty concrete and mortar beams with depths of either 200mm or 300mm, and notch depths of 40mm, 60mm, 80mm or 120mm were cast and tested to

determine their fracture characteristics.

Two series of fracture tests (one on concrete and one on mortar) were carried out. Series 'A' consisted of 18 prismatic, notched constant section concrete beams with support spans of 600mm or 900mm, and depths of 200mm or 300mm respectively. The span / depth ratio was constant at three. These beams had notch / depth ratios ranging from 0,2 to 0,4. Series 'B' consisted of 12 prismatic notched constant section mortar beams with dimensions identical to those in series 'A', differing only in that they were made from a coarse-grained mortar and not concrete.

The notches were all centrally located at midspan, and cut using a 3mm diamond-tipped sawblade. One face of each beam had a smooth finish so as to facilitate the glueing of clamps to hold five surface displacement measuring transducers set at a 100mm gauge length. A summary of the various specimens is given in table 3.1.

FIG 3.1 depicts a typical fracture beam while FIG's 3.2 and 3.3 show photographs of fracture beams at various stages of preparation and testing.

TABLE 3.1 SUMMARY OF FRACTURE BEAMS, SERIES A AND B

SERIES	NUMBER OF BEAMS	SPECIMEN NUMBER	OVERALL NOMINAL BEAM DIMENSIONS (mm) b x d x L	INITIAL NOTCH/DEPTH RATIO c_o/d	LOADING SPAN (mm) S	INITIAL LIGAMENT DEPTH h_o
A	7	1A;2A;3A;7A;13A;14A;15A	100x200x650	0,2	600	160
A	7	4A;5A;6A;8A;16A;17A;18A	100x200x650	0,4	600	120
A	2	9A;10A	100x300x950	0,2	900	240
A	2	11A;12A	100x300x950	0,4	900	180
B	4	1B;2B;3B;4B	100x200x650	0,4	600	120
B	4	5B;6B;7B;8B	100x200x650	0,2	600	160
B	4	9B;10B;11B;12B	100X300X950	0,4	900	180

TOTAL 30

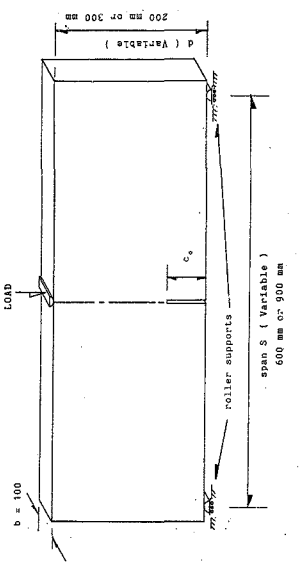


FIG 3.1 Typical fracture beam.

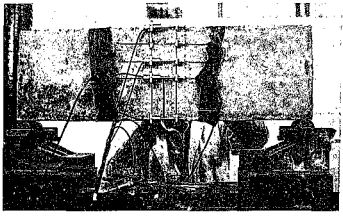


FIG 3.2 View of a fracture beam resting on its support rollers. Note the centrally cut notch and the surface and ultrasonic instrumentation (described elsewhere in the text).

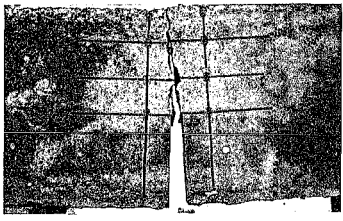


FIG 3.3 View of a cracked fracture beam after testing.

1. Certain beams had small variations in the dimensions b, d and c . These were accounted for in the calculations but, for simplicity sake, are not shown in table 3.1.

2. Specimens 13A and 14A suffered equipment malfunction during testing, so that data collected was of no value.

3.3 CONCRETE AND MORTAR MIXES

The concrete mix ratios were by mass:
1:0,55:2,19:2,86 (cement: water: sand: stone).
The slump for this mix varied between 30 and 40mm, and bleed was minimal.

The mortar mix ratios were by mass:
1:0,55:3,69 (cement: water: sand).
The visible bleed for this mix was minimal.

The mix proportions used are shown in Tables 3.2 and 3.3. Details of the mixing, curing, casting and the materials used are given in Appendix A.

A single batch of cement and aggregates was used throughout the testing.

TABLE 3.2 CONCRETE MIX PROPORTIONS

MATERIALS	MIX PROPORTIONS IN kg/m^3 (Dry materials)
CEMENT: Ordinary Portland	366
STONE : CRUSHED 19mm NOMINAL SINGLE SIZED - REEF QUARTZITE	1045
SAND : REEF QUARTZITE CRUSHER SAND	800
WATER : TAP WATER	200

TABLE 3.3 MORTAR MIX PROPORTIONS

MATERIALS	MIX PROPORTIONS IN kg/m^3 (Dry materials)
CEMENT : Ordinary Portland	448
SAND : REEF QUARTZITE CRUSHER SAND	1652
WATER : TAP WATER	245

3.4 MATERIALS CONTROL TESTS

For all the beams, control cubes (101,6mm) for compressive strength were cast. In addition, control prisms (100x100x200mm) for compressive elastic modulus were cast at regular intervals. A total of 54 control specimens were cast and tested to provide the material properties of the mortar and concrete used.

3.4.1 CUBE COMPRESSION TESTS

These tests were carried out using 101,6mm cubes and procedures were in accordance with SABS Standard Method 861[68].

Three cubes were cast for each mixing batch and tested on the same day as the beam tests. The cubes were cured with the beams, and all tests were done using the Amsler compression testing machine (see later).

3.4.2 PRISM TESTS FOR ELASTIC MODULUS

A total of 12 prism tests were carried out. The prisms were cast at the same time as the beams in 100x100x200mm moulds and tested at the same age as the fracture beams. Longitudinal strains were measured over a 100mm gauge length with a dial gauge compressometer, shown in FIG 3.4, and the method of the test was in accordance with the principles of BS 1881:

Part 5: 1970[69]. All the tests were undertaken using the Amsler compression testing machine.

3.4.3 RESULTS OF MATERIALS CONTROL TESTS

Tables 3.4 to 3.7 show the results for the materials control tests described above.

The cube tests that show slightly low values are those for beams 9B, 11B and 12B, the reason for which is unclear. The difference in strength may have had an effect on the fracture tests, but the scatter present in the results made it impossible to determine whether this was in fact so.

The elastic modulus of the concrete beams is higher than that of the mortar beams. However, there is good consistency for each batch tested for the concrete and the mortar beams. Since the elastic modulus does not form a part of the fracture analysis for this thesis, the purpose of these tests was to ensure consistency within the specimens. The difference in modulus between the concrete and the mortar beams may have had an effect on the fracture tests, but the inherent scatter present in the result made it impossible to determine whether this was in fact so.

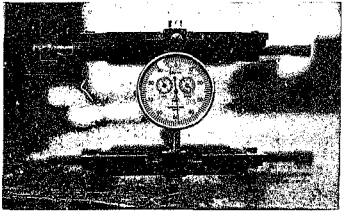


FIG 3.4 View of the dial gauge compressometer used for the elastic modulus tests.

TABLE 3.4 RESULTS FOR CUBE COMPRESSION TESTS ON CONCRETE

BATCH for beams:-	CUBE STRENGTH (MPa) (average of 3 cubes)	AGE AT TESTING (Days)
1A 2A 3A 4A	43,2	35
5A 6A 7A 8A	36,2	28
9A	37,3	30
10A 11A	38,4	30
12A	37,1	30
15A 16A	42,0	33
17A 18A	39,3	33

TABLE 3.5 RESULTS FOR CUBE COMPRESSION TESTS ON MORTAR

BATCH for beams:-	CUBE STRENGTH (MPa) (average of 3 cubes)	AGE AT TESTING (days)
1B 2B 3B	41,1	33
4B 5B	41,0	36
6B 7B 8B	36,7	25
9B	29,6	31
10B	35,6	31
11B	33,9	31
12B	32,3	31

TABLE 3.6 RESULTS FOR ELASTIC MODULUS TESTS ON CONCRETE

BATCH for beams:-	AVERAGE E (GPa) (3 prisms)	AVERAGE CUBE STRENGTH (MPa)	AGE AT TESTING (days)
9A 10A 11A 12A	33,5	37,6	30
15A 16A	37,0	42,0	33

TABLE 3.7 RESULTS FOR ELASTIC MODULUS TESTS ON MORTAR

BATCH for beams:-	AVERAGE E (GPa) (3 prisms)	AVERAGE CUBE STRENGTH (MPa)	AGE AT TESTING (days)
1B 2B 3B	29,7	41,1	33
9B 10B 11B 12B	27,0	32,8	31

3.5 EXPERIMENTAL APPARATUS

The instrumentation used for the tests comprised a load cell to measure midspan load, one transducer to measure mid-span deflection and five other transducers to record continuously the surface displacement across the fracturing section. Two recorders were used to plot the results autographically. Ultrasonic pulse equipment was also used to detect the onset of main crack growth.

3.5.1 DEFLECTION MEASURING RIG.

The beam deflections at midspan were measured using a modified version of the deflection rig used for Alexander's[4] work. The rig was supported on the horizontal top section of the beam on point supports placed directly above the loading supports of the beam. This eliminated any deflection due to local crushing at the loading supports. The mid-span deflections of the beams were measured by an LVDT (linear variable differential transformers) held in position by a clamp attached to the end of an arm suspended from the deflection rig. The beam was loaded through a loading roller with a centralised steel ball. A load cell was used to record the load. Photographs showing the arrangement are shown in FIG's 3.5 and 3.6. Further details of the deflection rig are given in appendix B.

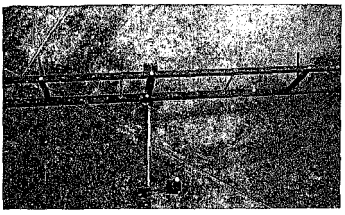


FIG 3.5 View of the deflection measuring rig. Note the supports at either ends and the arm for positioning the midspan deflection LVDT.

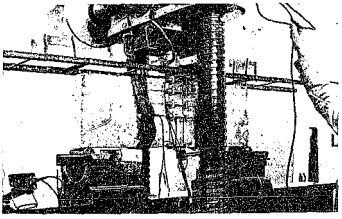


FIG 3.6 View of a fracture beam ready for testing. Note the deflection rig in position, and the midspan LVDT underneath the beam. Note also the centrally positioned surface displacement LVDTs and the ultrasonic probes held in position with rubber bands.

3.5.2 ELECTRONIC TRANSDUCERS

(i) LOAD CELL

This was used for all the tests and was calibrated using a Tinius-Olsen compression testing machine and later checked on the Amsler machine with the use of a digital multimeter (the calibrations were consistent). Further details are given in APPENDIX B.

(ii) LINEAR VARIABLE DIFFERENTIAL TRANSFORMERS (LVDTs)

A total of 6 LVDTs was used to record results continuously.

One LVDT was attached to the deflection rig (as explained in the previous section) and had its movable plunger core placed directly on the horizontal lower face of the beam next to the central notch. The other five LVDTs were attached to the vertical fracturing section of the beam and "spanned" the crack with a 100mm gauge length. The top and bottom LVDTs were positioned so as to measure extreme fibre displacements. The casings of these five LVDT's were held in place by aluminium clamps which were glued onto the beam surface. The cores rested on aluminium blocks which were placed at a distance of 100 mm across the fracturing section. These blocks had adjustable threaded screws to facilitate zeroing of the LVDTs.

Calibration of these instruments was carried out several times using an aluminium clamp and a micrometer both attached to a stiff steel plate. A multimeter was used to record the LVDT outputs in this case. Photographs showing the LVDT arrangements can be seen in FIG's 3.7 and 3.8.

Further details of the LVDTs are given in APPENDIX B.

3.5.3 RECORDING EQUIPMENT

Two types of autographic load and deflection measuring equipment were used.

(i) XY RECORDER

The XY recorder had an effective plotting area of 360mm (X scale) x 240mm (Y scale). This was used to record autographically the output from the load cell and the deflection rig LVDT. The load was recorded on the Y axis and the deflection on the X axis. Careful control was needed to ensure that the post-peak portion of the curve could be recorded and this was achieved in most cases.

(ii) MULTI-CHANNEL STRIP CHART RECORDER

This recorder was used continuously to plot the outputs from the five lateral displacement LVDTs. The

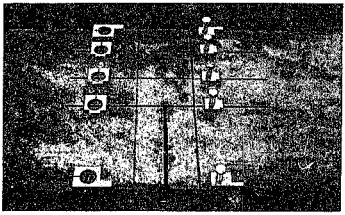


FIG 3.7 View of the LVDT clamps and blocks prior to gluing to the beam. Note the casing clamps on the left and the core support blocks with their adjustable screws on the right.

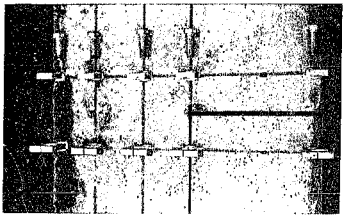


FIG 3.8 View of the LVDT clamps and blocks glued in position on a beam. Note the adjustable screws for the cores lying next to the blocks. (Note: Photograph rotated through 90°).

load cell output was recorded on a sixth channel to facilitate correlation between the strip chart records and the XY curves. Sensitivities were adjusted from cycle to cycle in each test so as to achieve maximum resolution, and calibrations were checked appropriately.

Further details of the equipment are given in APPENDIX B.

(iii) ULTRASONIC PULSE EQUIPMENT

An ultrasonic pulse recorder was used in most of the tests to help isolate the point of changeover from micro-cracking to main crack growth. The equipment comprised a transmitter and a receiver probe, both linked to a central unit which automatically measured the pulse transit time between the probes and displayed it on a digital meter.

The probes were placed on opposite sides of the beam and on opposite sides of the notch, at notch tip level. FIG 3.9 shows a detail of the probe positions. The ultrasonic pulse therefore had to travel through the material above the notch. The speed of this pulse would depend on the state of cracking of the material, ie pulse transit time would increase if cracking was present, and continue to do so as the cracking developed. The probes were held in position by rubber bands (see FIG 3.6) and a layer of petroleum jelly was

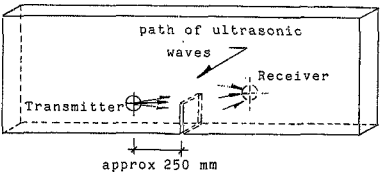


FIG 3.9 Detail of ultrasonic transducer probe positions on a typical fracture beam. Note that the probes are at notch tip level.

placed between the probe and the beam surface to ensure proper transmission of the ultrasonic pulses. Further details of the equipment are given in APPENDIX B.

3.5.4 TESTING MACHINE

An Amsler type 103 manually operated hydraulic compression testing machine was used for all beam tests and material control tests. It had a maximum load capacity of 2000 kN. Specimen loads were measured by the load cell which was clamped to the upper platen of the machine.

The beam support system was modified for the purposes of this work. This entailed specially machined smooth steel plates (made specially to fit onto the existing supports) on which two half-round steel rollers were placed. Free running, hardened steel, cylinder bearing races were placed between the half-rounds and the plates, thus allowing the beams to move freely laterally.

Alexander's[4] work drew attention to the importance of both laterally friction-free supports and a stiff testing machine. It was for this reason that the modified Amsler system was used. FIG's 3.10 and 3.11 show the support system used.

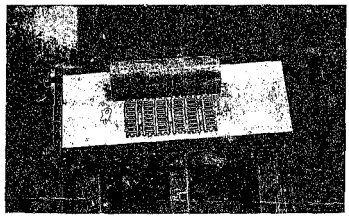


FIG 3.10 View of the rollers greased and ready to be placed between the half-round beam support and the machined steel plate.

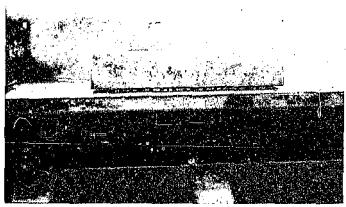


FIG 3.11 View of the rollers positioned between the half-round beam support and the machined steel plate.

3.6 TEST PROCEDURE

All the tests used a load-cycling technique to induce crack growth. Ultrasonic pulse times were recorded at the base and peak of each cycle while all other measurements were continuously recorded. (The ultrasonic equipment available was not able to record continuously)

3.6.1 SPECIMEN PREPARATION PRIOR TO TESTING

The beams were all damp-cured, under moist hessian and plastic sheeting, in a high humidity room with the temperature held at about 23° ± 2°. See APPENDIX A for further details. Approximately 2-3 hours before testing, the smooth side of each beam was thoroughly cleaned and accurately marked to facilitate glueing on of the aluminium LVDT clamps. The glue used was a rapid hardening preparation formulated for damp concrete which was ready for use within about 15 minutes. The beams were covered immediately after the glueing and kept damp until the test.

The specimens were placed on their roller-bearing bed and positioned using a tape measure. The lateral LVDTs were fastened in their clamps, and zeroed using the adjusting screws. The deflection rig was positioned and set. A thin layer of petroleum jelly was applied to the surfaces where the ultrasonic probes were

3.6 TEST PROCEDURE

All the tests used a load-cycling technique to induce crack growth. Ultrasonic pulse times were recorded at the base and peak of each cycle while all other measurements were continuously recorded. (The ultrasonic equipment available was not able to record continuously)

3.6.1 SPECIMEN PREPARATION PRIOR TO TESTING

The beams were all damp-cured, under moist hessian and plastic sheeting, in a high humidity room with the temperature held at about 23° ± 2°. See APPENDIX A for further details. Approximately 2-3 hours before testing, the smooth side of each beam was thoroughly cleaned and accurately marked to facilitate glueing on of the aluminium LVDT clamps. The glue used was a rapid hardening preparation formulated for damp concrete which was ready for use within about 15 minutes. The beams were covered immediately after the glueing and kept damp until the test.

The specimens were placed on their roller-bearing bed and positioned using a tape measure. The lateral LVDTs were fastened in their clamps, and zeroed using the adjusting screws. The deflection rig was positioned and set. A thin layer of petroleum jelly was applied to the surfaces where the ultrasonic probes were

to be placed. Initial readings of all instruments were then taken and the recorders were set.

3.6.2 LOADING

A technique of load-cycling was used to induce micro-cracking and stable main crack growth. The method was as follows:

1. A preliminary "setting" cycle of about 10% of estimated maximum load was applied. Strains were recorded during this cycle, but generally not used.

2. About three to four cycles were then applied before maximum load with typically about seven to ten cycles applied in total.

3. The load was applied at a steady rate with the typical time for one cycle being approximately 90 seconds. The rate of unloading was usually slightly greater than the rate of loading since it was more difficult to control load reduction than load application on the Amsler testing rig.

4. Control of any particular cycle was not difficult since the instrumentation made continuous recordings possible. The procedure was usually to allow very limited stable crack growth in the early cycles while trying to induce significant crack

growth in the cycles following maximum load. In many cases the load vs deflection curves reached plateaux in which the load remained almost constant while the deflection continued to increase.

5. Ultrasonic pulse transit times were measured at the start of each cycle and immediately before unloading of that cycle. It appeared that there was a significant difference between readings taken at the start and peak of a given cycle.

6. After failure the cracked beams were inspected for any notable features. A typical fracture test produced one load vs beam deflection record, in-plane displacement profile records and, in all but eight cases, ultrasonic pulse measurements. This data was analysed to isolate the features outlined in section 1.3.

FIG 3.12 illustrates a typical load vs beam deflection record. The relevant beam is N° 11B, d = 300mm. c_o/d = 0,40.

The first five cycles of the test are shown in this figure. The pre-loading (settling) cycle and the last three cycles are not shown. The following should be noted:

1. In this example maximum load was achieved on the

third cycle. The first two cycles show a sharp peak. It was hoped that these cycles would produce microcracking only.

2. The third cycle shows a tendency for an increase in deflection for no increase in load (only detailed analysis would show whether this was main crack growth or an increase in the size of the microcracked zone).

3. Cycles four and five show a definite increase in deflection for increase in load. Great care had to be taken in there cycles since the deflection had previously shown a tendency to accelerate and cause early failure.

4. The vertical portions immediately following the peak of each cycle represent rapid load dumping in order to arrest the deflection and prevent early failure.

3.7 SUMMARY

Chapter 3 has detailed the procedures for the fracture tests and selected materials control tests. A total of 30 (18 concrete and 12 mortar) notched fracture beams were tested. Two of the concrete beams tested suffered premature failure due to accidental overload.

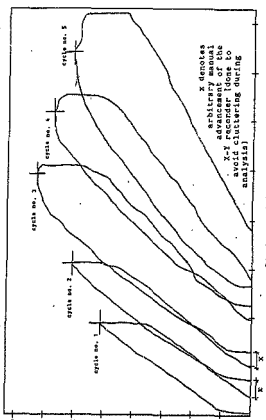


FIG 3.12 Typical load vs deflection record.

The beams had a constant width of 100mm and depths of either 200mm or 300mm. Sawn central notches were present in all cases with notch/depth ratios of 0,2 or 0,4. The beams had a constant span/depth ratio of 3. LVDTs (deflection measuring transducers) were fixed, via clamps glued onto the beam face, at mid-span and covering the beam height on one side of all beams at a gauge length of 100mm.

The beams were loaded cyclically at mid-span and supported on frictionless rollers. A load cell together with an LVDT produced a continuous output of load versus mid-span deflection on an XY recorder. LVDTs fixed to the sides of the beams produced continuous records of surface displacements across the fracturing section. Ultrasonic pulse velocity readings were taken at the peak and base of each load cycle.

4. FRACTURE TEST RESULTS

4.1 INTRODUCTION

The basic data from the fracture tests incorporated midspan load and deflection, ultrasonic pulse transit times and displacements across the notched section. Chapter 4 presents these results in their basic form.

4.2 LOAD-DEFLECTION RECORDS

The load versus deflection records of all twenty eight successful fracture tests were used to calculate the input of energy to the specimen for each cycle in a given test.

TABLE 4.1 gives a typical example of the data obtained from these records.

TABLE 4.1 TYPICAL EXAMPLE OF LOAD vs DEFLECTION DATA

SPECIMEN : N° 11B d = 300mm c_o/d = 0,40

CYCLE	Fmax (kN)	A (Nm)
1	2,5	0,05
2	3,0	0,08
3	3,6	0,16
4	3,3	0,16
5	3,0	0,17
6	2,5	0,15
7	1,7	0,12
8	1,0	0,08

Note:-

Fmax (kN) - maximum machine load for each cycle.

A (Nm) - area under load deflection curve for each cycle.

The records of the remaining twenty seven tests are tabulated in APPENDIX C.

The analysis of this data will be dealt with in the analysis section presented later.

The extraction of data from the autographic plots was carried out using a ruler, a pair of dividers and simple numerical methods.

The following explanation refers to FIG 4.1.

1. Choosing the point of maximum load, (Fmax), involved the use of a hand magnifying lens and a ruler. This point was interpreted as being the peak of the curve (as in cycles 1 and 2), or, in the case of a 'stable load plateau' (as in cycles 3,4 and 5), the point at which the load started to reduce.

   The reason for choosing the point at which the load started to reduce as the point of maximum load was that, shortly after the load began to reduce, it was necessary to rapidly 'dump' the load to prevent early failure of the beam. Since this point of 'dumping' was arbitrary, some other identifiable point (governed by the beam and not the machine operator) was required. The point at which the load began to reduce was the most logical to be chosen.

2. After the identification of Fmax, eight equal spaces were marked and measured using a divider and scale rule. Simpson's rule was then used to compute the area under that particular curve. While time consuming, this method was the most accurate available.

   FIG. 4.1 shows a typical area in question together with the eight spaces described.

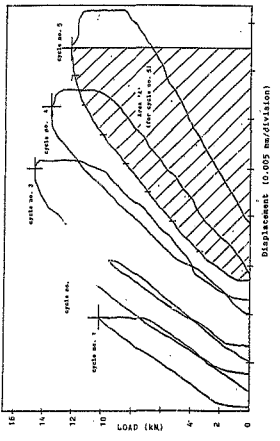


FIG 4.1 Typical area 'A' described in section 4.2 together with the eight equal spaces used to calculate 'A' by Simpsons rule. (The eight spaces can be seen marked on the trace of cycle 5).

NOTE: As can be seen in FIG. 4.1 the recording paper was manually advanced between cycles. This was done to avoid cluttering the record which would have made the data extraction more difficult.

4.3 *SURFACE DISPLACEMENTS ACROSS THE FRACTURING* SECTION

Continuous monitoring by five LVDTs mounted transversely across the fracture section yielded data that was used to plot displacement profiles for the test cycles of each beam. This was used to obtain crack lengths and positions of the neutral axis (see later).

The displacement profiles mentioned above are a plot of beam depth (on the vertical axis) versus the surface displacements across the fracturing section (at five different locations) relative to "zero displacement" at the start of a test. The five locations at which the displacements are measured are:- The extreme fibre position on the compressive face of the beam; two equidistant positions between the notch tip and the compressive face of the beam; the notch tip; and the extreme fibre position on the tensile face of the beam.

TABLE 4.2 gives a typical example of the data obtained from these records.

The values shown are the displacements at peak load (mm) for each cycle. The figures for all five LVDTs are given, together with the position of each LVDT above the base of the beam.

TABLE 4.2 EXAMPLE OF DISPLACEMENTS (mm) ACROSS A FRACTURING SECTION

SPECIMEN: N° 11B d = 300mm c_o/d = 0,40

DISPLACEMENTS AT PEAK CYCLE LOAD (mm)

LVDT		1	2	3	4	5
POSITION ABOVE TENSILE FACE (mm)		300,0	245,3	189,6	134,0	0,0
CYCLE		DISPLACEMENTS (mm)				
1		-0,003	-0,0013	6,3-04	0,0038	0,019
2		-0,0057	-0,0023	9,5-04	0,0070	0,032
3		-0,0074	-0,0026	0,0018	0,0110	0,046
4		-0,011	-0,0035	0,0050	0,0250	0,071
5		-0,012	-0,0031	0,0098	0,0370	0,090
6		-0,015	-0,0030	0,0198	0,0570	0,147
7		-0,017	0,0	0,0280	0,0820	0,184
8		-0,018	0,0167	0,0690	0,1400	0,284

NOTE: Positive value denotes tensile (opening) displacement.

The remaining data is tabulated in appendix C.

The analysis of this data will be dealt with in the analysis section presented later.

The outputs from the five displacement LVDTs were autographically recorded by a multi-channel strip chart recorder. The extraction of data from these plots was carried out using simple measuring equipment.

The use of a computer to process the information from these LVDTs would have greatly reduced the amount of work involved. This was, however, not possible since there was no data logging system available at the time.

The following explanation refers to FIG. 4.2.

1. The deflection peak was identified for each cycle. This was then clearly marked on each LVDT trace.

2. A pair of dividers and a scale rule were used to measure the trace movements and these were converted into actual deflections with the use of a simple computer programme.

3. During the course of a test, some of the traces had their sensitivities decreased as the deflections increased. This necessitated re-zeroing of the recorder.

4.4 ULTRASONIC TEST RECORDS

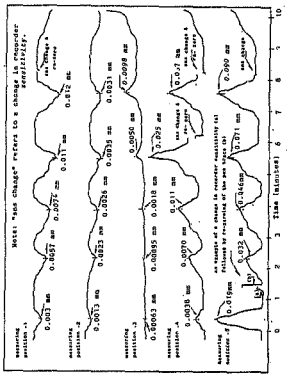
Ultrasonic pulse transit data was collected for twenty of the twenty eight tests conducted. This data was used to assess the extent of cracking of the fracture section during each cycle of each test.

TABLE 4.3 gives a typical example of the data obtained from these records.

TABLE 4.3 TYPICAL EXAMPLE OF ULTRASONIC RECORD

Specimen N° 11B $d = 300$ m $c_o/d = 0,40$

CYCLE	TR peak (µs)	TR base (µs)
1	106,8	106,8
2	107,0	106,8
3	107,2	106,9
4	108,2	107,3
5	109,1	107,7
6	110,6	108,4
7	113,4	109,6
8	138,2	113,7



Surface displacements (new values on chart)

FIG 4.2 Typical traces obtained from the LVDTs on the crack face of a fracturing beam. BEAM 11B

Note:-

TR peak (μS) ultrasonic transit time at the peak of a cycle.

TR base (μS) ultrasonic transit time at the start (base) of a cycle.

The records of the remaining nineteen tests are tabulated in APPENDIX C.

The analysis of this data will be dealt with in the analysis section presented later.

PART III

ANALYSIS AND INTERPRETATION OF DATA FROM FRACTURE TESTS

5. IDENTIFICATION OF THE POINT OF INITIATION OF MAIN CRACK GROWTH IN NOTCHED CONCRETE AND MORTAR BEAMS

5.1 INTRODUCTION

In the fracture tests conducted for this dissertation, the position of the neutral axis was found using the displacement profiles. Since these tests had the aim of identifying the point of change-over from micro-cracking to main crack growth, visible crack detection played little or no part, and it is for this reason that the J-integral concept is used in SECTION 5.3.

The continuously recording LVDTs were placed at five positions over the height of the fracturing section on a 100 mm gauge length. The data involved five surface displacements including that of the notch tip. Displacement profiles across the fracture section could then be plotted. This allowed surface crack widths to be measured.

The fracture section displacement results are presented in this section. Particular attention is given to isolating the point of change-over from micro-cracking to main crack growth.

5.2 SURFACE DISPLACEMENT PROFILES

Unlike Alexander's[4] work, this thesis concentrated

on investigating the change-over from micro-cracking to main crack growth in the fracture specimens. Therefore it was very important to collect accurate data from the early test cycles, and not only the later ones which Alexander did.

Displacement profiles were analysed to obtain an idea of tension and compression zone sizes, and the extent of the micro-cracked zone, at the start of main crack growth. This is dealt with later in section 6.2.

Displacement profiles for various concrete and mortar beams are shown in FIGs 5.1 TO 5.5.

I. CONCRETE

FIG 5.1 (BEAM 12A, d = 300, c_o/d = 0,4)

1. The profiles for the lower part of this beam become increasingly linear as the test progresses.

2. There is a steady rise in the neutral axis (N.A.) position from cycle to cycle. This is apparent from the start of the test.

3. The "initiation of main crack growth" (determined as in sections 5.4 and 5.10) was identified as occuring in cycle four.

FIG 5.2 (BEAM 18A, d = 200, c_o/d = 0,4)

1. The initiation of main crack growth occured during cycle four.

2. Beyond this point, the displacement profiles become increasingly linear indicating the development of a stress free crack. This is also accompanied by a rapid and extensive rise in neutral axis position.

II. MORTAR

FIG 5.3 (BEAM 10B, d = 300, c_o/d = 0,4)

1. The initiation of main crack growth occured during cycle five.

2. In spite of a large amount of deformation, this beam does not exhibit much neutral axis movement when compared with some of the other tests.

3. Gauge position N° 2 is very nearly a pivot point since the change in deformation is far smaller than for the other gauge positions. (Had the beam been subjected to further cyclic loading, there probably would have been a significant neutral axis movement with gauge position N° 2 showing an appreciable tensile deformation).

FIG 5.4 (BEAM 12B, d = 300, c_o/d = 0,4)

1. The initiation of main crack growth occured during cycle five.

2. A feature to note here is the degree of cracking which has taken place during this test. The neutral axis has moved to within a few millimetres of the top of the beam on the last cycle. The point of change-over (i.e. cycle five) from micro-cracking to main crack growth occurs during the cycle immediately preceding rapid movement of the neutral axis.

NOTE: Only about 20% of the tests developed cracking as advanced as that shown in FIG. 5.4. In many cases, sudden failure occurred only two cycles beyond main crack growth initiation.

STRAIN PROFILE IRREGULARITIES - AN UNEXPECTED PROBLEM

When the instrumentation system used in this research was designed, a considerable amount of thought went into the placing of the LVDTs for the recording of the surface displacement profiles dealt with in this section. A system based on Alexander's[4] work, but completely revised, was eventually decided upon. Alexander used mechanical strain gauges with a guage length of 100mm, and therefore could not continuously record

FIG 5.4 (BEAM 12B, d = 300, c_o/d = 0,4)

1. The initiation of main crack growth occured during cycle five.

2. A feature to note here is the degree of cracking which has taken place during this test. The neutral axis has moved to within a few millimetres of the top of the beam on the last cycle. The point of change-over (i.e. cycle five) from micro-cracking to main crack growth occurs during the cycle immediately preceding rapid movement of the neutral axis.

NOTE: Only about 20% of the tests developed cracking as advanced as that shown in FIG. 5.4. In many cases, sudden failure occurred only two cycles beyond main crack growth initiation.

STRAIN PROFILE IRREGULARITIES - AN UNEXPECTED PROBLEM

When the instrumentation system used in this research was designed, a considerable amount of thought went into the placing of the LVDTs for the recording of the surface displacement profiles dealt with in this section. A system based on Alexander's[4] work, but completely revised, was eventually decided upon. Alexander used mechanical strain gauges with a guage length of 100mm, and therefore could not continuously record

displacements. He found no profile irregularities for beams with a span to depth ratio of 4:1. However, with the same gauge length and at a span to depth ratio of 3:1, profile irregularities were encountered in about 35% of the tests carried out for this dissertation. This occurred in both concrete and mortar specimens.

A typical "irregular" profile is shown in FIG 5.5. (BEAM 5A, d = 200, $c_o/d = 0,4$). Points to note are as follows:

The displacements at the micro-cracked level are smaller than expected thereby giving the displacement profile a reverse curvature.

There is no correlation between this phenomenon and any geometrical or physical properties of the specimens tested. It appears to occur at random. The author offers the following explanation:

The smaller span to depth ratio (3:1 compared with 4:1 used in Alexander's work) used in this work may have induced greater lateral micro-cracking than was expected. It is possible that in about 35% of the tests conducted, this lateral micro-cracking extended far enough to interfere with the gauge clamps, thereby causing a form of strain release which allowed the clamps to rotate or move slightly closer together. This process then appeared as a reverse curvature in the micro-cracked zone.

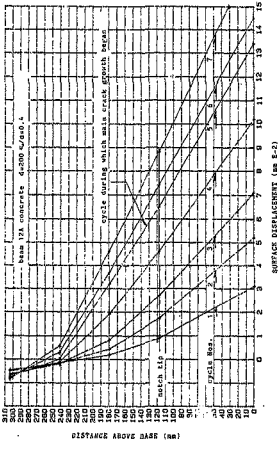


FIG 5.1 Surface displacement profile for beam 12A

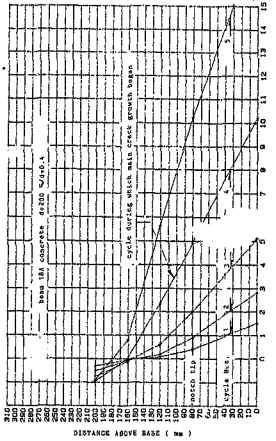


FIG 5.2 Surface displacement profile for beam 18A

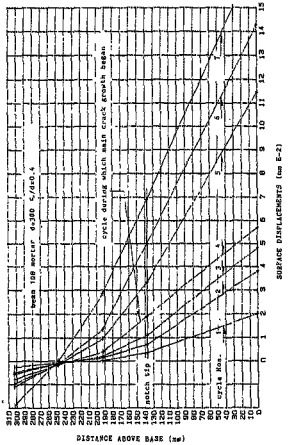


FIG 5.3 Surface displacement profile for beam 10B

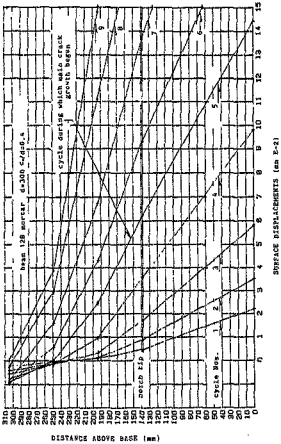


FIG 5.4 Surface displacement profile for beam 12B

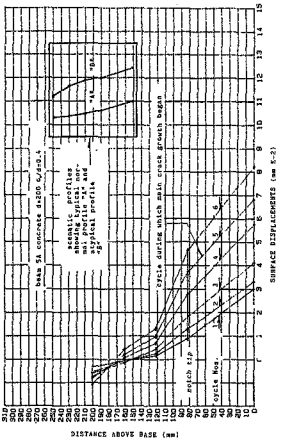


FIG 5.5 Atypical surface displacement profile for *beam 5A*

Unfortunately, there was no way of predicting this disturbance until the analysis was complete thereby forcing the author to reject affected profiles.

FIG. 5.5 shows a typical irregular profile (profile B) together with a "normal" profile (profile A). The reverse curvature of profile A can be clearly seen.

5.3 THE J-INTEGRAL

As was explained in section 2.2.5 the J-integral is a measure of fracture toughness, which in this case is related to the point of incipient crack growth (or point of changeover from micro-cracking to main crack growth). For the perfectly linear elastic case J_c equals G_c. However, cemented materials are not linear elastic and exhibit pseudo-plastic behaviour. For this reason, J_c provides a more accurate measure of the critical energy based fracture toughness parameter in the case of cemented materials.

The form of the J-integral used in this work is written as

$$J = \frac{2A}{W(d-c_o)} \qquad (5.1)$$

where: A = total area under load deflection curve for a particular cycle.

W = beam width

d = beam depth

c_o = initial notch depth

J was calculated for each load cycle of a fracture test.

It should be mentioned that the assumption of initial notch depth c_o remaining constant until the formation of a stress-free crack may not be strictly valid. It is possible that the presence of micro-cracking could reduce the effective ligament depth by de-stressing of the micro-cracked zone. However the extent of this reduction was impossible to determine in this work and therefore it was assumed, for the purposes of calculation, that the notch depth remained c_o until the initiation of main crack growth.

Any error incurred by using this assumption would, logically, have been similar for each test. Since the object of calculating J was to detect a sudden drop from one cycle to the next and not to produce a strictly correct numeric value, this error was assumed to be unimportant.

5.4 IDENTIFICATION OF THE CHANGEOVER FROM MICRO-CRACKING TO MAIN CRACK GROWTH USING THE J-INTEGRAL

The principle of the J-integral, together with information from the surface mounted LVDT at the notch tip, was used to identify the point of changeover from micro-cracking to main crack growth.

The J-integral may be interpreted, in practical terms, as the energy required for crack extension. Energy absorption must obviously increase before main crack growth can occur since the micro-cracked zone is growing. After the initiation of main crack growth, the micro-cracked zone reduces in size in a bend specimen, therefore absorbing less energy, while main crack growth reduces the ligament depth thereby reducing the energy demand. Thus it can be expected that J will reach a peak at the point of initiation of main crack growth and decrease as the main crack begins to propagate.

As described in section 4.1 the area under a given load-deflection curve (ie energy) was calculated up to the point of maximum load. Mindess[28] states:- "To be strictly valid, where deformation is not reversible, the J-integral refers to crack initiation rather than crack propagation. Thus we can only look at the critical value of J at the point of crack initiation." It is logical to assume that main crack growth would occur near or at peak load during the critical cycle of initiation of main crack growth. Therefore J has been calculated up to the peak load for each cycle.

In the series of diagrams FIG's 5.6 to 5.9 the surface displacement at the notch tip is plotted against the J-integral for the same cycle. The post peak portion of each curve is shown as a dotted line since c_o is

no longer constant at this stage, and the curve is therefore not representative of true J values.

The curves all show similar tendencies. An initial rapid increase in the J-integral value accompanied by a small increase in lateral displacement is followed by a peak value for J, which then starts to decline.

The following points should be noted:

1. The apex of the curve, representing the maximum value for J, is circled in the diagrams. This is assumed to be the point of initiation of main crack growth, according to the argument given above.

2. The J values plotted are not cumulative, but are the values calculated for each cycle. The curves were plotted in this way since the objective was to identify the difference in energy absorption from one cycle to the next. By doing this, a reduction in the J-value (identifying main crack growth) could be detected.

Tables 5.1 and 5.2 show the results for all the beams tested. The J-values shown in these tables (so called J_{cycle}) are the values for the critical cycle (where "critical" refers to the cycle during which main crack growth began).

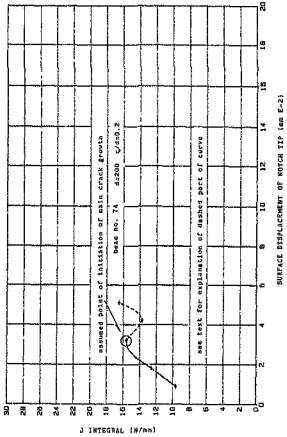


FIG 5.6 J-integral plotted against surface displacement of notch tip for beam 7A

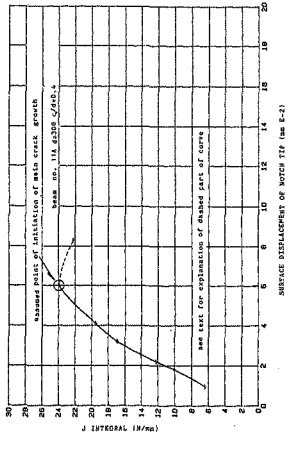


FIG 5.7 J-integral plotted against surface displacement of notch tip for beam 11A

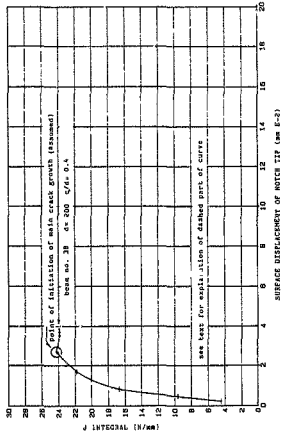


FIG 5.8 J-integral plotted against surface displacement of notch tip for beam 3B

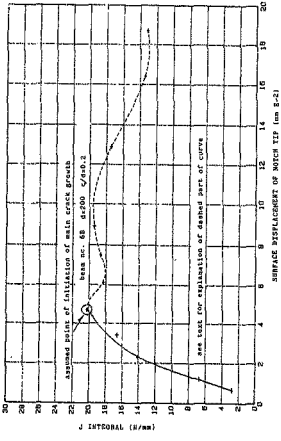


FIG 5.9 J-integral plotted against surface displacement of notch tip for beam 6B

It is important to note that the absolute numerical values of J for the critical cycle in each case are not that important. The objective of this section of the work was to identify the point at which J (calculated for each cycle) began to reduce, thereby indicating the cycle during which main crack growth began i.e. the critical cycle. (This was carried out in order to facilitate analysis in subsequent chapters of the critical cycle). It should be realised that the numerical value of J for the critical cycle is entirely dependent on the number of cycles carried out before the critical cycle. What is important, however, is the cumulative value of J based on an envelope curve joining the points of peak load for each cycle up to the critical cycle. This would represent the total energy absorption of the beam up to the point of main crack growth and could thus be thought of as a fracture parameter at the start of main crack growth. This cumulative J-value is discussed later in section 5.6.

TABLE 5.1 CRITICAL CYCLE FOR THE CONCRETE BEAMS

BEAM	$J_{cy,..}$ (N/mm)	CYCLE NUMBER
2A	2+,2	4
3A	14,6	4
4A	14,6	7
5A	9,7	5
6A	10,1	5
7A	15,6	4
8A	12,4	4
9A	18,9	4
10A	18,0	3
11A	23,9	6
12A	12,7	5
15A	28,3	5
16A	21,6	4
17A	15,5	5
18A	17,6	4

TABLE 5.2 CRITICAL CYCLE FOR THE MORTAR BEAMS

BEAM	J_{cycle} (N/mm)	CYCLE NUMBER
1B	11,4	6
2B	14,1	5
3B	24,2	5
4B	19,2	4
5B	24,5	4
6B	20,2	5
7B	21,9	5
8B	24,5	5
9B	17,6	6
10B	21,4	4
11B	19,4	6
12B	24,1	5

It should be mentioned that there is little point in computing the average values of J_{cycle} for concrete and mortar since, as mentioned above, these values are entirely dependent on the number of cycles carried out before the cycle during which main crack growth began.

5.5 COMPARISON OF THE MAXIMUM LOAD CYCLE AND THE CYCLE DURING WHICH MAIN CRACK GROWTH BEGAN

Tables 5.3 and 5.4 show a record of the cycle during which main crack growth began (based on the J value analysis) compared with the cycle during which the maximum load for a test occurred.

For the concrete beams, 80% of the tests showed maximum load occurring before the initiation of main crack growth, and the remaining 20% showed maximum load and the initiation of main crack growth occurring during the same cycle.

For the mortar beams, 83% of the tests showed maximum load occurring before the initiation of main crack growth, and the remaining 17% showed maximum load and the initiation of main crack growth occurring during the same cycle.

Thus, it can be said that for these tests maximum load occurred generally before the initiation of main crack growth. This means that there can be a reduction in the load carrying capacity of the beams due to the presence of micro-cracking only. TABLES 5.5 and 5.6 show this reduction expressed as a percentage of maximum load. These percentages vary widely making the computation of an average number questionable. The maximum percentages were 27,0% for concrete and 16,6% for mortar. As can be seen in tables 5.5 and 5.6 most values were far lower than these maximum values.

The physical interpretation of this phenomenon is that micro-cracking can cause sufficient damage to the material (be it concrete or mortar) for a reduction in load carrying capacity to occur. Although this reduction seems, usually, to be small, it cannot be disre-

garded. A cyclically loaded concrete or mortar structure (where the load approached the maximum load capacity of the material) could, according to the above, experience a reduction in strength without the presence of any visually detectable cracks. This is in agreement with work done by Tait[59].

TABLE 5.3 COMPARISON OF CRITICAL CYCLE (START OF MAIN CRACK GROWTH) AND MAXIMUM LOAD IN CONCRETE BEAMS

BEAM	CRITICAL CYCLE	MAXIMUM LOAD CYCLE
2A	4	4
3A	4	2
4A	7	4 AND 5
5A	5	4
6A	5	3
7A	4	3
8A	4	3
9A	4	4
10A	3	3
11A	6	4
12A	5	3 AND 4
15A	5	4
16A	4	3
17A	5	3
18A	4	3

TABLE 5.4 COMPARISON OF CRITICAL CYCLE (START OF MAIN CRACK GROWTH) AND MAXIMUM LOAD IN MORTAR BEAMS

BEAM	CRITICAL CYCLE	MAXIMUM LOAD CYCLE
1B	6	3
2B	5	4
3B	5	3 AND 4
4B	4	4
5B	4	1 AND 2
6B	5	4
7B	5	3 AND 4
8B	5	4
9B	6	5
10B	4	4
11B	6	4
12B	5	4

TABLE 5.5 REDUCTION IN THE LOAD CARRYING CAPACITY OF THE CONCRETE BEAMS DUE TO MICRO-CRACKING

BEAM	REDUCTION (as % of maximum load)
2A	0,0
3A	0,0
4A	26,2
5A	1,1
6A	7,7
7A	2,1
8A	1,0
9A	0,0
10A	0,0
11A	10,1
12A	2,3
15A	0,0
16A	1,5
17A	27,0
18A	4,0

TABLE 5.6 REDUCTION IN THE LOAD CARRYING CAPACITY OF THE MORTAR BEAMS DUE TO MICRO-CRACKING

BEAM	REDUCTION (as % of maximum load)
1B	15,7
2B	2,9
3B	5,9
4B	0,0
5B	6,6
6B	1,4
7B	1,0
8B	1,0
9B	2,9
10B	0,0
11B	16,6
12B	4,2

5.6 COMPARISON OF THE J-VALUES AT THE START OF MAIN CRACK GROWTH

In section 5.4 the J-value for each cycle was plotted against the surface displacement across the notch tip in order to identify the point of initiation of main crack growth. In this section, the cumulative J-value (J_c) up to the start of main crack growth (as identified in section 5.4) is examined for each beam. The effects of beam geometry and concrete strength are also examined. (This cumulative J-value can be thought of as a fracture parameter at the point of initiation of main crack growth.)

Tables 5.7 *and* 5.8 show the cumulative J-value at the start of main crack growth (J_c) together with the compressive cube strength of each beam or batch of beams.

J_c was calculated using an envelope curve joining the peaks of the individual cycle curves. In this way the recoverable elastic deformation for each cycle was eliminated. J_c therefore represents the irrecoverable energy absorbed by the beam up to the development of main crack growth, plus the recoverable elastic deformation for the cycle during which there was initiation of main crack growth.

TABLE 5.7 J_c VALUES FOR CONCRETE

BEAM	d(mm)	c_o/d	J_c (N/mm)	COMPRESSIVE STRENGTH (MPa)
2A	200	0,2	24,5	43,2
3A	200	0,2	16,5	43,2
4A	200	0,4	34,0	43,2
5A	200	0,4	26,5	36,2
6A	200	0,4	16,1	36,2
7A	200	0,2	20,1	36,2
8A	200	0,4	19,8	36,2
9A	300	0,2	24,2	37,3
10A	300	0,2	19,4	38,4
11A	300	0,4	39,9	38,4
12A	300	0,4	22,0	37,1
15A	200	0,2	34,0	42,0
16A	200	0,4	28,0	42,0
17A	200	0,4	36,0	39,3
18A	200	0,4	24,6	39,3

AVERAGE J_c FOR CONCRETE 25,7 N/mm

COEFFICIENT OF VARIATION 28,5%

Statistical test shows no outliers due to the limited number of results.

TABLE 5.8 J_c VALUES FOR MORTAR

BEAM	d(mm)	c_o/d	J_c (N/mm)	COMPRESSIVE STRENGTH (MPa)
1B	200	0,4	22,0	41,1
2B	200	0,4	19,6	41,1
3B	200	0,4	22,9	41,1
4B	200	0,4	25,6	40,6
5B	200	0,2	33,5	40,6
6B	200	0,2	26,6	36,7
7B	200	0,2	30,4	36,7
8B	200	0,2	31,5	36,7
9B	300	0,4	38,0	29,6
10B	300	0,4	28,6	35,6
11B	300	0,4	42,5	33,9
12B	300	0,4	36,9	32,3

AVERAGE J_c FOR MORTAR 29,8 N/mm

COEFFICIENT OF VARIATION 23,4%

Statistical test shows no outliers due to the limited number of results.

The scatter present in these results dictates that only a general idea of J_c as a fracture parameter can be gained from this work.

It could be argued that the value of J for the critical cycle (so called J_{cycle}) should be compared with the present cumulative J at the start of main crack

growth (so called J_c) but this is of very limited value because, as discussed in section 5.4, the J_{cycle} value depends fundamentally on the number of cycles taken to reach the point at which J decreases. This comparison, although considered, was thus not undertaken.

The overall averages obtained from TABLES 5.7 and 5.8 can be regarded as guidelines. With this in mind, it is apparent that the average J_c for mortar is essentially the same as the average J_c for concrete. This indicates that mortar has the same fracture toughness as concrete.

It should be noted that many investigators have found scatter to be a major problem in the fracture testing of concrete. Some (eg. Petersson[23]) suggest that few certain conclusions can be drawn in this field because of the problem of scatter.

5.7 THE VALUE OF J AT THE START OF MICRO-CRACKING (J_i)

This section is based on the ASTM-E813-81 method for the calculation of the J-integral at the initiation of crack growth in metals[70].

Referring to FIGURE 5.10, this method involves the linear regression of several points on a J versus

crack mouth displacement (Δa_p) curve to intersect a so called blunting line. The blunting line is an estimate of notch tip stretch effects and is calculated from material flow properties. The intersection point between the linear regression line fit of the data and the blunting line defines J_i, which is the value of the J-integral at the start of crack formation.

For concrete and mortar, a similar argument may be applied. The start of cracking will, however, take the form of micro-cracking as opposed to the formation of a single crack. J_i for concrete and mortar can therefore be thought of as the value of the J-integral at the start of micro-cracking.

The term blunting does not strictly apply to concrete and mortar since these materials are not ductile. Blunting can, however, be thought of as as displacement without any significant cracking and will thus be very small in the case of concrete and mortar. In effect the initial notch faces move apart; this is the concrete analogy of "blunting" in metals. For the ASTM - E 813 method, the blunting line is based on the expression:

$$J = 2\sigma_y \Delta a_p \qquad (5.2)$$

where

σ_y = yield stress of material

For the concrete and mortar specimens tested for this

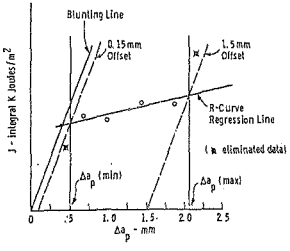


FIG 5.10 Linear regression fit of J-integral data (ASTM-813-81 method[70])

dissertation, the approximate yield stress is approxi-mately 3MPa (approximately 10 percent of the ultimate compressive stress).

Expression (5.2) therefore becomes approximately:

$$J = 6 \times \Delta c_o \ J/m^2 \qquad (5.3)$$

This line is shown on FIGURES 5.11 and 5.13 and as can be seen, it is very steep and lies very close to the y-axis (line of zero notch tip displacement). Bearing in mind the inherent scatter already present in the results obtained for this dissertation, the blunting effect was assumed to be zero and J_i was taken to be the intercept between the regression line and the y-axis. The additional error introduced by this assumption is negligible when compared to that of the already observed inherent scatter.

In this section, curves of the J-integral versus notch tip displacement and the J-integral versus the cumulative change in peak ultrasonic pulse transit time were analysed according to the ASTM-813[70] method for all the beams tested.

FIGURES 5.11 to 5.14 show typical curves obtained together with the regression line described above.

Tables 5.9 and 5.10 show the results of the J_i intercept obtained for all the beams tested. The results

from the notch tip displacement curves and the ultrasonic pulse transit time curves are shown in the same table. In certain cases, it was not possible to obtain a representative regression. These cases are shown as "no intercept" in the tables. Bearing in mind the scatter prevalent in the results throughout this dissertation, good agreement (with the exception of certain outliers) between the J_i results from the notch tip displacement and the cumulative difference in ultrasonic pulse transit time curves is apparent. The average values for J_i are essentially the same for both sets of curves and for both concrete and mortar.

As mentioned earlier, J_i can be thought of as the J-integral at the start of micro-cracking at the notch tip, and can therefore be regarded as a measure of the J_i fracture toughness of the material. From these results it can therefore be said that the fracture toughness at the start of micro-cracking is essentially the same for concrete and for mortar. It should be noted that J_c (fracture toughness at the start of main crack growth (sections 5.6 and 5.9 respectively) were also found to be essentially the same for concrete and mortar. J_i is about 40% of J_c for both concrete and mortar, which is consistent with the J fracture toughness behaviour of metals and alloys[71].

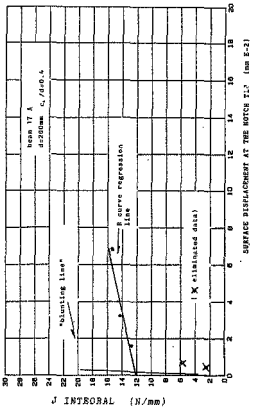


FIG 5.11 Evaluation of J_i using the ASTM-813 method[70] on a graph of the J-integral *versus* the surface displacement at the notch tip. BEAM 17A

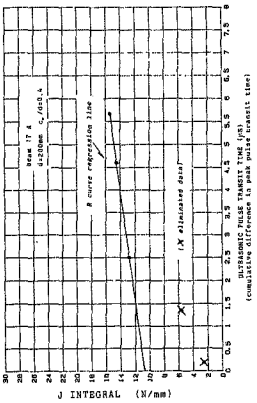


FIG 5.12 Evaluation of J_i using the ASTM-813 method[70] on a graph of the J-integral versus the cumulative difference in peak ultrasonic pulse transit time. BEAM 17A

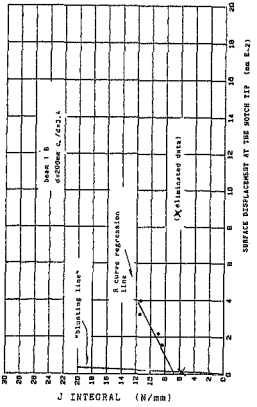


FIG 5.13 Evaluation of J_i using the ASTM-813 method[70] on a graph of the J-integral versus the surface displacement at the notch tip. BEAM 1B

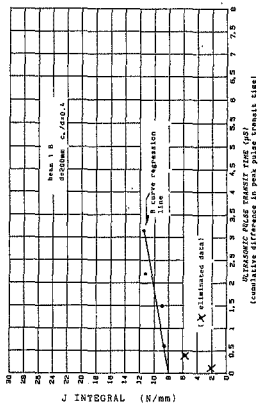


FIG 5.14 Evaluation of J_i using the ASTM-813 method[70] on a graph of the J-integral versus the cumulative difference in peak ultrasonic pulse transit time. BEAM 1B

TABLE 5.9 J_i FOR THE CONCRETE BEAMS

BEAM	d(mm)	C_o/d	J_i from J vs notch tipe displacement (N/m)	J_i from J vs cumulative change in peak pulse transit time. (N/m)
2A	200	0,2	No intercept	-
3A	200	0,2	No intercept	-
4A	200	0,4	13,0	-
5A	200	0,4	6,0	-
6A	200	0,4	6,0	-
7A	200	0,2	8,0	-
8A	200	0,4	No intercept	-
9A	300	0,2	No intercept	5,8
10A	300	0,2	No intercept	12,0
11A	300	0,4	10,0	11,0
12A	300	0,4	9,5	5,5
15A	200	0,2	11,8	No intercept
16A	200	0,4	15,8	14,0
17A	200	0,4	12,0	12,0
18A	200	0,4	11,5	12,0
			AVERAGE J_i : 10,4 COEFFICIENT OF VARIATION : 30%	AVERAGE J_i : 10,3 COEFFICIENT OF VARIATION : 32%

TABLE 5.10 J_i FOR THE MORTAR BEAMS

BEAM	d(mm)	C_o/d	J_i *from J vs* notch tipe displacement (N/m)	J_i *from J vs* cumulative change in peak pulse transit time. (N/m)
1B	200	0,4	7,0	8,0
2B	200	0,4	5,3	7,3
3B	200	0,4	10,3	9,75
4B	200	0,4	10,0	9,2
5B	200	0,2	15,0	17,2
6B	200	0,2	8,0	8,0
7B	200	0,2	11,5	No intercept
8B	200	0,2	10,0	8,5
9B	300	0,4	8,8	12,0
10B	300	0,4	11,3	12,0
11B	300	0,4	15,3	11,0
12B	300	0,4	18,2	11,0
			AVERAGE J_i : 10,9 COEFFICIENT OF VARIATION : 34%	AVERAGE J_i : 10,4 COEFFICIENT OF VARIATION : 27%

5.8 DEPENDENCE OF J_i AND J_c ON SPECIMEN GEOMETRY

The inherent scatter in the results for J_i and J_c and the lack of sufficient data for beams of different geometries makes it difficult to correlate these parameters with specimen geometries. Nevertheless, the comparison was deemed worthwile and is discussed below.

Tables 5.11 to 5.14 show the results for J_c and J_i grouped together for beams of different geometry.

It can be seen from these tables that:

1. The average J_i values for the concrete beams show a tendency to decrease with increasing beam size, and to increase with an increased c_o/d radio. The lack of sufficient data renders this uncertain, however.

2. The average J_i values for the mortar beams show a tendency to increase with increasing beam size, and to decrease with an increased c_o/d ratio. In other words, the degree of micro-cracking shows a tendency to increase in the case of larger beams, and to increase for a smaller notch/depth ratio. This is in agreement with work done by

Alexander[4] who found the micro-cracked zone size to be larger for larger beams.

3. The results for the mortar and concrete beams are in contrast here. However, the lack of sufficient data in the case of the concrete beams leads to the belief that the results for the mortar beams are more representative of actual trends.

4. The average J_c values for the concrete beams show a tendency to increase for an increased beam size, and to decrease for an decrease in c_o/d ratio (excepting for geometries C and D which have essentially the same averages. The lack of sufficient data makes this uncertain, however.

5. The average J_c values for the mortar beams show a tendency to increase for increasing beam depth, and to decrease for a decreasing c_o/d ratio. This is in agreement with the values of J_c obtained for the concrete beams.

6. It is significant that, with the exception of the J_i values obtained for the concrete beams, both J_i and J_c show a tendency to increase with increasing beam depth which is consistent with work done by Alexander[4] (mentioned in point 2 above).

It should be noted that there is little agreement

between the results obtained by other investigators in this field. Halvorsen[18] finds J to be dependent on specimen geometry, while Carrato[63] concludes that J is independent of specimen size, notch type, notch size and notch thickness.

In the following Tables 5.11 to 5.14 the geometry groupings are as follows:

Geometry A : d = 200 ; $c_o/d = 0,4$

Geometry B : d = 300 ; $c_o/d = 0,4$

Geometry C : d = 200 ; $c_o/d = 0,2$

Geometry D : d = 300 ; $c_o/d = 0,2$

TABLE 5.11 AVERAGE J_i VALUES FOR CONCRETE BEAMS OF DIFFERENT GEOMETRY

GEOMETRY	A	B	C	D
	13,0	10,0	8,0	5,8
	6,0	9,5	11,8	12,0
	6,0	11,0		
	14,0	5,5		
	12,0			
	15,8			
	12,0			
	11,5			
	12,0			
AVERAGES	11,4 ± 30%	9,0 ± 27%	9,9 ± 27%	8,9 ± 49%

TABLE 5.12 AVERAGE J_i VALUES FOR MORTAR BEAMS OF DIFFERENT GEOMETRY

GEOMETRY	A	B	C	D
	7,0	6,6	15,0	
	8,0	11,3	8,0	
	5,3	15,3	11,5	
	9,8	18,2	10,0	NO DATA
	7,3	12,0	17,0	
	10,3	12,0	8,0	
	10,0	11,0	8,5	
	9,2	11,0		
AVERAGES	8,4 ± 21%	12,5 ± 24%	11,1 ± 32%	

TABLE 5.13 AVERAGE J_c VALUES FOR CONCRETE BEAMS OF DIFFERENT GEOMETRY

GEOMETRY	A	B	C	D
	34,0	39,0	24,5	24,2
	26,5	22,0	16,5	19,4
	16.1		20,1	
	19,8		34,0	
	28,0			
	36,0			
	24,6			
AVERAGES	26,4 ± 26%	31,0 ± 41%	23,8 ± 32%	21,8 ± 16%

TABLE 5.14 AVERAGE J_c VALUES FOR MORTAR BEAMS OF DIFFERENT GEOMETRY

GEOMETRY	A	B	C	D
	22,0	38,0	33,5	
	19,6	28,6	26,6	
	22,9	42,5	30,4	NO DATA
	25,6	36,9	31,5	
AVERAGES	22,5 ± 9%	36,5 ± 16%	30,5 ± 1 5	

5.9 NOTCH TIP DISPLACEMENT (COD) AT INITIATION OF MAIN CRACK GROWTH

Tables 5.15 and 5.16 list the notch tip displacements at the point of initiation of main crack growth. Also shown, are the average displacements together with the coefficients of variation for the concrete and the mortar results.

The notch tip displacement can, in this instance, be thought of as the crack tip opening displacement (COD), since the crack is just starting to grow from the notch tip at this stage of the test. It can also be thought of as a fracture parameter at the start of main crack growth.

TABLE 5.14 AVERAGE J_c VALUES FOR MORTAR BEAMS OF DIFFERENT GEOMETRY

GEOMETRY	A	B	C	D
	22,0	38,0	33,5	
	19,6	28,6	26,6	
	22,9	42,5	30,4	NO DATA
	25,6	36,9	31,5	
AVERAGES	22,5 ± 9%	36,5 ± 16%	30,5 ± 10,5	

5.9 NOTCH TIP DISPLACEMENT (COD) AT INITIATION OF MAIN CRACK GROWTH

Tables 5.15 and 5.16 list the notch tip displacements at the point of initiation of main crack growth. Also shown, are the average displacements together with the coefficients of variation for the concrete and the mortar results.

The notch tip displacement can, in this instance, be thought of as the crack tip opening displacement (COD), since the crack is just starting to grow from the notch tip at this stage of the test. It can also be thought of as a fracture parameter at the start of main crack growth.

Significant points are:

1. There is considerably less scatter for the mortar results than there is for the concrete results. This is to be expected since mortar is more homogeneous than concrete.

2. The average COD for concrete is essentially the same as the average COD for mortar.

The scatter in the results for concrete is very large. This is probably due to the heterogeneous nature of the material. It should be borne in mind that these COD values represent suface measurements on one side of the beam only. Therefore, the presence of a large piece of aggregate immediately beneath the surface could affect the COD significantly. In the case of mortar, the aggregate particles are smaller (thus implying a more homogeneous material) and consequently the measurements would not presumably be so greatly affected.

The average values in TABLES 5.15 and 5.16 compare very well with the COD values found by Alexander[4] in his work - he found the COD during crack extension to vary from 0,037 mm to 0,064 mm, the larger beams (500mm) obtaining the higher values.

TABLE 5.15 COD AT START OF MAIN CRACK GROWTH FOR THE CONCRETE BEAMS

BEAM	NOTCH TIP DISPLACEMENT (COD) (mm)	d(mm)	c_o/d
2A	0,025	200	0,2
3A	0,034	200	0,2
4A	0,081 *	200	0,4
5A	0,028	200	0,4
6A	0,029	200	0,4
7A	0,032	200	0,2
8A	0,050	200	0,4
9A	0,035	300	0,2
10A	0,021	300	0,2
11A	0,041	300	0,4
12A	0,046	300	0,4
15A	0,040	200	0,2
16A	0,046	200	0,4
17A	0,068	200	0,4
18A	0,049	200	0,4

AVERAGE NOTCH TIP DISPLACEMENT	: 0,039 mm
COEFFICIENT OF VARIATION	: 32 %

NOTE: The value marked * in TABLE 5.11 was identified as a statistical outlier using Dixon's outlier test[64].

TABLE 5.16 COD AT START OF MAIN CRACK GROWTH FOR THE MORTAR BEAMS

BEAM	NOTCH TIP DISPLACEMENT (COD) (mm)	d (mm)	σ_o/d
1B	0,040	200	0,4
2B	0,051	200	0,4
3B	0,037	200	0,4
4B	0,033	200	0,4
5B	0,045	200	0,2
6B	0,047	200	0,2
7B	0,035	200	0,2
8B	0,034	200	0,2
9B	0,026	300	0,4
10B	0,033	300	0,4
11B	0,057	300	0,4
12B	0,062	300	0,4

AVERAGE NOTCH TIP DISPLACEMENT	: 0,046 mm
COEFFICIENT OF VARIATION	: 23,6%

5.10 THE USE OF ULTRASONIC TECHNIQUES

5.10.1 INTRODUCTION

An ultrasonic technique was used to monitor the crack growth in twenty out of the total of twenty-eight useful tests. This technique was aimed mainly at detecting the onset of main crack growth once the micro-cracked zone had reached its maximum size for a particular specimen.

The use of ultrasonics for testing damage in concrete has been well proven. Blight[65] used the technique to study cracking in concrete caused by alkali-aggregate reaction and found it excellent for detecting damage such as micro-cracking, and Tait[59] used ultrasonics to monitor damage in cyclically loaded concrete specimens.

Details of the equipment used and of the experimental set-up have been presented in sections 3.5 and 3.6. The information collected comprised transit times measured at the start and peak of each cycle. It was this 'dual' measuring that helped with the extraction of conclusive results from the data obtained.

This section deals with the identification of the point of change-over from micro-cracking to main crack growth, as obtained from the ultrasonic results.

5.10.2 IDENTIFICATION OF THE ONSET OF MAIN CRACK GROWTH USING ULTRASONICS

Two different approaches were used to attempt to detect the onset of main crack growth.

The first one, which uses principles very similar to those in section 5.4 involves the comparison of changes in peak ultrasonic transit time from one cycle to the next, with the energy parameter 'J' described previously in section 5.4. It can be said that this method is complementary to that in section 5.4 because of the similarity of the principles employed. Therefore, as a second approach the concept of permanent damage (explained in section 5.10.2.2) was also used. In this case, the cumulative difference in peak transit time from one cycle to the next was plotted against the cumulative difference in trough transit time from one cycle to the next.

5.10.2.1 PULSE TRANSIT TIME AND FRACTURE ENERGY

As was described in section 5.4, it was reasoned that the cyclic absorption of energy in a notched fracture beam would increase until a point was reached where a stress-free crack was generated, at which stage the beam would show a reduction in energy absorption, and would continue deflecting while absorbing less energy

from cycle to cycle. The parameter of energy measurement chosen was a form of the J-integral expressed as in equation 5.1.

In the series of diagrams FIG's 5.15 to 5.18 cumulative changes in peak transit time are plotted against the J-integral for the same cycle. The J-integral was computed on a cyclic basis in these cases.

The cumulative change in peak transit time was chosen since it was postulated that the development of a stress-free crack would show as a marked increase in ultrasonic pulse transit time. The transit time at the peak of each cycle was subtracted from that of the previous cycle and these changes in peak time were then plotted cumulatively against the J-integral as described above.

It must be stressed that the absolute numerical values of the transit times are not important since the distance between probes and the dimensions of the specimen varied from test to test. It is only the cumulative change in transit time that is of any interest here.

It is important to note that, after the value of the J-integral has started to reduce and main crack growth has begun, the expression 5.1 is no longer valid since c becomes an unknown. This section of each curve is therefore shown as a dotted line.

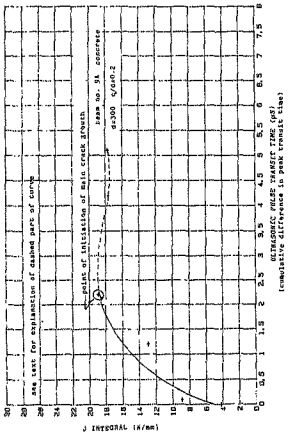


FIG 5.15 J-integral plotted against cumulative difference in peak ultrasonic pulse transit time for beam 9A

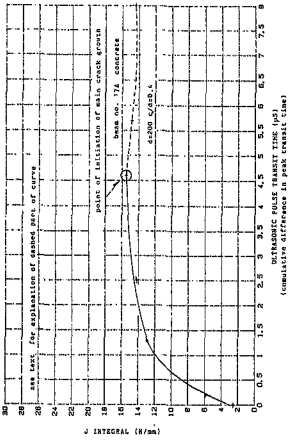


FIG 5.16 J-integral plotted against cumulative difference in peak ultrasonic pulse transit time for beam 17A

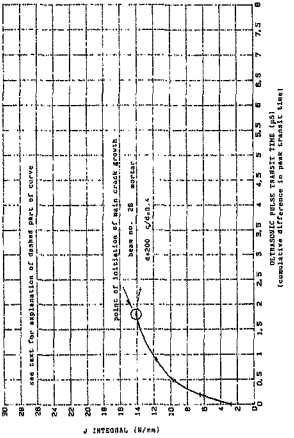


FIG 5.17 J-integral plotted against cumulative difference in peak ultrasonic pulse transit time for beam 2B

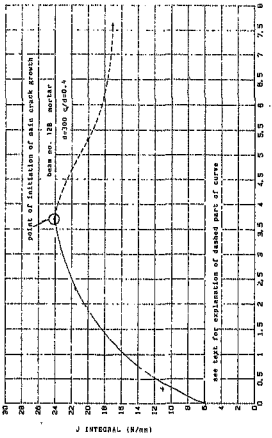


FIG 5.18 J-integral plotted against cumulative difference in peak ultrasonic pulse transit time for beam 12B

All the curves show the the same pattern of an initial sharp increase in the J-integral value for a small increase in transit time, followed by a peak value of J. This reinforces the idea that main crack growth initiates together with a drop in energy absorption rate.

The following points should be noted:

1. The apex of each curve (shown as circled in the diagrams) represents the maximum value for J and therefore the point of initiation of main crack growth.

2. In several tests, the J-integral began to show an increase leading to a second peak. Although this part of the curve is not valid since c is unknown, a second peak suggests the possible formation of a second crack. This should perhaps be borne in mind by future researchers.

TABLE 5.17 and TABLE 5.18 show the results obtained for all the beams on which ultrasonics was used.

TABLE 5.17 IDENTIFICATION OF THE CYCLE DURING WHICH MAIN CRACK GROWTH BEGAN FOR CONCRETE BEAMS USING AN ULTRASONIC TECHNIQUE

BEAM	J_{cycle}	CYCLE NUMBER
9A	18,9	4
10A	18,0	3
11A	19,5	6
12A	12,7	5
15A	28,3	5
16A	21,6	4
17A	15,5	5
18A	17,6	4

NOTE:

Since this method has made use of the J-integral to identify the point of initiation of main crack growth, the results are the same as those obtained in section 5.4.

TABLE 5.18 IDENTIFICATION OF THE CYCLE DURING WHICH MAIN CRACK GROWTH BEGAN FOR MORTAR BEAMS USING AN ULTRASONIC TECHNIQUE

BEAM	J_{cycle}	CYCLE NUMBER
1B	11,4	6
2B	14,1	5
3B	24,2	5
4B	19,2	4
5B	24,5	4
6B	20,2	5
7B	21,9	5
8B	24,5	5
9B	17,6	6
10B	21,4	4
11B	19,4	6
12B	24,1	5

As was said before, the similarity between this method and that dealt with in section 5.4 means that these results are complementary to those in section 5.4 and do not break new ground. The concept of permanent damage, dealt with in the following section, makes more use of ultrasonics as a technique on its own.

5.10.2.2 PULSE TRANSIT TIME AND THE CONCEPT OF PERMANENT DAMAGE

When a matrix is subjected to low levels of stress, micro-cracking occurs within that matrix. When this stress is removed, the recovery of the material is

partially elastic and re-alignment of the deformed particles is very nearly perfect. As the micro-cracking progresses to the point of initiation of main crack growth, damage becomes more pronounced and permanent. Once a stress-free crack has developed there is incomplete crack-closure on unloading due to relative displacement of crack surfaces and debris lodging in the crack.

This can be seen in the photographs of FIG. 5.19. Using the preceding discussion as a basis, it was reasoned that if ultrasonic pulse transit times were measured at the peak of a cycle and then at the trough (zero load point) of the same cycle, some measure of permanent damage could be obtained.

The series of graphs FIG's 5.20 to 5.26 show a plot of cumulative difference in peak pulse transit time on the horizontal axis and cumulative difference in trough pulse transit time on the vertical axis. The cumulative difference in pulse transit time was calculated by subtracting the pulse transit time (peak or trough) of cycle one from cycle two, and then cycle two from cycle three, and then cycle three from cycle four etc until the end of a test. These differences were then added cumulatively for both peak and trough pulse transit time and plotted for each cycle as described. A steep line, or section of a curve, therefore indicates considerable permanent damage while a

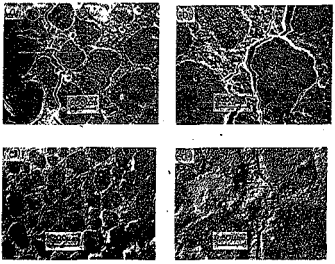
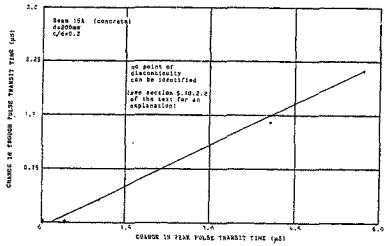


FIG 5.19 Crack patterns obtained from mortars loaded within the sample chamber of an SEM:
(a), (b) compact tension specimens;
(c), (d) compression specimens.
(from ref 66)



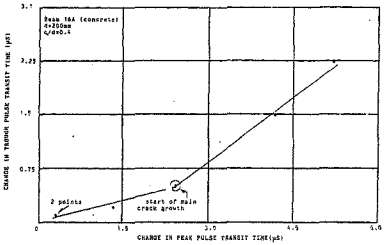


FIG 5.20 (a)&(b) Plots of cumulative change in trough pulse transit time vs cumulative change in peak pulse transit time for beams 15A & 16A

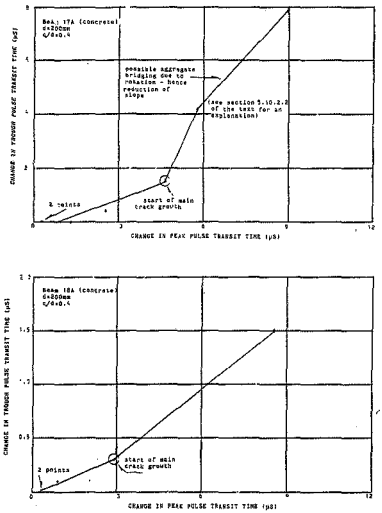


FIG 5.21 (a)&(b) Plots of cumulative change in trough pulse transit time *vs* cumulative change in peak pulse transit time for beams 17A & 16A

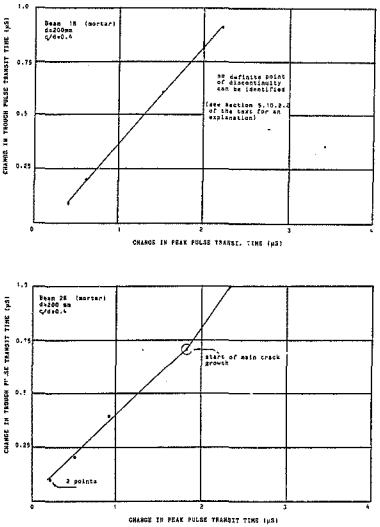
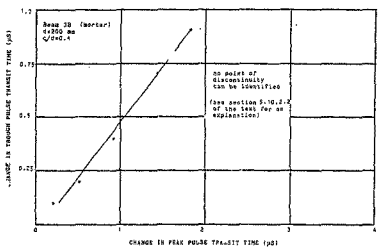


FIG 5.22 (a)&(b) Plots of cumulative change in trough pulse transit time vs cumulative change in peak pulse transit time for beams 1B & 2B



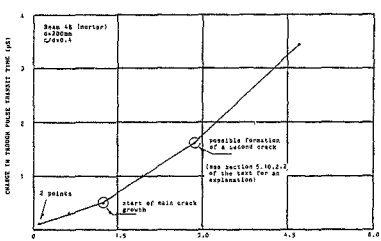


FIG 5.23 (a)&(b) Plots of cumulative change in trough pulse transit time vs cumulative change in peak pulse transit time for beams 3B & 4B

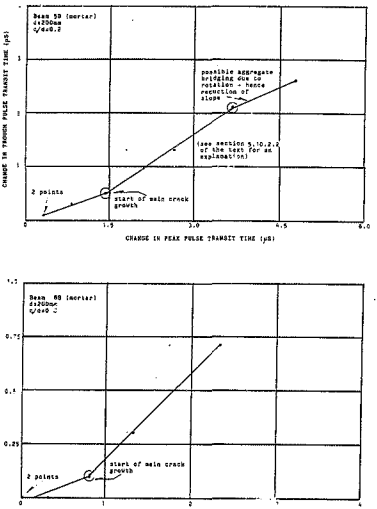


FIG 5.24 (a)&(b) Plots of cumulative change in trough pulse transit time vs cumulative change in peak pulse transit time for beams 5B & 8B

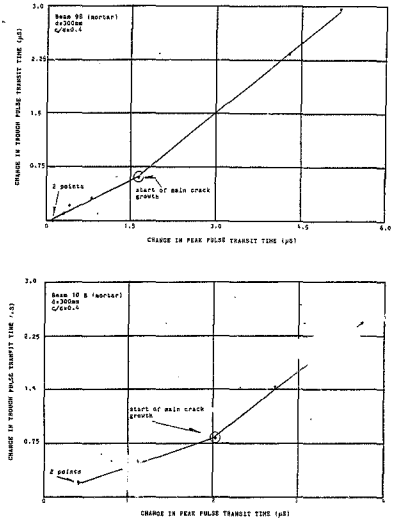
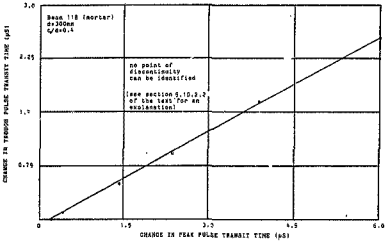


FIG 5.25 (a)&(b) Plots of cumulative change in trough pulse transit time vs cumulative change in peak pulse transit time for beams 9B & 10B



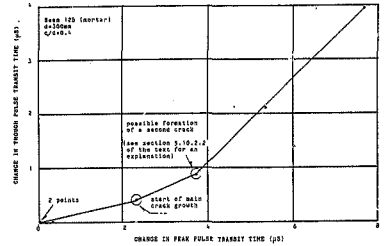


FIG 5.26 (a)&(b) Plots of cumulative change in trough pulse transit time vs cumulative change in peak pulse transit time for beams 11B & 12B

less steep line indicates efficient re-alignment and less permanent damage. In many cases, there is a point of discontinuity which could indicate the point of change-over from micro-cracking to main crack growth.

The reliability of this method proved not to be as good as it was hoped to be. In several cases the tests were inconclusive since there was no apparent point of discontinuity. It is reasoned that this may have occurred as a result of aggregate bridging across the crack after closing which could have provided a path for the ultrasonic waves and hence resulted in a transit time change not representative of the damage present.

In a number of other cases (FIG 5.23(b) and FIG 5.26(b)) there was more than one point of discontinuity. In these instances the first point of discontinuity was interpreted as the onset of main crack growth and the second as the possible formation of another crack, or increasing damage due to micro-cracking.

In cases where there was a sudden steepening of the graph (indicating increased permanent damage) followed by a decrease in slope, (see FIG 5.21(a) and FIG 5.24(a)) it is possible that rotation of the crack, during the cycles following the onset of main crack growth, could have caused the wedging of a piece of

dislodged aggregate thereby permitting the ultrasonic waves to travel a shorter path. This would show as the decrease in slope on the graph, after the onset of main crack growth.

TABLES 5.19 and 5.20 show the results of the identification of the cycle during which main crack growth started, obtained from the use of this technique. A comparison between these figures and those obtained from the use of the fracture energy method is also given in each table. (Only five of the concrete beams are shown since this technique was employed after several specimens had already been tested).

In spite of the lack of reliability of this method in terms of success rate, it is important to note that out of ten successful tests, only two were in disagreement with the results obtained in sections 5.4 and 5.10.2. One of these (FIG 5.26(b) - BEAM 12B) showed two points of discontinuity. The second point was identified as the onset of main crack growth in sections 5.4 and 5.6.2, but FIG 5.26(b) suggests that there may have been two cracks. The other (FIG 5.24(b) - BEAM 8B) showed the onset of main crack growth to be one cycle earlier than was found in sections 5.4 and 5.10.2. It is possible that the degree of micro-cracking present in the earlier cycle was sufficient to show up as damage, and thus suggest the development of a main crack. Alternatively, the

beam may have, through aggregate interlock, been able to absorb more energy than is normal following main crack growth, thus only showing a drop in the J-integral after main crack growth and not simultaneously with it. It is impossible to say which one of the methods is correct in this case.

The author concludes that this technique could be far more useful if continuous measuring techniques were employed. A continuously recorded ultrasonic pulse velocity measurement would serve the purpose of indicating trends that would be impossible to determine from only two measurements per cycle. However, this was not possible since no such equipment was available at the time of testing.

It is also reasoned that ultrasonic methods may be of more value in tests which involve a large number of cycles (from one hundred to several thousand) since the damage is gradual in these cases. In tests such as those carried out in this dissertation, damage may be very sudden due to the limited number of cycles (less than 10) and the difference in pulse transit time from one cycle to the next is equally sudden, with a "grey area" in between. It is this "grey area" that is of particular importance in determining the onset of main crack growth.

TABLE 5.19 IDENTIFICATION OF THE ONSET OF MAIN CRACK GROWTH (CRITICAL CYCLE) FOR CONCRETE BEAMS USING AN ULTRASONIC TECHNIQUE TO RECORD PERMANENT DAMAGE.

BEAM	CRITICAL CYCLE *(Using permanent damage technique)*	CRITICAL CYCLE *(Using energy technique)*
12A	FAULTY DATA	5
15A	NO DEFINITE POINT	5
16A	4	4
17A	5	5
18A	4	4

TABLE 5.20 IDENTIFICATION OF THE ONSET OF MAIN CRACK GROWTH (CRITICAL CYCLE) FOR MORTAR BEAMS USING AN ULTRASONIC TECHNIQUE TO RECORD PERMANENT DAMAGE.

BEAM	CRITICAL CYCLE (Using permanent damage technique)	CRITICAL CYCLE (Using energy technique)
1B	NO DEFINITE POINT	6
2B	5	5
3B	NO DEFINITE POINT	5
4B	4	4
5B	4	4
6B	NO DATA	5
7B	NO DEFINITE POINT	5
8B	4	5
9B	6	6
10B	4	4
11B	NO DEFINITE POINT	6
12B	4 & 5	5

5.11 CONCLUDING DISCUSSION

The major purpose of the work covered in Chapter 5 was to identify the onset of main crack growth during a fracture test and to provide a fracture parameter at this point. The following conclusions in this regard can be drawn:-

1. The design of instrumentation should be very carefully considered. A possible interference from

surface micro-cracking may have caused the strain profile irregularities discussed in Section 5.2. A remedy for this problem would have been to place the instrumentation clamps at a wider gauge length, thereby ensuring that surface micro-cracking would not interfere with the LVDTs.

2. The J-integral seems to be useful for helping to identify the onset of main crack growth. The J-integral, calculated for each cycle and then plotted against the in-plane displacement at the notch tip for the same cycle, reached a peak for every fracture test carried out. This peak (or rather the drop following a peak) was interpreted as the onset of main crack growth, (as explained in section 5.4)

3. The use of ultrasonic pulse velocity measurements, when plotted against the J-integral provided a back-up for the results determined in 2. above.

The use of ultrasonic pulse velocity measurement as a technique on its own proved to be of limited value for the tests conducted in this dissertation. A lack of successful tests proved to be a major problem. However, out of a total of ten successful tests, eight yielded results in agreement with those obtained in 2. above. The technique used the concept of permanent damage, and

evidence of sudden permanent damage was interpreted as the onset of crack growth.

It was mentioned that the use of a continuous recording system for recording pulse velocity would have been of more value than the limited equipment that was available for the work covered in this dissertation.

4. The J-integral, calculated as a cumulative value based on the envelope curve joining the peak load points for each cycle up to the cycle during which main crack growth began, can be thought of as a fracture toughness parameter relating to the point of initiation of main crack growth (J_c). J_c was found to be essentially the same for mortar and concrete.

5. Analysis of the curves for the J-integral versus notch tip displacement, and the J-integral versus cumulative change in peak ultrasonic pulse transit time according to the ASTM-813 method[72], produced a fracture toughness parameter at the start of micro-cracking (J_i). J_i for concrete was found, within the scatter limits, to be approximately the same as J_i for mortar, and approximately 40% of J_c.

6. Average J_i values show a tendency, in general, to increase with increasing beam size thus supporting the finding by Alexander[4] that the degree of micro-cracking was greater for larger beams. Average J_c values also show a tendency, in general, to increase with increasing beam depth. A lack of sufficient data and the inherent scatter present in the results render these tendencies approximate, however. It should be mentioned that there is little agreement among researchers as to the dependance of J on specimen geometry (see section 2.2.2).

7. The notch tip displacement at the point of initiation of main crack growth can be thought of as the crack opening displacement (COD) since the crack is propagating from the notch tip at this stage. The average COD for concrete is approximately the same as the average COD for mortar. The scatter in these results was larger for concrete than it was for mortar (30% variation compared with 20% variation). This is probably due to the heterogeneous nature of concrete when compared with mortar. It should also be borne in mind that the COD measurements were taken in one position and on one side of the test beam only. Material irregularities could therefore be responsible for the large scatter in the case of concrete. The COD can be thought of as a fracture parameter at the start of main crack growth.

8. In most of the tests, peak load occurred before the initiation of main crack growth. This indicates that there can be a reduction in the load carrying capacity of concrete and mortar due to the presence of micro-cracking only. This reduction varied up to 27% for concrete and up to 17% for mortar.

Chapter 5 provides a basis for the analysis of fracture zones in concrete and mortar at the start of main crack growth. This is dealt with in Chapter 6.

6. MATERIAL CHARACTERISATION FROM FRACTURE ZONE SIZE MEASUREMENTS

FIGURE LEGEND

The legend shown below applies to those figures which contain reference to the various fracture beams.

BEAM GEOMETRY	CONCRETE	MORTAR
d = 200 mm C_o/d = 0,2	1	5
d = 300 mm C_o/d = 0,2	2	6
d = 200 mm C_o/d = 0,4	3	7
d = 300 mm C_o/d = 0,4	4	8

TABLE 6.1 General figure legend.

6.1 INTRODUCTION

Fracture of a heterogeneous material like concrete is extremely complex. Cracking may occur by means of cleavage within the material leaving stress-free surfaces. Alternatively, gradual micro-cracking can initiate in areas of high stress concentration. This microcracking can occur, on a microscopic scale, either between the aggregate-matrix interfaces or within the matrix itself - initiated perhaps by drying shrinkage cracks or small air voids trapped during the mixing. Stress transfer across this micro-cracked zone is, in general, still possible.

Four distinct stress zones may be identified in a notched fracture beam[4]. FIG. 6.1 shows these as:

1. A destressed zone characterised by a stress-free crack of depth c.

2. A micro-cracked zone, also called a fracture zone, which includes a zone of aggregate pull-out, and extends immediately ahead of the main crack tip. Stress transfer may occur within this zone.

3. An intact tension zone, in which the material is essentially undamaged and stress-strain relationships are linear. The stress at the limit of this zone approaches the bulk tensile strength of the material.

4. A compression zone above the neutral axis in which the material is also essentially undamaged and stress-strain relationships are linear.

FIG. 6.1 shows that the total tension zone consists of the micro-cracked zone and the intact tension zone. The residual ligament depth h is defined as the difference between the beam depth d and the stress free crack depth c. It is within depth h that stress transfer can occur.

The presence of a notch in a fracture beam has a profound effect on the stress distribution in that beam

during fracture. It is therefore desirable that the stress zones are l understood. Considering the three zones described in FIG 6.1 the following is true:-

The strain distribution within the micro-cracked zone is not linear and displacements relate to localised cracking. The stress-free zone below the main crack tip (or notch if main crack growth has not yet been initiated) consists of either totally damaged material or no material at all (notch). For equilibrium within the beam, the force in the tension zone must balance that within the compression zone. But, since concrete is weaker in tension than it is in compression, the size of the tension zone must be greater than that of the compression zone. For a particular material, a characteristic relationship between the sizes of these two zones should exist. Experimental displacement results are analysed in this section in order to determine the characteristic relationship described above, and thereby to effect material characterisation at the start of main crack growth for both concrete and mortar.

6.2 TENSION AND COMPRESSION ZONE SIZES

The two zone depths are described by the following equations: (see FIG 6.1)

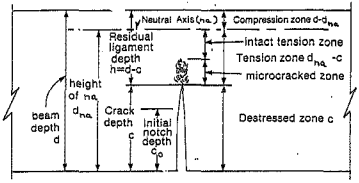


FIG 6.1 Definition of stress zones in a concrete or mortar beam during fracture (from ref 4).

$$\text{Compression zone depth} = d - d_{na} \qquad (6.1)$$

$$\text{Tension zone depth} = d_{na} - c \qquad (6.2)$$

The tension zone consists of the zone below the neutral axis, and the compression zone comprises that material above the neutral axis.

FIG's 6.2 and 6.3 show a plot of the relationship between the tension and compression zone size for sixteen fracture beams. Since one of the main aims of this work was to characterise concrete and mortar at the stage of change-over from micro-cracking to main cracking, only the results at this point (as determined in the previous section) are shown here. The plots were arrived at by using the recorded displacement profiles to determine d_{na} at the start of main crack growth for each beam. c is simply the notch depth for that beam. (Diagrams showing progressive micro-cracking, up to the point of initiation of main crack growth, will be shown following the discussion on FIG's 6.2 and 6.3).

FIG 6.2

This shows the results for seven concrete beams. Points to note are as follows:

1. The results have a best fit line, passing through the origin, with the equation

$$d - d_{na} = 0{,}56\ (d_{na} - c) \qquad (6.3)$$

2. Scatter is present (coefficient of variation is 13%) so the above equation can be regarded as a general trend.

3. The physical meaning of equation 6.3 is that the tension zone at the start of main crack growth is just under twice the size of the compression zone.

FIG. 6.3

This shows the results for nine mortar beams.

1. The results have a best fit line with the equation

$$d - d_{na} = 0{,}60\ (d_{na} - c) \qquad (6.4)$$

2. Once again the scatter is significant (coefficient of variation is 10%) - equation 6.4 is therefore a trend.

3. According to the equations (6.3) and (6.4), the ratio of tensile to compressive zone sizes is slightly less for mortar than it is for concrete.

FIG's 6.2 and 6.3 show lines which represent specific material behaviour. The line for a perfectly linear

elastic brittle material shows a linear stress distribution, ie equal compression and tension zone sizes. Since concrete and mortar are quasi-ductile and inelastic materials it is expected that they should lie well below the line for a perfectly linear elastic material.

It should also be noted that the average for the mortar beams lies somewhat closer to the "ideal" line than the average for the concrete beams. While this difference is not great, it is consistent with the expectation that mortar more closely approximates a linear elastic material than concrete does. The line representing the relationship between compression and tension zone sizes in a beam during fracture can therefore be thought of as a material characteristic.

It should be mentioned that Alexander[4], in his work, obtained an average value for the relationship between tension zone and compression zone sizes as follows;

$$d - d_{na} = 0{,}461\ (d_{na} - c) \quad \text{(concrete only)}$$

This means that the material tested in this work showed a larger compression zone depth at the start of main crack growth (when compared with the tension zone depth), than that tested by Alexander[4]. This is most likely due to the fact that the work in this

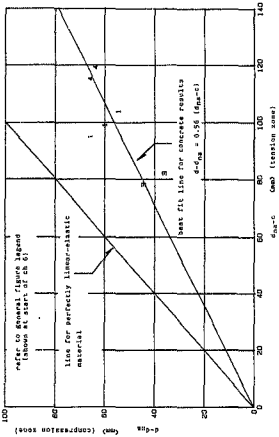


FIG 6.2 Plot of compression zone depth ($d-d_{na}$) versus tension zone depth ($d_{na}-c$) for the concrete beams

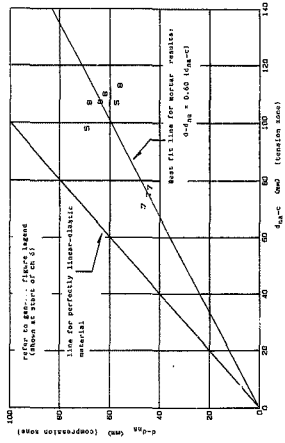


FIG 6.3 Plot of compression zone depth ($d-d_{na}$) versus tension zone depth ($d_{na}-c$) for the mortar beams

dissertation relates to the point of initiation of main crack growth while that of Alexander relates to conditions well after main crack growth. Since the state of damage (extent of cracking) of the material at the start of main crack growth is less than that well after main crack growth, the overall integration of tensile stress can be higher thus implying a smaller tension zone size.

FIG's 6.4 and 6.5 show plots of progressive micro-cracking up to the point of initiation of main crack growth.

Several of the tests had their starting points lying on the line for a perfectly elastic material thereby indicating equal sizes of the compression and the tension zone. As these tests progressed, the tension zone size increased as would be expected.

6.3 THE POSITION OF THE NEUTRAL AXIS DURING FRACTURE

The position of the neutral axis at the point of change-over from micro-cracking to main crack growth gives a good idea of the extent and positions of the tension and compression zones in the beam at this point. Section 6.3 deals with this by establishing a relationship between the neutral axis position and the geometrical parameter h, where h = d-c (residual ligament depth). h was chosen in order to facilitate comparison between the different beams.

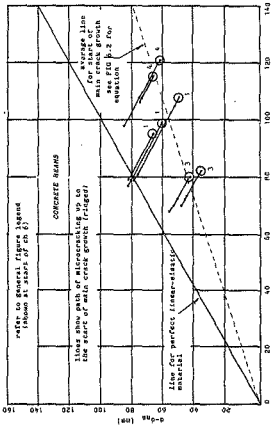


FIG 6.4 Plot of compression versus tension zone sizes during progressive micro-cracking up to the start of main crack growth (concrete beams)

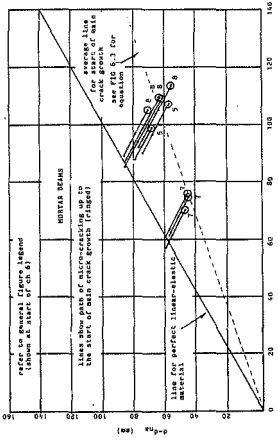


FIG 6.5 Plot of compression versus tension zone sizes during progressive micro-cracking up to the start of main crack growth (mortar beams)

From equations 6.3 and 6.4 the following relationships can be derived:

For concrete:

$$d-d_{na} = 0,56\ (d_{na}-c)$$

Which can be written as

$$(d-c)-(d_{na}-c) = 0,56\ (d_{na}-c)$$

giving

$$d_{na}-c = 0,64\ (d-c) \qquad (6.5)$$

For mortar:

(by the same process)

$$d_{na}-c = 0,63\ (d-c) \qquad (6.6)$$

FIG's 6.6 and 6.7 show these relationships. Also shown is the neutral axis position for an ideal brittle and elastic material (i.e. equal compression and tension zone sizes). It is important to note that the experimental points shown represent beams at the point of incipient fracture (i.e. point of change-over from micro-cracking to main crack growth). The results for

the mortar beams lie slightly closer to the ideal material line than the results for the concrete beams. This is to be expected since mortar more closely approximates an ideal brittle and elastic material than concrete does. (see discussion in Section 6.2)

The physical interpretation of the above is that at the point of incipient fracture of a beam, the neutral axis lies above the notch tip, about two thirds of the distance between the notch tip and the upper face of the beam.

6.4 DETERMINING THE MICRO-CRACKED ZONE SIZE FROM THE DISPLACEMENT PROFILES

To accurately record the shape of the displacement profile in a beam, many gauge points spread evenly over the fracture section would be necessary. This is extremely difficult since a shortage of space determines the maximum number of instruments that can be used. However Alexander[4] proposes a simple method for overcoming this problem as far as the determination of the micro-cracked zone size is concerned. This method was adopted for use in this work, and is described below:

(NOTE: Other more sophisticated techniques such as Moiré Interferometry and Laser Holography are also possible, but were not available for this work.)

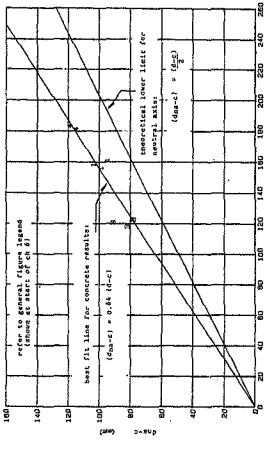


FIG 6.6 Position of the neutral axis at the start of main crack growth (concrete beams)

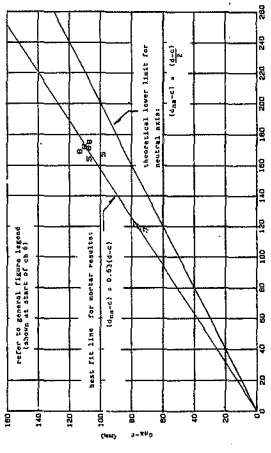


FIG 6.7 Position of the neutral axis at the start of main crack growth (mortar beams)

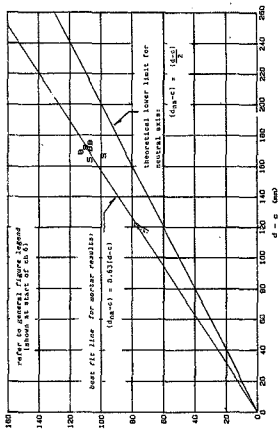


FIG 6.7 Position of the neutral axis at the start of main crack growth (mortar beams)

The micro-cracked zone is bounded at one end by a stress-free crack tip and at the other by the transition from damaged to intact material. Depending on the degree of damage, the material will exhibit a corresponding stiffness. This will vary from the high stiffness of intact material to the low stiffness of cracked material. The micro-cracked zone will exhibit a stiffness at a particular point that is being continually reduced as the zone extends, until a limiting lower value is reached. This is usually when the micro-cracked zone has reached its full extent at that particular point. Therefore, two distinct stiffnesses can be identified:- that of fully intact material, and that of fully damaged material. The micro-cracked zone will lie somewhere between these two extremes. Thus a point of discontinuity, marked by the intersection of two lines with slopes representing the stiffness of intact and fully damaged material, should be an indication of the limit of the micro-cracked zone.

FIG. 6.8 shows a schematic strain profile which illustrates the theory outlined above. The construction required is executed as follows:

1. The slope of the displacement profile in the lower (i.e. notched and micro-cracked) portion of the beam represents the fully damaged stiffness. The line with this slope (Line A) is extended upwards.

2. If the displacement at measuring position N° 2 is compressive, or does not exceed about 100×10^{-6} tensile strain units then it is assumed that this point lies within fully intact material. The displacement at position N° 1 is always compressive and well within the "intact range". Therefore the displacement profile of intact material is given by the line joining the displacements at measuring positions N° 1 and N° 2. This line (LINE B) is then extended to meet the extension of Line A. The point of discontinuity thus formed represents the upper limit of the micro-cracked zone.

3. Since this construction is carried out on the critical cycle (cycle during which the micro-cracked zone reached maximum size) for each test, the crack length c is equal to the notch depth c (i.e. main crack growth has not yet begun). Therefore the difference in height between the notch tip and the limit of the micro-cracked zone (point of discontinuity) is the depth of this zone.

4. This method fails if the displacement at measuring position N° 2 indicates a damaged material. The limits are taken as being no greater than 100×10^{-6} to 150×10^{-6} strain units[4].

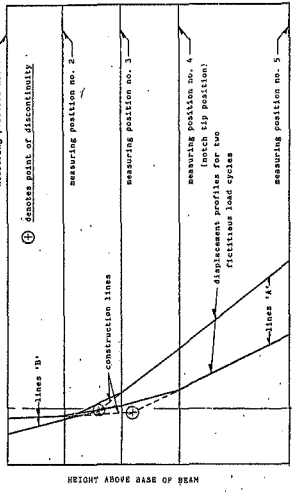


FIG 6.8 Schematic surface strain profile used to determine the size of the micro-cracked zone at the start of main crack growth (from ref 4)

The displacement profiles of 16 beams (7 concrete and 9 mortar) were analysed in this way. FIG's 6.9 and 6.10 show the results plotted as a function of ligament depth h. Points to note are:

1. These figures represent the fracture condition at the point of changeover from micro-cracking to main crack growth.

2. The best-fit straight line through all the results (passing through the origin) for CONCRETE has the following equation:-

   Micro-cracked zone depth = 0,424 h (6.7)

3. The best-fit straight line through all the results (passing through the origin) for MORTAR has the following equation:-

   Micro-cracked zone depth = 0,410 h (6.8)

4. A difference in results for beams of different geometry was evident. However because of the limited amount of data available, it is difficult to determine whether these differences are due to an actual trend or to experimental scatter.

Tables 6.2 and 6.3 show the results for different beam geometries. With the exception of the d = 300, c_o/d = 0,4 beams in Table 6.3, consistency of results within a given geometry was good.

Bearing in mind the scatter present in general, the following trend can be determined from Table 6.2:-

Concrete beams with smaller notch/depth ratios seem to have a smaller relative micro-cracked zone size than beams with larger notch depth ratios. For mortar this is unclear.

From equations 6.7 and 6.8 it can be seen that the overall average micro-cracked zone size is slightly smaller for mortar than it is for concrete. However, considering the scatter in these results, this difference is not significant.

Alexander[4] found the average micro-cracked zone depth for concrete beams tested in his work to be 0,463 h and further found that beams of a large depth had larger relative micro-cracked zone sizes than beams of a small depth. It is significant that the overall average for the tests conducted in his work is very close to that obtained in this work. Alexander[4] found no correlation between micro-cracked zone size and notch/depth ratio.

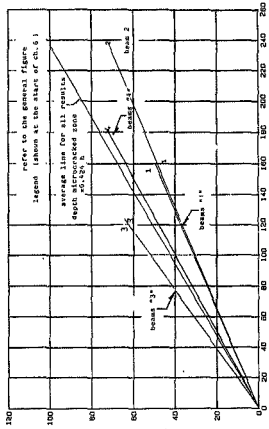


FIG 6.9 Size of the micro-cracked zone at the start of main crack growth (concrete beams)

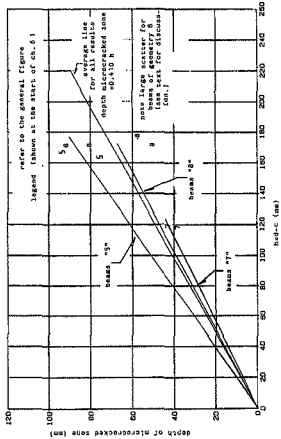


FIG 6.10 Size of the micro-cracked zone at the start of main crack growth (mortar beams)

TABLE 6.2 THE SIZE OF THE MICRO-CRACKED ZONE IN CONCRETE BEAMS

BEAM GEOMETRY	MICRO-CRACKED ZONE DEPTH (AVERAGE)	NUMBER OF SPECIMENS
d = 200 mm $c_o/d = 0,4$	0,540 h 0,520 h 0,500 h	2
d = 300 mm $c_o/d = 0,4$	0,508 h 0,504 h 0,500 h	2
d = 200 mm $c_o/d = 0,2$	0,279 h 0,309 h 0,339 h	3
d = 300 mm $c_o/d = 0,2$	0,302 h	1

TABLE 6.3 THE SIZE OF THE MICRO-CRACKED ZONE IN MORTAR BEAMS

BEAM GEOMETRY	MICRO-CRACKED ZONE DEPTH (AVERAGE)		NUMBER OF SPECIMENS
d = 200 mm c_o/d = 0,4	0,325 h 0,397 h 0,358 h	0,360 h	3
d = 300 mm c_o/d = 0,4	0,295 h 0,470 h 0,500 h 0,330 h	0,398 h	4
d = 200 mm c_o/d = 0,2	0,562 h 0,463 h	0,512 h	2

6.5 CONCLUDING DISCUSSION

The following general conclusions may be drawn from the discussion in Chapter 6. It must be emphasised that the following comments refer to conditions at the *start of main crack growth.*

1. Both concrete and mortar beams show unequal sizes of compression and tension zones during fracture. For concrete, the size of the compression zone is

56% of the size of the tension zone, while for mortar the size of the compression zone is 60% of the size of the tension zone. These relationships can be regarded as a material characteristic at the point of initiation of main crack growth. It is to be expected that these materials behave in a non-linear fashion since they are quasi-ductile and have a stress distribution affected by the presence of a micro-cracked zone. It should be noted that the relationship for mortar lies slightly closer to an ideal linear - elastic brittle relationship (equal tension and compression zone sized) than the relationship for concrete. While this difference is slight, it is to be expected since mortar more closely approximates a linear elastic material than concrete does.

2. Plots of progressive micro-cracking up to the point of initiation of main crack growth showed that several of the beams had their starting points (first or second cycles) lying on the line for a perfectly linear - elastic material, thereby indicating equal compression and tension zone sizes. As these tests progressed and significant micro-cracking occurred, the zone sizes deviated from this until they reached the situation described in point 1. above.

3. Plots of the neutral axis position at the point of initiation of main crack growth showed that, at this stage during fracture, the neutral axis lies above the notch tip, about two thirds of the distance betwe' the notch tip and the upper face of the beam. (This is true for both concrete and mortar)

4. Distortion of t -plane displacement profile of the beams was used to determine the size of the microcracked zone in 10 beams. This was found to be about 42% of the residual ligament depth for concrete and about 41% of the residual ligament depth for mortar. A difference in results for beams of different geometry was evident, but due to the limited amount of data it was difficult to determine whether this was due to scatter or an actual trend. These results compare well with those of Alexander[4] who found that (for concrete beams of a similar nature to those tested in this work) the micro-cracked zone size was about 46% of residual ligament depth. Referring again to the difference in results for beams of different geometry, the trend (bearing scatter in mind) for the concrete tests seems to show that beams with smaller notch depth ratios have a smaller micro-cracked zone size than beams with larger notch depth ratios.

7. DISCUSSION, CONCLUSIONS AND RECOMMENDATIONS FOR FUTURE WORK

The purpose of this chapter is to summarise the conclusions drawn in earlier chapters and to present an overall view of the work carried out for this dissertation. The objectives are outlined, a summary of experimental results is given and finally conclusions and recommendations for further work are presented.

7.1 OBJECTIVES

The main objectives for this work were prompted by the recommendations for future research given by Alexander[4] in his earlier thesis. The most important message that came across from Alexander's work was the need for a fracture parameter at the point of initiation of main crack growth and characterisation of fracture behaviour at this point. A literature study confirmed this need and most researchers agreed that one of the most difficult aspects of a fracture test is to identify the point of change-over from micro-cracking to main crack growth in a test.

7.2 SUMMARY OF EXPERIMENTAL WORK

A total of 30 notched, rectangular beams of constant width 100mm and with depths of either 200mm or 300mm were tested. The span to depth ratio was kept constant at 3:1. Notch/depth ratios used were either

0,2 or 0,4 and all notches were cut after casting using a diamond tipped saw blade. Beams of concrete and mortar were tested. The fracture tests involved the use of a compression machine to load the beams in bending which rested on supports made as frictionless as possible.

Load cycling was carried out to induce stable crack growth. Deflections and loads at midspan were measured. LVDTs were used to monitor the surface displacements across the fracture face. Transverse ultrasonic pulse measurements were recorded for each load cycle.

Materials control tests shows that, except for two beams in which the cube strength was slightly low, good quality control was achieved throughout the testing. Cube strengths varied from 36 MPa to 43 MPa for concrete and from 32,5 MPa to 41 MPa for mortar. Elastic modulus values ranged from 33,5 GPa to 36,9 GPa for concrete and from 27,0 GPa to 29,7 GPa for mortar.

7.3 SUMMARY OF RESULTS

7.3.1 IDENTIFICATION OF THE POINT OF INITIATION OF MAIN CRACK GROWTH

The placing of instrumentation should be carefully considered. Possible interference from in-plane micro-

cracking may have caused the strain profile irregularities discussed in section 5.2. A wider gauge length should be considered.

The J-integral proved to be useful for identifying the onset of main crack growth. The J-integral, calculated for each cycle and plotted against the surface displacement across the notch tip, reached a peak for every fracture test carried out. This peak was interpreted as the start of main crack growth (as explained in section 5.4)

The use of ultrasonic pulse velocity measurements when plotted against the J-integral, provided a back-up for the results determined from the J-integral plotted against the surface displacements across the notch tip.

The use of an ultrasonic pulse velocity technique utilizing the principle of permanent damage to identify the start of main crack growth proved to be of limited value due to a low success rate in achieving conclusive results. Those results that were conclusive did, however, compare well with the results obtained using the J-integral technique.

The J-integral, calculated as a cumulative cyclic value up to the point of initiation of main crack growth, can be thought of as a fracture parameter J_c.

cracking may have caused the strain profile irregularities discussed in section 5.2. A wider gauge length should be considered.

The J-integral proved to be useful for identifying the onset of main crack growth. The J-integral, calculated for each cycle and plotted against the surface displacement across the notch tip, reached a peak for every fracture test carried out. This peak was interpreted as the start of main crack growth (as explained in section 5.4)

The use of ultrasonic pulse velocity measurements when plotted against the J-integral, provided a back-up for the results determined from the J-integral plotted against the surface displacements across the notch tip.

The use of an ultrasonic pulse velocity technique utilizing the principle of permanent damage to identify the start of main crack growth proved to be of limited value due to a low success rate in achieving conclusive results. Those results that were conclusive did, however, compare well with the results obtained using the J-integral technique.

The J-integral, calculated as a cumulative cyclic value up to the point of initiation of main crack growth, can be thought of as a fracture parameter J_c.

Bearing in mind the inherent scatter present in the results (coefficients of variation of 28% for concrete and 23% for mortar), it was concluded that the average J_c for concrete was essentially the same as the average J_c for mortar.

The J-integral, calculated according to the ASTM-813 method[70], produced a fracture parameter J_i at the start of micro-cracking. Bearing in mind the scatter present in the results (coefficients of variation of 30% for both concrete and mortar) the average J_i for concrete is essentially the same as the average J_i for mortar. J_i is about 40% of J_c for both concrete and mortar.

J_c was found, on average, to increase for an increase in beam depth and to decrease for a decreasing notch/depth ratio.

J_i was found, on average, to increase for an increase in beam depth and to decrease for a decreasing notch/depth ratio. These findings support those of Alexander[4] who found the micro-cracked zone size to be larger for beams of greater depth.

The notch tip displacement at the start of main crack growth (COD) was found to be approximately the same for mortar as it was for concrete. The average for concrete was 0,039 mm while for mortar it was 0,046 mm. The scatter in the results was larger for concrete

(coefficient of variation 30%) than it was for mortar (coefficient of variation 20%). This was thought to be due to the heterogeneous nature of concrete when compared with mortar. The notch tip displacement can be thought of as a fracture parameter at the start of main crack growth.

In 80% of the tests, peak load occurred before the initiation of main crack growth. This indicates that there can be a reduction in load carrying capacity due to the presence of micro-cracking only. This reduction varied up to 27% for concrete and up to 17% for mortar.

7.3.2 MATERIAL CHARACTERISATION FROM FRACTURE ZONE SIZE MEASUREMENTS

Both concrete and mortar beams showed unequal sizes of compression and tension zones at the point of initiation of main crack growth during fracture. For concrete, the size of the compression zone was 56% of the size of the tension zone, while for mortar the size of the compression zone was 60% of the size of the tension zone. It is thought that these relationships can be regarded as a material characteristic. The relationship for mortar was found to lie closer to the perfectly linear elastic material relationship than that for concrete. This was expected since mortar more closely approximates a linear elastic material than

concrete does. Plots of progressive micro-cracking up to the point of initiation of main crack growth showed that several of the beams had their starting point lying on the line for a perfectly linear - elastic material.

Plots of neutral axis position at the start of main crack growth showed that the neutral axis lay above the notch tip, about two thirds of the distance between the notch tip and the upper face of the beam, for both concrete and mortar.

In-plane displacement measurements across the cracking face [illegible]ms were used to determine the size of the micro-cracked zone at the start of main crack growth. This was found to be about 42% of the residual ligament depth for concrete and about 41% of the residual ligament depth for mortar.

7.4 MAJOR CONCLUSIONS

1. Results from a total of 28 notched concrete and mortar beams of width 100 mm and with depths of either 200 mm or 300 mm have been presented. About 30% of these results could not be used for surface displacement results due to the probable interference of surface micro-cracking with instrumentation clamps. A remedy for this problem is thought to be the use of a wider gauge length.

2. Both displacement and ultrasonic pulse velocity measurements proved to be useful techniques for detecting the initiation of main crack growth, although the reliability of providing clear results was not as good as was hoped for with the ultrasonic technique.

3. The J-integral, calculated from an envelope curve joining the maximum load points of each cycle up to the start of main crack growth, can be thought of as a fracture parameter J_c. J_c was found to be essentially the same for mortar as for concrete.

4. The J-integral, calculated according to the ASTM-813 method[70], can be thought of as a fracture parameter at the start of micro-cracking J_i. J_i was found to be essentially the same for mortar as for concrete.

5. Both J_c and J_i were found to increase for an increase in beam depth and to decrease for a decrease in notch/depth ratio for both the concrete and the mortar beams.

6. The notch tip displacement (COD) can be thought of as a fracture parameter at the start of main crack growth. The COD for concrete was approximately the same as the COD for mortar.

7. It was found that a reduction in the load carrying capacity of both concrete and mortar is possible due to the presence of micro-cracking only.

8. Displacement measurements showed that relationships between compression and tension zone sizes at the start of main crack growth can be thought of as characteristic of material behaviour. Both concrete and mortar were shown to depart from the ideal linear - elastic condition, with mortar being slightly closer to this condition than concrete. The tension zone was roughly twice the size of the compression zone in both cases.

9. Displacement measurements across the cracking face were used to determine the size of the micro-cracked zone at the start of main crack growth. This was 42% of the residual ligament depth for concrete and 41% of the residual ligament depth for mortar.

10. Scatter was a problem in all of the results. This meant that specific trends were difficult to identify and only general conclusions could be drawn. It is the opinion of the author that fracture tests on heterogeneous materials such as concrete and mortar are of questionable value (due to scatter) if performed using a small number of cycles (less than 20). It is suggested that, due

to the presence of large irregularities and flaws across the fracturing section, the change of behaviour from one cycle to the next can be drastic - with a grey area between. A method of testing involving a larger number of cycles (from 20 to several thousand) may, through the induction of gradual damage, help to reduce scatter such as that encountered in the tests carried out for this dissertation.

7.5 OVERALL EVALUATION AND DISCUSSION

In spite of the considerable inherent scatter present in the results obtained for this dissertation, and the limited amount of data available, it was possible to identify general trends which were consistent, in most cases, for both concrete and mortar. Agreement with results obtained by Alexander[4] was also apparent. From the literature survey conducted, it was clear, however, that there is very little agreement amongst researchers in the field of fracture mechanics for cemented materials.

It is quite possible that the effects of specimen type and testing methods, could greatly affect the results obtained for a particular material. What is required, therefore, is a standardisation for both specimen type and testing method and subsequent comparison of results obtained by various researchers.

Even with this standardisation, however, the heterogeneous nature of cemented materials will continue to introduce considerable scatter into the results obtained for any test. Until a complex set of fracture models has been developed to explain the fracture processes in these materials, fracture mechanics for cemented materials will remain an academic rather than an engineering pursuit.

7.6 RECOMMENDATIONS FOR FUTURE RESEARCH

1. Pursuit of the use of ultrasonics as a means of detecting the degree of micro-cracking and the onset and degree of main crack growth.

2. Investigation into the surface spreading of the micro-cracked zone.

3. Investigation of the development of more than one main crack during cyclic loading.

4. Investigation into testing methods which, by their nature, reduce experimental scatter to a point where accurately conclusive trends can be identified.

APPENDIX A

DETAILS OF CONCRETE MIXES AND PRODUCTION PROCEDURES FOR FRACTURE TESTS.

A.1 MATERIALS

A.1.1 CEMENT

Ordinary Portland cement, obtained during May 1986 in a single batch from the Anglo-Alpha cement factory in Roodepoort, Transvaal.

The cement was obtained fresh from the mill and placed in sealed bins on arrival.

A.1.2 AGGREGATES

STONE

Crushed Reef quartzite of nominal 10 mm single-size. The average properties of this stone, according to Davis[67], are:-

Relative Density (R.D) = 2,71

Loose Bulk Density (L.B.D.) = 1330 -1350 kg/m^3

This stone falls, geologically, into the rocks of Witwatersrand Supergroup.

Mortar shrinkage is, on average, about 0,055% with a maximum measured of 0,069%.

SAND

Reef Quartzite Crusher Sand was used for both the concrete and the mortar. The average properties, according to Davis[67], are:-

R.D. = 2,70

Fineness Modulus (F.M.) = 2,94

The mortar shrinkage for this sand is low and varies between the limits 0 047% and 0,069%.

A.2 BATCHING AND MIXING

All the aggregate materials were weigh-batched using an accurate laboratory scale. They were air dried in the laboratory (average temperature 20°C, average relative humidity 55 per cent) and stored dry.

The dry solids were placed in a 40 litre capacity horizontal pan mixer with the water being introduced over a period of about 30 seconds. Mixing was then continued for a further 90 seconds. The slumps of the con-

crete and mortar varied from 30mm to 50mm and 40mm to 60mm respectively which allowed placing by hand and moderate mechanical vibration.

A.3 CASTING AND CURING

A.3.1 MOULDS

The four inch cubes and four inch x eight inch Youngs modulus prisms were cast in standard steel moulds.

The fracture beams were cast on their sides on shutterboard on the floor. The sides of the moulds were made from 100mm deep shutterboard sections bolted onto rectangular double-angle steel frames. Spacer boards were used to form the ends of the beams and were held in position by carpenters clamps. The side shutters were clamped at each end with threaded rods.

A.3.2 CASTING PROCEDURE

The beams were all cast in a horizontal position on the laboratory floor. Great care had to be taken to ensure that the mould base was horizontal so as to eliminate any twist in the beams. The moulds were filled from drums brought from the pan mixer. A small poker vibrator was used to ensure proper compaction. Very little bleed was detectable for any of the beams.

Control cubes and elastic modulus prisms were compacted by placing the moulds on a vibrating table for about one minute. Moulds were stripped one to two days after casting.

A.3.3 CURING

Immediately after casting, the specimens were covered with plastic sheeting for about twenty four hours. The moulds were then stripped, and the beams and their control specimens were placed together in a pile under damp hessian cloth and plastic sheeting. The hessian was kept damp until testing time. All of the curing took place in a high humidity room with the temperature held at about 23°C.

APPENDIX B

DETAILS OF EXPERIMENTAL APPARATUS

B.1 DEFLECTION RIG

The deflection rig to support the midspan deflection LVDT was originally fabricated by Alexander[4], but needed modification for use in the experimental work for this thesis.

The rig was manufactured primarily from 25 x 3mm steel angle and 20 x 3m flat steel strip. Other components included threaded rods to act as spacers or support pins. The entire rig was bolted together, and was fully adjustable for different sized fracture beams. This was achieved by having movable end suppports. FIG B.1 shows rhe rig set for a 900mm long beam. The modification to the rig consisted of an "L-shaped" adjustable stiff steel tubing which was attached to the top of the rig. The L-shape was arranged in such a way that a single LVDT could be supported directly underneath the centre of the beam in order to measure midspan deflection. This can be seen in FIG B.1.

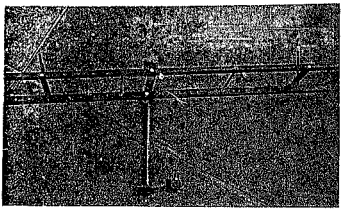


FIG B.1 Deflection measuring rig set for a 900mm long beam.

B.2 ELECTRONIC TRANSDUCERS AND POWER SUPPLY MODULES

B.2.1 ELECTRONIC LOAD CELL

Made by Kyowa Electronic instruments Co. Ltd, Tokyo, Japan.

Type:	Kyowa strain gauge based load cell, compression / tension.
Series No:	LLI-2TE
Capacity:	20kN
Bridge Voltage:	10,0 V.D.C.
Output Voltage Sensitivity:	2mV/V ± 0,2%

B.2.2 LINEAR VARIABLE DEFFERENTIAL TRANSFORMERS (LVDTs)

Made by RDP Electronics Ltd, Wolverhampton, UK.

Transducer length:	53mm) Type D2/200A
Transducer diameter:	21mm)
Linear Range:	± 5,0mm
Linearity:	Approx 0,25% full scale
Excitation:	6.0V D.C

B.2.3 POWER SUPPLY MODULES

Separate power supply modules were used to power the load cell and the LVDTs.

Type:	Regulated DC power supply modules. 0-20V; 0-1A

Made by Metronix Corporation, Tokyo, Japan.
Powered by 220V A.C. Mains Voltage.

B.3 RECORDING EQUIPMENT

B.3.1 XY RECORDER

Made by JJ Lloyd Instruments Ltd, Southhampton, UK.

Type:	PL 2500
Serial No:	775
Effective writing area:	240mm (Y scale) 360mm (X scale)

Recorder also had a chart drive motor with variable speed drive.

Linearity:	> 0,1% f.s.d.

MULTI CHANNEL RECORDER

Linearcorder Mark VII WR3101, Made by Graphtec Corp., Tokyo, Japan.

Six channels of varying paper width, electronic heat pens.

Accuracy:	within ± 0,5% over full scale
Sensitivity:	± 2,5V/cm.
Variable Chart Spaed:	14 Speeds

B.3.3 ULTRASONIC PULSE EQUIPMENT

Type:	Dr Steinkamp Ultrasonic Tester, BP IV.
Natural frequency of Standard transducers:	40-50 Hz
Frequency response:	20-200 Hz
Transducers (pulse transmitter and receiver):	electro-acoustical type liquid crystal display of transit time in µs.

APPENDIX C

RECORDS OF TEST RESULTS

Tables C.1 and C.2 show the results for all the tests carried out for this dissertation.

FIGs C.1 to C.4 show the plots of the J-integral versus surface displacement at the notch tip, the J-integrel versus cumulative difference in peak ultrasonic pulse transit time, and linear regression to evaluate J_1 according to the ASTM-813[70] method.

TABLE C.1 Results of all the tests for maximum force during each cycle (Fmax), J - integral for each cycle (Jcycle), ultrasonic pulse transit time for each cycle and exact beam dimensions.

Δmax IS THE DEFLECTION OF THE BEAM AT FMAX FOR EACH CYCLE
Δp IS THE IRRECOVERABLE DEFLECTION FOR EACH CYCLE

BEAM	CYCLE	FMAX (KN)	A (Nm)	J (N/mm)	PEAK PULSE TRANSIT TIME (μs)	TROUGH PULSE TRANSIT TIME (μs)	BEAM DEPTH d (mm)	BEAM WIDTH b (mm)	NOTCH DEPTH a (mm)	ΔMAX (mm)	Δp (mm)
2A	1	2,93	0,028	3,02			204	100	43	0,0220	0,0017
	2	3,53	0,040	4,77						0,0220	0
	3	4,00	0,005	5,57						0,0230	0,0017
	4	4,20	0,193	24,20						0,0520	0,0074
	5	5,20	0,158	19,60						0,0360	0,0095
	6	4,30	0,107	13,50						0,0490	0,0081
	7	4,20	0,116	14,40						0,0520	0,0090
	8	3,63	0,107	13,30						0,050	FAIL
3A	1	4,83	0,049	6,05			202	100		360	0
	2	4,73	0,078	9,63						220	0
	3	4,63	0,079	9,78						0,0340	0
	4	4,73	0,119	14,60						0,0480	0,0078
	5	3,95	0,103	12,70						0,0490	0,0028
	6	3,35	0,077	19,80						0,0560	FAIL
4A	1	2,38	0,039	4,47			203	100	84	0,0220	0,0016
	2	2,3	0,34	5,71						0,0270	0,0045
	3	2,60	0,48	8,07						0,0320	0,0054
	4	2,56	0,059	9,92						0,0370	0,0099
	5	2,56	0,082	13,80						0,0470	0,0079
	6	2,40	0,084	14,10						0,0560	0,0120
	7	1,90	0,087	14,60						0,0650	FAIL

NOTE: ULTRASONIC TESTS WERE NOT CONDUCTED FOR BEAMS 2A TO 8A HENCE THE ABSENCE OF RESULTS IN TABLE C.1

	1	1,76	0,012	7,09			200	100	82	0,0113	0
	2	2,15	0,030	5,98						0,0215	0,0180
	3	2,29	0,040	6,78						0,0320	0,0071
5A	4	2,33	0,047	7,97						0,0390	0,0017
	5	2,30	0,057	9,66						0,0480	0,0065
	6	2,23	0,051	8,64						0,0498	0,0059
	7	2,18	0,065	11,00						0,0570	FAIL
	1	1,93	0,017	2,81			205	100	84	0,0123	0,0026
	2	2,25	0,026	4,30						0,0170	0,0038
	3	2,76	0,046	7,60						0,0250	0,0058
6A	4	2,73	0,053	8,76						0,0276	0,0017
	5	2,55	0,066	10,10						0,0300	0,0072
	6	2,30	0,059	9,75						0,0310	0,0085
	7	2,20	0,085	14,00						0,0366	FAIL
	1	2,08					204	100	45	0,0093	0,0080
	2	4,67	0,076	9,60						0,0260	0,0020
7A	3	4,83	0,100	12,60						0,0320	0,0028
	4	4,73	0,124	15,60						0,0390	0,0070
	5	4,10	0,109	13,70						0,0420	0,0050

	6	3,70	0,131	14,50						0,0532	FAIL
	1	2,38	0,041	6,09			200	100	81	0,0270	0,0056
	2	2,50	0,046	7,73						0,0270	0,0030
	3	2,63	0,060	10,00						0,0360	0,0090
8A	4	2,60	0,074	12,40						0,0400	0,0038
	5	2,50	0,072	12,10						0,0420	0,0150
	6	1,88	0,064	10,80						0,0490	0,0198
	7	1,60	0,061	10,30						0,0528	FAIL
	1	4,00	0,052	4,16	77,7	77,6	303	103	60	0,0230	0,0037
	2	5,25	0,111	8,87	77,8	77,6				0,0367	0,0019
9A	3	5,88	0,161	12,90	78,9	78,0				0,0459	0,0035
	4	6,05	0,236	18,90	79,9	78,4				0,0571	0,0061
	5	5,56	0,220	17,60	81,9	79,1				0,0630	0,0039
	6	5,05	0,222	17,70	82,8	79,8				0,0710	FAIL
	1	1,83	0,010	0,79			308	102	58	0,0276	0,0003
	2	4,43	0,067	5,30	74,1					0,0276	0,0007
	3	6,35	0,225	18,00	74,5	74,3				0,0540	0,0065
10A	4	6,18	0,219	17,50	76,4	74,9				0,0570	0,0050
	5	6,05	0,265	21,20	77,4	75,3				0,0710	0,0072

	6	5,73	0,243	21,00	78,3	75,8				0,0760	0,0070
	7	5,05	0,246	19,70	79,2					0,0790	FAIL
	1	3,03	0,059	6,89	75,9	75,6	303	102	122	0,0330	0,0130
	2	3,63	0,092	9,97	76,2	75,6				0,0450	0,0050
	3	3,70	0,113	12,20	76,7					0,0490	0,0060
11A	4	3,84	0,136	14,90	77,0	76,1				0,0440	0,0070
	5	3,70	0,180	19,50	78,8					0,0730	0,0090
	6	3,45	0,221	23,90	81,0	77,7				0,0930	0,0230
	7	3,18	0,205	22,20						0,0970	FAIL
	1	1,48	0,006	0,69			300	101	117	0,0033	0,0025
	2	3,10	0,056	6,06	73,0	72,8				0,0320	0,0057
	3	3,28	0,081	8,76	73,8	72,9				0,0410	0,0057
12A	4	3,28	0,104	11,20	75,0	73,1				0,0500	0,005
	5	3,20	0,117	12,66	77,0	74,1				0,0570	0,0136
	6	2,73	0,103	11,20	98,4	75,4				0,0530	0,0137
	7	2,23	0,096	10,40	99,6	76,3				0,0650	0,012
	8	2,00	0,085	10,20						0,0710	FAIL
	1	3,00	0,021	2,64	70,2	70,3	202,5	101	44,2	0,0109	0
	2	3,55	0,038	4,69	70,2	70,3				0,0175	0

15A	3	4,50	0,075	9,33	70,6	70,3				0,0215	0
	4	5,55	0,156	19,50	71,2	70,5				0,0478	0
	5	5,75	0,224	28,30	74,3	71,6				0,0640	0,0111
	6	4,60	0,205	28,60	75,8	72,6				0,0728	0,0182
	7	3,40	0,166	20,80	76,7					0,0769	FAIL
16A											
	1	1,70	0,016	2,65	74,2	74,1	202,5	103	85	0,0180	0,0006
	2	2,70	0,048	7,77	74,5	74,2				0,0320	0,0017
	3	3,25	0,113	18,40	75,5	74,3				0,0530	0,007
	4	3,30	0,133	21,40	76,6	74,6				0,0640	0,010
	5	2,80	0,125	20,80	78,3	75,2				0,0696	0,024
	6	2,13	0,17	19,00	79,5	74,3				0,0800	FAIL
17A											
	1	1,65	0,016	2,55	59,1	58,9	202,5	104	82	0,0155	0,0048
	2	2,40	0,037	5,90	59,3	58,9				0,0250	0,0050
	3	3,05	0,981	12,90	60,4	58,1				0,0370	0,0060
	4	2,80	0,089	14,20	61,6	59,3				0,0480	0,0150
	5	2,25	0,097	15,50	63,7	60,0				0,0640	0,0290
	6	1,75	0,093	14,80	64,8	61,5				0,0740	0,0320
	7	1,28	0,089	14,20	69,0	62,6				0,0740	FAIL
	1	1,73	0,018	2,73	95,5	93,2	202,5	106	80	0,0180	0

18A	2	2,58	0,068	7,40	95,8	93,2				0,0230	0	
	3	3,15	0,71	10,0	96,4	95,3				0,0440	0,0040	
	4	3,03	0,114	17,6	98,4	95,4				0,0520	0,0280	
	5	2,23	0,099	15,3	104,0	96,4				0,0580	0	
18												
	1	1,48	0,013	2,02	71,7	71,7	207	104	87	0,0198	0,003	
	2	2,33	0,037	5,73	71,8	71,6				0,0250	0,003	
	3	2,55	0,053	8,16	72,1	71,6				0,0310	0,004	
	4	2,55	0,055	8,61	73,3	71,7				0,0330	0,005	
	5	2,55	0,071	11,40	73,2	72,1				0,0390	0,005	
	6	2,15	0,071	11,44	73,9	72,4				0,0440	0,007	
	7	1,85	0,080	12,80	74,9					0,0560	FAIL	
26												
	1	1,60	0,017	2,75	68,8	68,7	205	103	85	0,0160	0,0003	
	2	2,30	0,040	6,47	69,0	68,8				0,0230	0,0016	
	3	2,55	0,060	9,71	69,3	68,9				0,0310	0,0028	
	4	2,56	0,072	11,70	69,7	69,1				0,0440	0,0037	
	5	2,50	0,087	14,10	70,6	69,4				0,0520	0,0057	
	6	2,30	0,089	15,50	71,1	69,7				0,0580	0,0067	
	7	2,14	0,086	15,90						0,0660	FAIL	
"												
	1	1,34	0,014	4,45	77,4	77,3	205	107	87	0,0173	0,0040	

38	2	2,15	0,050	9,42	77,6	77,4				0,0230	0,0050
	3	2,53	0,052	16,70	77,9	77,5				0,0320	0,0057
	4	2,53	0,068	21,80	78,3	77,7				0,0400	0,0057
	5	2,42	0,076	24,20	78,8	78,0				0,0480	0,0077
	6	2,20	0,070	23,90	79,2	78,2				0,0510	0,0027
	7	2,05	0,075	24,00	80,3					0,0550	FAIL
48	1	1,38	0,013	2,01	74,9	74,7	202	107	86	0,0107	0,0020
	2	2,60	0,047	7,49	75,0	74,8				0,0260	0,0028
	3	3,27	0,093	15,30	75,5	75,0				0,0430	0,0057
	4	3,33	0,119	19,20	76,1	75,2				0,0560	0,0100
	5	2,85	0,111	17,90	76,8	75,7				0,0570	0,0096
	6	2,60	0,106	17,10	77,7	76,3				0,0620	0,0060
	7	2,24	0,104	16,80	79,5	78,1				0,0720	0,0590
	8	1,25	0,084	13,60	113,2					0,0780	FAIL
58	1	5,60	0,160	18,94	67,2	66,6	203	103	37	0,0470	0,0093
	2	5,50	0,166	19,45	67,5	66,7				0,0490	0,0023
	3	5,45	0,174	20,40	68,0	66,9				0,0520	0
	4	5,23	0,207	24,30	68,6	67,1				0,0630	0,0030
	5	4,93	0,204	24,15	69,8	67,9				0,0660	0,0100
	6	3,65	0,158	18,70	70,8	68,7				0,0678	0,0207

	7	2,60	0,124	14,68	71,9	69,2				0,0720	0,0057	
	8	2,87	0,129	15,20	74,2	132,0				0,0720	FAIL	
68	1	2,70	0,123	2,76	66,7	66,6	204	101	36	0,0142	0	
	2	4,20	0,057	6,74	66,8	66,7				0,0760	0,0014	
	3	5,50	0,119	14,02	67,2	66,8				0,0936	0,0027	
	4	5,78	0,141	16,60	67,6	67,0				0,0960	0,0031	
	5	5,70	0,171	20,20	68,0	67,2				0,0880	0,0043	
	6	5,30	0,155	18,26	68,4	67,4				0,0800	0,0038	
	7	4,88	0,158	18,60	68,9	67,6				0,0736	0,0037	
	8	4,28	0,165	19,44	69,3	67,9				0,0620	0,0039	
	9	3,75	0,148	17,44	70,2	68,6				0,0630	0,0036	
	10	2,65	0,114	13,43	71,0	69,3				0,0620	0,0028	
	11	1,90	0,111	13,08						0,0720	FAIL	
78	1	2,79	0,080	3,55	78,2	78,1	200	102	35	0,0196	0	
	2	4,56	0,099	11,70	78,6	78,1				0,0270	0	
	3	5,00	0,133	15,70	79,2	78,7				0,0460	0,0026	
	4	5,00	0,178	21,10	79,8	78,8				0,0550	0,0037	
	5	4,98	0,185	21,90	80,2	79,0				0,0600	0,0042	
	6	4,10	0,192	16,90	80,5	79,1				0,0560	0,0027	
	7	4,30	0,162	21,60						0,0700	FAIL	

88	1	2,00	0,094	1,48	68,9	68,8	205	100	38	0,0126	0,0020	
	2	3,68	0,052	6,23	68,9	68,8				0,0226	0,0030	
	3	5,05	0,116	13,30	69,2	68,8				0,0390	0,0050	
	4	5,52	0,148	19,50	69,7	68,9				0,0498	0,0094	
	5	5,65	0,205	24,80	70,2	69,1				0,0830	0,0050	
	6	4,68	0,162	19,40	71,2	69,5				0,0540	0,0059	
	7	4,10	0,176	21,10	126,9					0,0830	FAIL	
98	1	1,04	0,009	0,93	93,7	93,7	306	102	131	0,0157	0,0030	
	2	2,16	0,033	3,92	93,5	93,7				0,0233	0,0140	
	3	2,90	0,075	8,40	94,0	93,8				0,0440	0,0070	
	4	3,40	0,108	12,10	94,1	93,9				0,0520	0,0060	
	5	3,50	0,138	15,50	94,5	94,0				0,0620	0,0060	
	6	3,40	0,157	17,60	95,3	94,3				0,0720	0,0116	
	7	3,20	0,155	17,40	97,9	96,0				0,0376	0,0310	
	8	1,90	0,138	15,50	98,9	96,5				0,0560	FAIL	
	1	2,56	0,062	6,87	82,2	82,0	302	105	130	0,0230	0,0030	
	2	3,06	0,091	10,00	82,2	82,0				0,0330	0,0020	
	3	3,69	0,154	17,30	82,6	82,2				0,0720	0,0057	
	4	3,83	0,193	21,40	83,3	82,5				0,0860	0,0116	

108	5	3,40	0,186	20,46	84,2	82,8					0,0910	0,0141
	6	2,85	0,163	18,10	84,9	83,5					0,0960	0,0226
	7	2,10	0,133	14,70	85,9	84,4					0,1000	0,0336
	8	1,40	0,087	9,63	88,8						0,0970	FAHL
118	1	1,56	0,023	2,61	106,9	106,8	301	103	130		0,0230	0,0200
	2	2,48	0,050	5,68	107,0	106,8					0,0350	0,0067
	3	3,00	0,082	9,31	107,2	106,9					0,0460	0,0051
	4	3,60	0,136	17,72	108,2	107,3					0,0680	0,0118
	5	3,30	0,157	14,80	109,1	107,7					0,0750	0,0110
	6	3,00	0,171	19,61	110,6	108,4					0,0890	0,0230
	7	2,48	0,151	17,15	113,4	109,6					0,0970	0,0270
	8	1,71	0,116	13,20	138,2	113,7					0,1020	0,0790
	9	0,99	0,077	9,74							0,1140	FAHL
128	1	1,56	0,016	1,80	103,1	102,8	304	105	135		0,0153	0,0040
	2	2,53	0,052	5,86	103,0	102,8					0,0316	0,0032
	3	3,35	0,098	11,00	103,3	102,8					0,0487	0,0062
	4	3,90	0,191	21,50	104,3	103,2					0,0797	0,0079
	5	3,74	0,214	24,10	105,7	104,0					0,0899	0,0230
	6	2,68	0,178	20,10	107,3	105,0					0,0976	0,0460
	7	1,85	0,151	17,04	109,6	106,8					0,1150	0,0720

	8	1,05	0,076	13,00	43,8	109,2				0,1076	0,0850
	9	0,65	0,053	5,97						0,1164	FAIL

TABLE C.2 Results of all ... tests for surface displacements across the fracturing section for each cycle.

ALL LVDT READINGS ARE IN mm
NEGATIVE VALUES DENOTE COMPRESSIVE DISPLACEMENTS

DISTANCE FROM BASE OF BEAM (mm)						
LVDT:		1	2	3	4	5
BEAM	CYCLE					
2A		204	150,3	96,67	43	0
	1	-0,0084	$-8,66\times10^{-4}$	$3,15\times10^{-4}$	0,00492	0,0057
	2	-0,0089	-0,0012	$3,15\times10^{-4}$	0,00459	0,012
	3	-0,0047	-0,0012	$6,3\times10^{-4}$	0,0058	0,015
	4	-0,0108	-0,0020	0,0057	0,025	0,0396
	5	-0,0108	-0,10	0,012	0,0298	0,0478
	6	-0,0097	$-4,33\times10^{-4}$	0,013	0,0345	0,548
	7	-0,0110	+0,002	0,0178	0,0477	0,710
3A		202	148	94	40	0
	1		$-0,0012$	$1,26\times10^{-03}$	$5,26\times10^{-03}$	0,0145
	2		$-0,0013$	$1,89\times10^{-03}$	$8,2\times10^{-03}$	0,020
	3		$-0,0014$	$2,52\times10^{-03}$	0,010	0,023
	4		$-0,0014$	$1,26\times10^{-02}$	0,034	0,060
	5		$-8,77\times10^{-4}$	$1,70\times10^{-02}$	0,039	0,066
	6		$+1,01\times10^{-03}$	0,021	0,048	0,074
4A		203	163,33	123,67	84	0
	1		$-1,15\times10^{-03}$	$3,2\times10^{-03}$	$1,46\times10^{-02}$	$2,5\times10^{-02}$
	2		$-1,44\times10^{-03}$	$5,0\times10^{-03}$	0,015	0,027
	3		$-1,59\times10^{-03}$	$7,9\times10^{-03}$	0,019	0,036
	4		$-1,44\times10^{-03}$	$1,26\times10^{-02}$	0,027	0,047
	5		$-2,88\times10^{-4}$	$2,1\times10^{-02}$	0,039	0,068

	6		$^{T}2,74^{-03}$	2,8 -02	0,059	0,095
	7		$^{T}0,0082$	0,052	0,081	0,117
5A		200	160,67	121,3	82	0
	1		-5,77-04	1,26-03		1,61-02
	2	-0,0034	-5,77-04	1,97-03	8,77-03	0,030
	3	-5,7-03	-6,77-04	2,5 -03	1,28-02	0,033
	4	-6,26-03	-1,44-04	4,4 -03	1,81-02	0,041
	5	-7,79 -03	-5,77-04	6,9 -03	0,0275	0,055
	6	-8,5-03	$T_{1,87}$-03	9,7 -03	0,037	0,068
	7	-0,011	$T_{4,04}$-03	1,3 -02	0,046	0,082
6A		205	164,67	124,3	84	0
	1	-0,0037	-2,88-04	0,0035	0,0058	0,019
	2	-0,0048	-1,44-04	0,0050	0,0082	0,0263
	3	-0,0065	$T_{2,88}$-04	0,0118	0,0149	0,043
	4	-0,0077	$T_{6,49}$-04	0,0134	0,0193	0,0552
	5	-0,0091	$T_{0,0015}$	0,0255	0,029	0,076
	6	-0,0097	$T_{0,0020}$	0,0297	0,0304	0,085
7A		204	181	98	45	0
	1	-0,0026	-5,77-04	0,00	0,0020	0,0057
	2	-0,0065	-0,0019	6,3 -04	0,0091	0,0220
	3	-0,0077	-0,0019	0,0082	0,0181	0,034
	4	-0,0094	-0,0016	0,0088	0,032	0,055
	5	-0,0105	-0,0016	0,0145	0,042	0,069
	6	-0,011	-0,0016	0,0195	0,051	0,082
		200	160,33	120,67	81	0

8A	1	-4,84-03	-2,8-04	5,7-03	2,1-02	2,58-02
	2	-5,7-03	-4,3-04	8,5-03	0,025	0,041
	3	-6,8-03	-0,0	1,35-02	0,038	0,053
	4	-9,1-03	+2,8-04	1,98-02	0,050	0,069
	5	-1,1-02	+4,76-03	0,0214	0,075	0,099
	6	-1,3-02	+8,9-03	0,045	0,089	0,125
	7	-0,0154	+0,0148	0,060	0,127	0,179
9A		303	222	141	60	0
	1	-4,6-03	-8,66-04	0	5,8-03	1,37-02
	2	-6,8-03	-1,15-03	6,3-04	0,011	0,025
	3	-9,4-03	-1,58-03	1,37-03	0,026	0,038
	4	-1,1-02	-1,87-03	2,35-03	0,0345	0,058
	5	-1,36-02	-2,20-03	1,29-02	0,049	0,081
	6	-0,0145	-1,73-03	0,0195	0,062	0,097
10 A		303	222	140	58	0
	1	-3,54-04	-2,88-04	0,00	0,00283	
	2	-0,00313	-0,0010	0,00126	0,0058	
	3	-0,0103	-0,00188	0,0047	0,0213	
	4	-0,011	-0,00188	0,0090	0,032	
	5	-0,0122	-0,00166	0,0176	0,056	
	6	-0,0133	-0,00130	0,025	0,0672	
		303	242,6	182,3	122	0
	1	-4,8-03	-1,15-03	2,8-03	9,6-03	2,7-02
	2	-5,9-03	-1,14-03	4,17-03	0,018	0,049
	3	-6,8-03	-1,73-03	6,0-03	0,022	0,058

11A	4	-8,5-03	-2,02-03	1,0-02	0,032	0,079
	5	-1,02-02	-2,0 -03	1,5 -02	0,041	0,097
	6	-1,4-02	-1,4 -03	2,7-02	0,060	0,116
	7	-0,0165	-0,0	0,049	0,083	0,160
		303	241	179	117	0
12A	1	-. ,- -03	-0,00144	1,9 -03	9,0 -03	3,1-02
	2	-5,1-03	-0,0012	4,4 -03	0,0175	0,052
	3	-6,3-03	-0,0019	8,2 -03	0,027	0,071
	4	-6,8-03	-0,0015	1,92-02	0,046	0,102
	5	-7,4-03	-0,0	0,032	0,065	0,124
	6	-7,9-03	-0,0029	0,037	0,074	0,145
	7	-0,0085	-0,0056	0,046	0,088	0,172
15A		205	151,4	97,8	44,2	0
	1	-0,0046	-5,2-04	0,0	0,0050	
	2	-0,0054	-5,8-04	6,3-05	0,0061	
	3	-0,0068	-5,8-04	9,45-05	0,0094	0,018
	4	-0,0097	-6,35-04	0,0028	0,019	0,035
	5	-0,015	-8,65-04	0,0113	0,0403	0,067
	6	-0,0159	0,0	0,023	0,060	0,093
16A		205	164,3	123,6	83	0
	1	-0,0031	-7,22-04	3,15-04	0,0041	0,0132
	2	-0,0054	-0,0012	0,00126	0,0090	0,025
	3	-0,0085	-0,0017	0,0057	0,0228	0,0484
	4	-0,0110	-0,0014	0,0158	0,046	0,077
	5	-0,0125	-0,0017	0,0252	0,0894	0,124

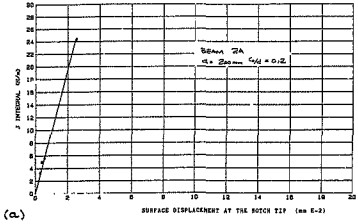
17A		205	164	123	82	0
	1	-0,0034	-289-04	6,3 -04	0,0044	0,0189
	2	-0,0051	-4,33-04	0,0014	0,0070	0,0215
	3	-0,0091	-1,5-04	0,0038	0,0161	0,0425
	4	-0,013	-0,00	0,0133	0,0833	0,0705
	5	-0,0185	+0,0052	0,036	0,0689	0,132
	6	-0,0194	+0,011	0,056	0,0996	0,181
18A		200	159,96	119,9	79,9	0
	1	-0,0033	-5,77-04	6,3-04	0,0038	0,015
	2	-0,0056	-9,24-04	0,0016	0,0088	0,028
	3	-0,0079	-0,0013	0,0058	0,0196	0,051
	4	-0,0098	-0,00	0,023	0,049	0,102
	5	-0,0094	+0,0018	0,0567	0,1023	0,179
18		207	167	127	87	0
	1	-0,0074	-0,0019	6,3-04	0,0099	0,0816
	2	-0,0094	-0,0017	0,0022	0,016	0,051
	3	-0,010	-0,0017	0,0031	0,022	0,058
	4	-0,013	-0,0017	0,008	0,033	0,082
	5	-0,017	-0,0016	0,011	0,0398	0,096
28		205	165	125	85	0
	1	-0,004	-1,22-04		0,004	0,024
	2	-0,006	-8,66-04		0,014	0,040
	3	-0,007	-0,001		0,024	0,054
	4	-0,0085	-8,66-04		0,035	0,067
	5	-0,010	-0,0	0,0028	0,051	0,087

	6	-0,9108	+0,0038	0,082	0,089	0,094
3B		205	164,6	124,3	84	0
	1	-0,0068	-0,0011	9,45-04	0,0047	0,019
	2	-0,006	-0,0017	0,0019	0,0082	0,029
	3	-0,0085	-0,0017	0,0050	0,017	0,048
	4	-0,011	-0,0014	0,0095	0,027	0,075
	5	-0,014	-0,0013	0,0145	0,037	0,094
	6	-0,015	-0,0011	0,0176	0,043	0,104
	7	-0,017	-7,22-04	0,020	0,049	0,106
4B		202	163,6	124,6	86	0
	1	-0,0028	-8,66-04	6,3-04	0,0035	0,0145
	2	-0,0068	-0,002	0,0016	0,0094	0,035
	3	-0,010	-0,0024	0,0041	0,0199	0,059
	4	-0,013	-0,0024	0,0095	0,0333	0,083
	5	-0,014	-4,33-04	0,016	0,048	0,102
	6	-0,016	+0,0016	0,026	0,063	0,131
	7	-0,019	+0,013	0,057	0,121	0,231
	8	-0,017	+0,017	0,065	0,128	0,253
5B		203	148,3	93,67	39	0
	1	-0,010	-0,001	0,0028	0,0215	0,034
	2	-0,011	-0,0016	0,0047	0,027	0,041
	3	-0,0116	-0,001	0,0095	0,035	0,054
	4	-0,0125	-8,66-04	0,0135	0,045	0,065
	5	-0,014	+0,004	0,0296	0,074	0,099
	6	-0,014	+0,0087	0,035	0,089	0,115

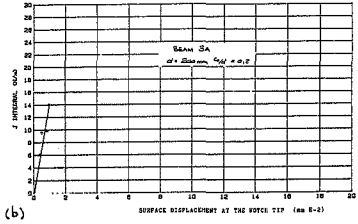
	7	-0,014	+0,013	0,041	0,102	0,131
	8	-0,0145	+0,016	0,044	0,111	0,142
6B		204	148	92	36	0
	1	-0,0039	-8,66·10⁻⁴	9,45·10⁻⁴	0,0067	0,0086
	2	-0,0063	-0,001	0,0016	0,012	0,015
	3	-0,0091	+0,0023	0,0032	0,023	0,027
	4	-0,0108	-0,0026	0,0050	0,034	0,037
	5	-0,0113	-0,0026	0,0095	0,047	0,050
	6	-0,0119	-0,0023	0,016	0,061	0,062
	7	-0,0128	-0,0020	0,0233	0,075	0,077
	8	-0,014	-0,0020	0,0277	0,089	0,093
	9	-0,015	-0,0016	0,053	0,129	0,133
	10	-0,0165	-0,00	0,081	0,164	0,166
	11	-0,0159	+0,0039	0,082	0,187	0,193
7B		200	145·	90	35	0
	1	-0,0039	0,0	0,001	0,0041	0,0083
	2	-0,0071	-2,88·10⁻⁴	0,0035	0,015	0,016
	3	-0,0085	0,0	0,0050	0,0224	0,026
	4	-0,0094	+5,77·10⁻⁴	0,010	0,0354	0,044
	5	-0,0011	+5,77·10⁻⁴	0,016	0,0454	0,058
	6	-0,010	+0,0014	-,0186	0,044	0,057
8B		205	149,3	93,66	38	0
	1	-0,0054	-0,0012	0,0016	0,0081	0,013
	2	-0,0074	-0,0016	0,0032	0,0146	0,024
	3	-0,0085	-0,0016	0,0050	0,0222	0,031

	4	-0,010	-0,0016	0,009	0,034	0,041
	5	-0,011	-0,0013	0,017	0,046	0,055
	6	-0,010	$-4,33\cdot10^{-4}$	0,018	0,049	0,056
9B		306	250	194	138	0
	1	-0,0048	-0,001	0,0	0,0017	0,028
	2	-0,0071	-0,0016	$6,3\cdot10^{-4}$	0,007	0,043
	3	-0,0083	-0,0019	0,0013	0,0111	0,057
	4	-0,0097	-0,0020	0,0022	0,016	0,069
	5	-0,0171	-0,0020	0,005	0,026	0,090
	6	-0,0157	-0,0038	0,0277	0,050	0,168
	7	-0,0168	-0,0189	0,061	0,120	0,244
10B		302	247	192	137	0
	1	-0,0051	$-8,46\cdot10^{-4}$	0,0013	0,007	0,038
	2	-0,0057	-0,0011	0,0019	0,011	0,048
	3	-0,0079	-0,0016	0,0038	0,019	0,057
	4	-0,0097	-0,0017	0,0095	0,033	0,118
	5	-0,011	-0,0012	0,0135	0,050	0,148
	6	-0,019	-0,00	0,0284	0,069	0,178
	7	-0,014	-0,0081	0,102	0,095	0,221
	8	-0,013	-0,0098	0,118	0,101	0,226
11B		301	245,3	189,6	134	0
	1	-0,003	-0,0013	$6,3\cdot10^{-4}$	0,0088	0,019
	2	-0,0057	-0,0023	$9,43\cdot10^{-4}$	0,0070	0,082
	3	-0,0074	-0,0026	0,0018	0,011	0,046
	4	-0,011	-0,0035	0,0050	0,025	0,071

	5	-0,012	-0,0081	0,0098	0,037	0,090
	6	-0,015	-0,0080	0,0198	0,057	0,147
	7	-0,017	0,0	0,028	0,082	0,184
	8	-0,018	+0,0167	0,069	0,140	0,284
		304	248,6	193,3	138	0
	1	-0,0023	-5,77·04	9,45-04	0,0047	0,022
	2	-0,0043	-0,00115	0,0013	0,0088	0,035
	3	-0,0057	-0,0014	0,0032	0,017	0,058
	4	-0,0077	-0,0014	0,0095	0,0357	0,098
128	5	-0,0091	-0,00	0,0246	0,062	0,117
	6	-0,0097	+0,0058	0,048	0,093	0,171
	7	-0,0085	+0,0159	0,0671	0,137	0,244
	8	-0,0028	+0,0297	0,111	0,192	0,330
	9	-0,00	+0,0387	0,148	0,251	0,427

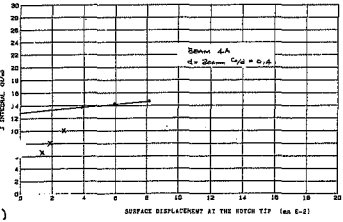


(a)

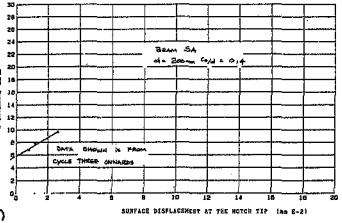


(b)

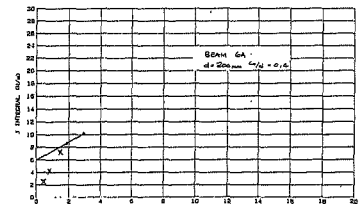
FIG C.1 Plots of the J - integral versus surface displacement at the notch tip for the concrete beams, and linear regression according to the ASTM-813 method.


Beam 4A
d = 20cm c/d = 0.16
J INTEGRAL, KN/M
SURFACE DISPLACEMENT AT THE NOTCH TIP (in E-2)

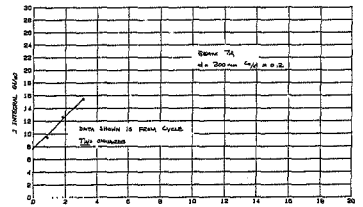
(c)


Beam 5A
d = 20cm c/d = 0.16
DATA ENDING IS FROM
CYCLE THREE ONWARDS
J INTEGRAL, KN/M
SURFACE DISPLACEMENT AT THE NOTCH TIP (in E-2)

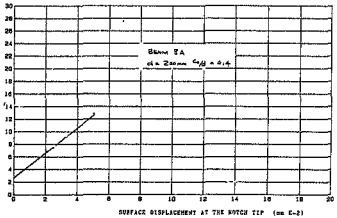
(d)


BEAM 6A
d = 200 mm
J INTEGRAL KJ/M2
SURFACE DISPLACEMENT AT THE NOTCH TIP (mm X-D)

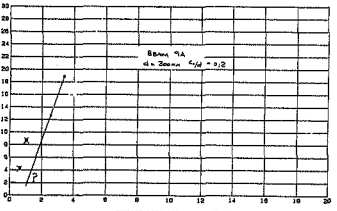
(e)


BEAM 7A
d = 200 mm
J INTEGRAL KJ/M2
SURFACE DISPLACEMENT AT THE NOTCH TIP (mm X-D)

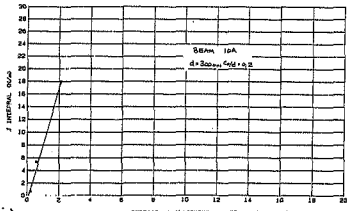
(f)


Beam 9A
a = 20mm $c_{/d}$ = 0.4
J INTEGRAL (KJ/m)
SURFACE DISPLACEMENT AT THE NOTCH TIP (mm E-2)

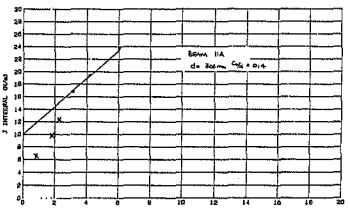
(g)


Beam 9A
a = 20mm $c_{/d}$ = 0.2
J INTEGRAL (KJ/m)
X
P
SURFACE DISPLACEMENT AT THE NOTCH TIP (mm E-2)

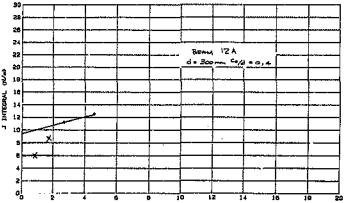
(h)


BEAM 10A
d = 300mm c/d = 0.2
J INTEGRAL KN/M
SURFACE DISPLACEMENT AT THE NOTCH TIP (mm E-2)

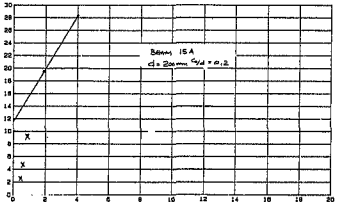
(i)


BEAM 11A
d = 300mm c/d = 0.4
J INTEGRAL KN/M
SURFACE DISPLACEMENT AT THE NOTCH TIP (mm E-2)

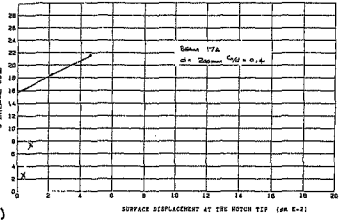
(j)


Beam 12A
d = 20cm a/d = 0.4
J INTEGRAL (N/m)
SURFACE DISPLACEMENT AT THE NOTCH TIP (mm E-2)

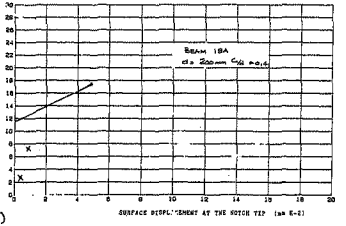
(k)


Beam 15A
d = 20cm a/d = 0.2
J INTEGRAL (N/m)
SURFACE DISPLACEMENT AT THE NOTCH TIP (mm E-2)

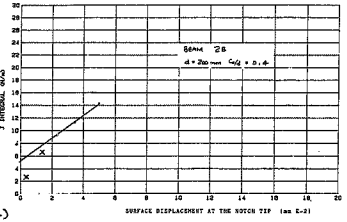
(l)


Beam 17A
a = 200mm a/d = 0.4
J INTEGRAL (N/m)
SURFACE DISPLACEMENT AT THE NOTCH TIP (mm E-2)

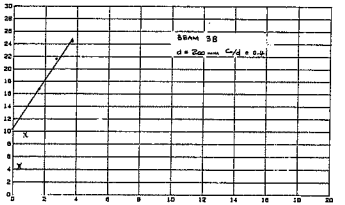
(m)


Beam 18A
a = 200mm a/d = 0.4
J INTEGRAL (N/m)
SURFACE DISPLACEMENT AT THE NOTCH TIP (mm E-2)

(n)

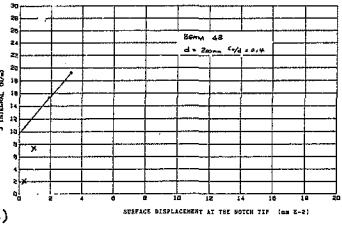


(a)

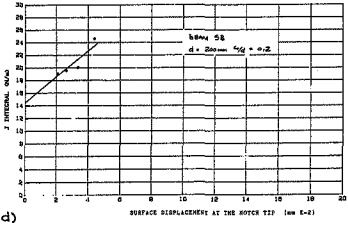


(b)

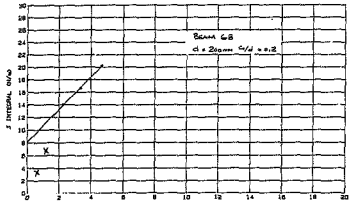
FIG C.2 Plots of the J - integral versus surface displacement at the notch tip for the mortar beams, and linear regression according to the ASTM-813 method.


Beam 48
d = 20mm
J INTEGRAL (KN/m)
SURFACE DISPLACEMENT AT THE NOTCH TIP (mm E-2)

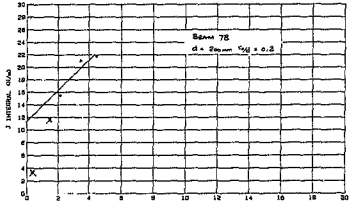
(c)


Beam 58
d = 20mm
J INTEGRAL (KN/m)
SURFACE DISPLACEMENT AT THE NOTCH TIP (mm E-2)

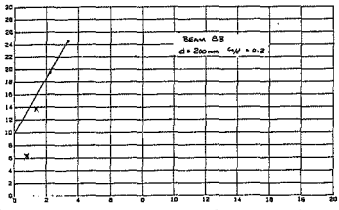
(d)


Beam 6B
d = 20mm c/d = 0.2
J INTEGRAL N/mm
SURFACE DISPLACEMENT AT THE NOTCH TIP (mm E-2)

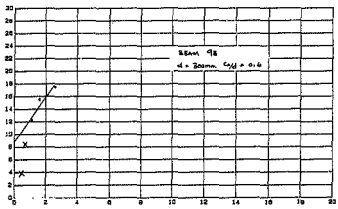
(e)


Beam 7B
d = 20mm c/d = 0.3
J INTEGRAL N/mm
SURFACE DISPLACEMENT AT THE NOTCH TIP (mm E-2)

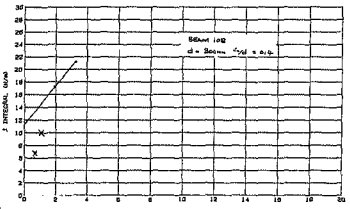
(f)


Beam 6S
d = 20cm c_{ij} = 0.2
J INTEGRAL (KJ/m2)
SURFACE DISPLACEMENT AT THE NOTCH TIP (mm E-2)

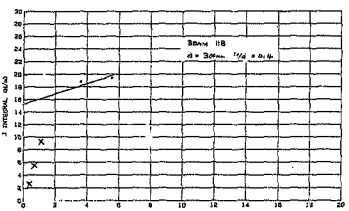
(g)


Beam 9S
d = 20cm c_{ij} = 0.4
J INTEGRAL (KJ/m2)
SURFACE DISPLACEMENT AT THE NOTCH TIP (mm E-2)

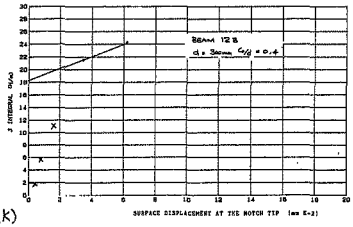
(h)


Beam 102
d = 30mm
J INTEGRAL KN/M
SURFACE DISPLACEMENT AT THE NOTCH TIP (mm E-2)

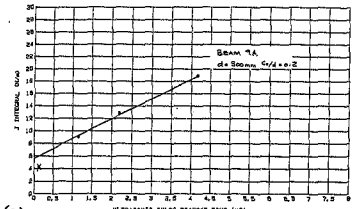
(i)


Beam 118
d = 30mm
J INTEGRAL KN/M
SURFACE DISPLACEMENT AT THE NOTCH TIP (mm E-2)

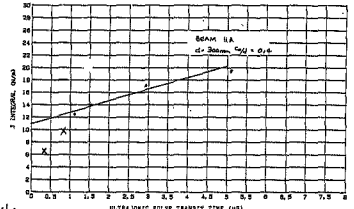
(j)


BEAM 12 B
a/w = 3mm Crij = 0.4
J INTEGRAL (N/m)
SURFACE DISPLACEMENT AT THE NOTCH TIP (mm E-2)

(k)

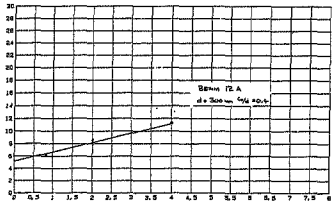


(a)

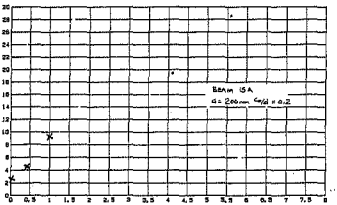


(b)

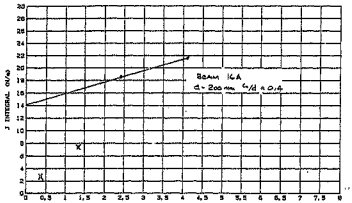
FIG C.3 Plots of the J - integral versus the cumulative difference in peak ultrasonic pulse transit time for the concrete beams, and linear regression according to the ASTM-813 method.


J INTEGRAL, KN/M
Beam 12A
d = 300 mm, a/d = 0.45
0 0.5 1 1.5 2 2.5 3 3.5 4 4.5 5 5.5 6 6.5 7 7.5 8
ULTRASONIC PULSE TRANSIT TIME (μs)
(cumulative difference in peak pulse transit time)

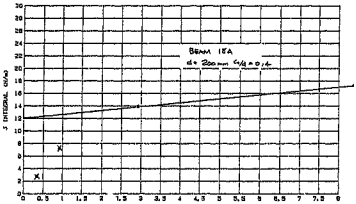
(c)


J INTEGRAL, KN/M
Beam 15A
d = 200 mm, a/d = 0.2
0 0.5 1 1.5 2 2.5 3 3.5 4 4.5 5 5.5 6 6.5 7 7.5 8
ULTRASONIC PULSE TRANSIT TIME (μs)
(cumulative difference in peak pulse transit time)

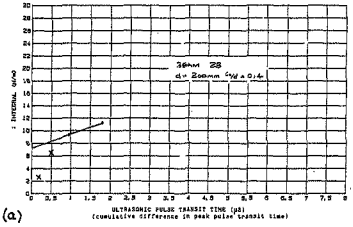
(d)


BEAM 16A
d = 200 mm a/d = 0.4
J INTEGRAL (KN/m)
ULTRASONIC PULSE TRANSIT TIME (μs)
(cumulative difference in peak pulse transit time)

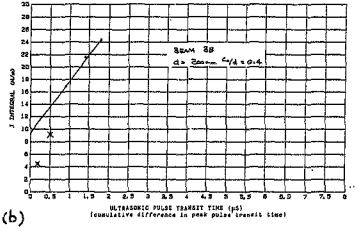
(e)


BEAM 18A
d = 200 mm a/d = 0.4
J INTEGRAL (KN/m)
ULTRASONIC PULSE TRANSIT TIME (μs)
(cumulative difference in peak pulse transit time)

(f)

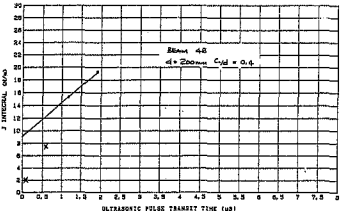


(a)

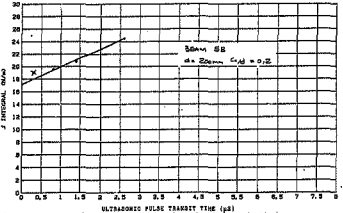


(b)

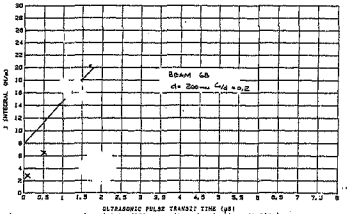
FIG C.4 Plots of the J - integral versus the cumulative difference in peak ultrasonic pulse transit time for the mortar beams, and linear regression according to the ASTM-813 method.


Beam 4B
d = 20mm C/d = 0.4
J INTEGRAL cm/cm2
ULTRASONIC PULSE TRANSIT TIME (μs)
(cumulative difference in peak pulse transit time)

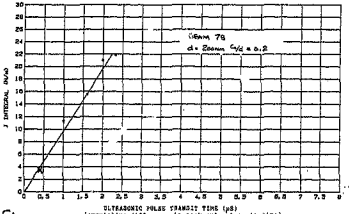
(c)


Beam 8B
d = 20mm C/d = 0.2
J INTEGRAL cm/cm2
ULTRASONIC PULSE TRANSIT TIME (μs)
(cumulative difference in peak pulse transit time)

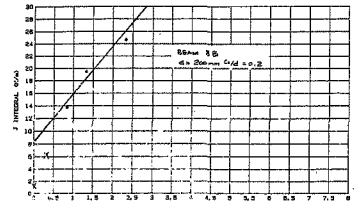
(d)


J INTEGRAL (KA/m)
BEAM 6B
d= 200mm c/a = 0.2
ULTRASONIC PULSE TRANSIT TIME (μs)
(cumulative difference in peak pulse transit time)

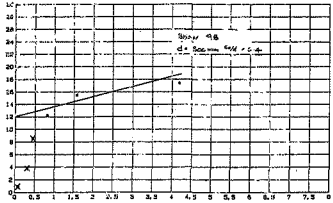
(e)


J INTEGRAL (KA/m)
BEAM 7B
d= 200mm c/a = 0.2
ULTRASONIC PULSE TRANSIT TIME (μs)
(cumulative difference in peak pulse transit time)

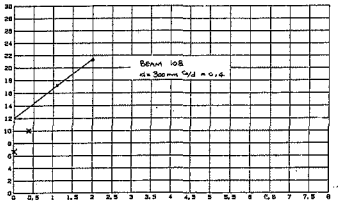
(f)


Beam 8B
d = 20mm c/d = 0.2
J INTEGRAL (N/m)
ULTRASONIC PULSE TRANSIT TIME (μs)
(cumulative difference in peak pulse transit time)

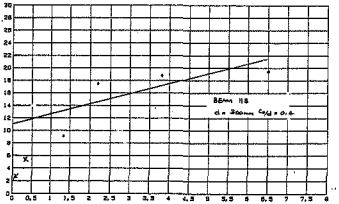
(g)


Beam 9B
d = 5mm c/d = 0.8
J INTEGRAL (N/m)
ULTRASONIC PULSE TRANSIT TIME (μs)
(cumulative difference in peak pulse transit time)

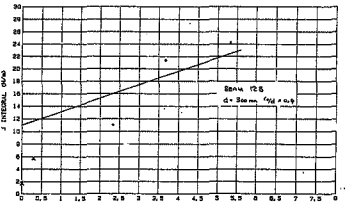
(h)


Beam 10B
d = 300mm Cyl = o.c.
J INTEGRAL, KN/m
ULTRASONIC PULSE TRANSIT TIME (μS)
(cumulative difference in peak pulse transit time)

(i)


Beam 11B
d = 300mm Cyl = o.c.
J INTEGRAL, KN/m
ULTRASONIC PULSE TRANSIT TIME (μS)
(cumulative difference in peak pulse transit time)

(j)


J INTEGRAL (KN/m)
Beam 12.5
d = 30 mm a/d = 0.4
ULTRASONIC PULSE TRANSIT TIME (μs)
(cumulative difference in peak pulse transit time)

(k)

REFERENCES

1. Carpinteri, A. Mechanical damage and crack growth in concrete, Dordrecht: Martinus Nijhoff Publishers, 1986.

2. Sih, G.C. and DiTommaso, A. Fracture mechanics of concrete, Dordrecht: Martinus Nijhoff Publishers, 1985.

3. Carpinteri, A. and Ingraffea, A.R. (Ed's). Fracture mechanics of concrete, The Hague: Martinus Nijhoff Publishers, 1984.

4. Alexander, M.G. Fracture of plain concrete - a comparative study of notched beams of varying depth, PhD Thesis, University of the Witwatersrand, Johannesburg, 1985.

5. Griffith, A.A. The phenomena of rupture and flow in solids, Philosophical Transactions, Royal Society of London, Series A, Vol. 221, 1920, pp. 163-198.

6. Quoted in Gordon, J.E. New Science of Strong Materials, Penguin Books, 1968, pp. 115-117.

7. Blight, G.E. Fracture of pavement materials, Proc. ASCE, Vol. 99, No. TE4, 1973, pp. 801-819.

8. Kaplan, M.F. Crack propagation and the fracture of concrete, Journal of the American Concrete Institute, 58(1961) pp. 591-610.

9. Glucklich, J. Static and fatigue fractures of Portland cement mortar in flexure, in Proceedings of the First International Conference on Fracture, Japan, 1965, The Japanese Society for Strength and Fracture of Materials, 1966, Vol. 3, pp. 1343-1382.

10. Moavenzadeh, F. and Kuguel, R. Fracture of concrete, Journal of Materials, 4(1969) pp. 497-519.

11. Koyanagi, W. and Sakai, K. Observations on the crack propagation process of mortar and concrete, in Review of the Twenty-Fifth General Meeting, The Cement Association of Japan, Tokyo, 1971, pp. 153-157.

12. Brown, J.H. Measuring the fracture toughness of cement paste and mortar, Magazine of Concrete Research, 24(1972) pp. 185-196.

13. Blight, G.E. Possible applications of an energy approach to design in non-metallic construction materials, Proceedings of 1st Australian Conference on Engineering Materials, University of New South Wales, Sydney, Australia, 1974.

14. Cooper, A.G. and Figg, J. Fracture studies of set cement paste, Journal of the British Ceramic Society, 71(1972) pp. 1-4.

15. Walsh, P.F. Fracture of plain concrete, Indian Concrete Journal 46(1972) pp. 469-470,476.

16. Mindess, S. and Nadeau, J.S. Effect of notch width on K_{IC} for mortar and concrete, Cement and Concrete Research, 6(1976) pp. 529-534).

17. Morita, K. and Kato, K. Fundamental study on evaluation of fracture toughness of artificial lightweight aggregate concrete, in Review of the Thirty-Third General Meeting, The Cement Association of Japan, Tokyo, 1979, pp. 175-177.

18. Halvorsen, G.T. Toughness of Portland cement concrete, PhD Thesis, University of Illinois, Urbana, 1979.

19. Rokugo, K. Experimental evaluation of fracture toughness parameters of concrete, M.S. Thesis, Dept. of Civil Engineering, University of Illinois at Urbana - Champaign, 1979.

20. Carrato, J.L. Experimental evaluation of the J-integral, M.S. Thesis, Dept. of Civil Engineering, University of Illinois at Urbana-Champaign, 1980.

21. Kim, M.M., Ko, H.-Y. and Gerstle, K.H. Determination of fracture toughness of concrete, in W.F. Chen and E.C. Ting (eds.) Fracture in Concrete, Proceedings of an ASCE Session, Florida, 1980, American Society of Civil Engineers, New York, 1980, pp. 1-14.

22. Petersson, P.E. Fracture energy of concrete: method of determination, Cement and Concrete Research, 10(1980) pp. 78-89.

23. Petersson, P.E. Fracture energy of concrete: practical performance experimental results, Cement and Concrete Research, 10(1980) pp. 91-101.

24. Nallathambi, P., Karihaloo, B.L. and Heaton, B.S. Effect of specimen and crack sizes, water/cement ratio and coarse aggregate texture upon fracture toughness of concrete, Magazine of Concrete Research, 36(1984) pp. 227-236.

25. Bazant, Z.P. and Cedolin, L. Approximate linear analysis of concrete fracture by R-curves, Journal of Structural Engineering, 110(1984) pp. 1336-1355.

26. Hillerborg, A. The theoretical basis of a method to determine the fracture energy G_F of concrete, Matériaux et Constructions, 18(1985) pp. 291-296.

27. Shah, S.P. (e.d.), Application of fracture mechanics to Cementitions composites, Proceedings of the NATO Advanced Research Workshop on Application of Fracture Mechanics to Cementitions Composites, Northwestern University, September 1984; Martinus Nijhoff Publishers, The Netherlands, 1985, p. 714.

28. Mindess, S. Application of fracture mechanics to concrete, in W.F. Chen and A.D.M. Lewis (eds.), Recent Advances in Engineering Mechanics and their Impact on Civil Engineering Practice, Vol. II, American Society of Civil Engineers, New York, 1983, pp. 794-797.

29. Ziegeldorf, S. Phenomenological aspects of the fracture of concrete, in Fracture Mechanics of Concrete, Ed. F.H. Wittman, Amsterdam: Elsevier, 1982, pp. 31-40.

30. Grudemo, A. Microcracks, fracture mechanics and strength of the cement paste matrix, Cem. Concr. Res. 9 (1979), pp. 19-34.

31. Moavenzadeh, F.; Kuguel, R.; Fracture of concrete, J. of Mat., JMLSA, 4 (1969) pp. 497-519.

32. Naus, D.J. and Lott, J.L. Fracture toughness of Portland cement concretes, Proc. ACI, Vol. 66, 1969, pp. 481-489.

33. Glucklich, J. Fracture of plain concrete, Proc. ASCE, Vol. 89, No. EM6, Dec. 1963, pp. 127-138.

34. Sih, G.C. and DiTommaso, A. Fracture mechanics of concrete, Dordrecht: Martinus Nijhoff Publishers, 1985, p. 72.

35. Mindess, S. The application of fracture mechanics to cement and concrete: a historical review, in Fracture Mechanics of Concrete, Ed. F.H. Wittman, Amsterdam: Elsevier, 1983, p. 9.

36. Ziegeldorf, S. A model law for the notch sensitivity of brittle materials, Muller, H.S. and Hilsdorf, H.K. Cem. Concr. Res., 10 (1980), pp. 589-599.

37. Swamy, R.N. Linear elastic fracture mechanics parameters of concrete, in Fracture Mechanics of Concrete, Ed. F.H. Wittman, Amsterdam: Elsevier, 1983, p. 415.

38. Swamy, R.N., in Ed. F.D. Lydon, Developments in Concrete Technology - I, Applied Science Publishers Ltd, London, 1979, pp. 221-281.

39. Nishioka, K., Yamakawa, S., Hirakawa, K. and Akihama, S., Proceedings, RILEM Symposium 1978, Testing and Test Methods of Fibre Cement Composites, The Construction Press, Lancaster, pp. 87-98.

40. Brandt, A. Crack propagation energy in steel fibre reinforced concrete, The Inter. J. of Cement Composites, 2 (1980) 35-42.

41. Halvorsen, G.T. J-integral study of steel fibre reinforced concrete, The Inter. J. of Cement Composites, 2(1980) 13-22.

42. Mai, Y.W. Strength and fracture properties of asbestos-cement mortar composites, Journal of Materials Science, 14(1979) 2091-2102.

43. Lenain, J.C. and Bunsell, A.R. The resistance to crack growth of asbestos cement, Journal of Materials Science, 14(1979) 321-332.

44. Mai, Y.W., Foote, R.M. and Cotterell, B. Size effects and scaling laws of fracture in asbestos cement, The Inter. J. of Cement Composites, 2(1980) 23-34.

45. Hillerborg, A., Modeer, M. and Petersson, P.E. Analysis of crack formation and crack growth in concrete by means of fracture mechanics and finite elements, Cement and Concrete Research, 6(1976) 773-782.

46. Modeer, M. Report TVBM - 1001, University of Lund, 1979.

47. Hillerborg, A. The Inter. J. of Cement Composites, 2(1980) 177-184.

48. Rice, J.R. A path independent integral and the approximate stress analysis of strain concentration by notches and cracks, Journal of Applied Mechanics, Trans. ASME, Vol. 35, June 1968, pp. 379-386.

49. Rolfe, S.T. and Barsom, J.M. Fracture and fatigue control in structures, applications of fracture mechanics, Prentice-Hall, Englewood Cliffs: 1977, p. 549.

50. Begley, J.A. and Landes, J.D. The J-Integral as a Fracture Criterion, ASTM STP 514, American Society for Testing Materials, Philadelphia, 1972, p. 1-20.

51. Bucci, R.J., Paris, P.C., Landes, J.C. and Rice, J.R J-Integral Estimation Procedures, ASTM STP 514, American Society for Testing Materials, Philadelphia, 1972, pp. 40-69.

52. Rice, J.R., Paris, P.C. and Merkle, J.G. Some Further Results on J-Integral Analysis and Estimates, ASTM STP 536, American Society for Testing Materials, Philadelphia, 1973, pp. 231-245.

53. Landes, J.D. and Begley, J.A. Test Results from J-Integral Studies: An Attempt to Establish a J_{Ic} Testing Procedure, ASTM STP 560, American Society for Testing Materials, Philadelphia, 1974, pp. 170-186.

54. Hayes, D.J. Some applications of elastic-plastic analysis of fracture mechanics, Ph. D. dissertation, Imperial College, London, 1970.

55. Broek, D. Elementary Engineering Fracture Mechanics, Leyden: Noordhoff, 1974, p. 135.

56. Irwin, G.R. and Kies, J.A. Fracturing and fracture dynamics, Welding Journal Research Supplement, Vol. 17, Feb. 1952, p. 95-100.

57. Irwin, G.R. and Kies, J.A. Critical energy rate analysis of fracture strength, Welding Journal Research Supplement, Vol. 33, 1954, pp. 193ff.

58. Higgins, D.D. and Bailey, J.E. Fracture measurements on cement paste, Journal of Material Science, Vol. 11, 1976, pp. 1995-2003.

59. Tait, R.B. Fatigue and fracture of cement mortar, PhD Thesis, University of Cape Town, South Africa, 1984.

60. Yokomichi, H., Fujita, Y. and Saeki, N. Experimental researches on crack propagation of plain concrete, in Review of the Twenty-Seventh General Meeting, the Cement Association of Japan, Tokyo, 1973, pp. 144-147.

61. Petersson, P., -E. Comments on the method of determining the fracture energy of concrete by means of three-point bend tests on notched beams, Report TVBM-3011, Division of Building Materials, Lund Institute of Technology, Lund, Sweden, 1982.

62. Rokugo, K., Kesler, C.E. and Lawrence, F.V. Evaluation of fracture toughness of concrete by J-integral method, in Proceedings, JCI (Japanese Concrete Institute), Second Conference, (1980) pp. 125-128.

63. Carrato, J.L. Experimental evaluation of the J-integral, M.S. Thesis, Dept. of Civil Engineering, University of Illinois at Urbana-Champaign, 1980.

64. Dunn, O.J. and Clark, V.A. Applied Statistics: analysis of variance and regression, New York: John Wiley & Sons, 1974.

65. Blight, G.E., McIver, J.R., Schutte, W.K. and Rimmer, R. The effects of alkali-aggregate reaction on reinforced concrete structures made with Witwatersrand Quartzite aggregate, Proceedings 5th International Conference on Alkali-Aggregate Reaction in Concrete, Cape Town, 1981, Paper S252/15, pp. 1-12.

66. Swamy, R.N. Linear Elastic Fracture Mechanics Parameters of concrete, in Fracture Mechanics of Concrete, Ed. F.H. Wittman, Amsterdam: Elsevier, 1983, p. 439.

67. Davis, D.E. The Concrete-Making properties of South African aggregates, Ph. D. Thesis, University of the Witwatersrand, Johannesburg, 1975.

68. South African Bureau of Standards. Compressive strength of Concrete, Pretoria: South African Bureau of Standards, SABS Standard Method 863, pp. 1-6.

69. British Standards Institution. Methods of testing hardened concrete for other than strength, London: British Standards Institution, BS 1881, Part 5, 1970, pp. 13-17.

70. American Society for Testing and Materials, Standard Test for J_i a Measure of Fracture Toughness, ASTM Standard Method E813-81.

71. Tait, R.B; Cortie M.B. A Fracture Toughness assessment of Thick IZETT steel using J-integral methods. Department of Metallurgy Fracture Research Group report FRG/C/86/27, University of Witwatersrand, September 1986.

BIBLIOGRAPHY

GENERAL COMPREHENSIVE REFERENCES ON FRACTURE

1. Alexander, M.G. **Fracture of plain concrete - a comparative study of notched beams of varying depth**, PhD Thesis, University of the Witwatersrand, Johannesburg, 1985.

2. Wittman, F.H. (Ed), **Fracture Mechanics of Concrete**, Developments in Civil Engineering, Vol. 7, Amsterdam: Elsevier, 1983.

3. Wittman, F.H. (Ed), **Fracture Toughness and Fracture Energy of Concrete**, Developments in Civil Engineering, Vol. 18, Amsterdam: Elsevier, 1985.

4. Carpinteri, A. **Mechanical damage and crack growth in concrete**, Dordrecht: Martinus Nijhoff Publishers, 1986.

5. Sih, G.C. and DiTommaso, A. **Fracture Mechanics of Concrete**, The Hague, Martinus Nijhoff Publishers, 1985.

6. Carpinteri, A. and Ingraffea, A.R. (Ed's) **Fracture Mechanics of Concrete**, The Hague, Martinus Nijhoff Publishers, 1984.

Author Gill Laurence Mark
Name of thesis Micro-cracking And Crack Growth In Notched Concrete And Mortar Beams. 1988

PUBLISHER:
University of the Witwatersrand, Johannesburg
©2013

LEGAL NOTICES:

Copyright Notice: All materials on the University of the Witwatersrand, Johannesburg Library website are protected by South African copyright law and may not be distributed, transmitted, displayed, or otherwise published in any format, without the prior written permission of the copyright owner.

Disclaimer and Terms of Use: Provided that you maintain all copyright and other notices contained therein, you may download material (one machine readable copy and one print copy per page) for your personal and/or educational non-commercial use only.

The University of the Witwatersrand, Johannesburg, is not responsible for any errors or omissions and excludes any and all liability for any errors in or omissions from the information on the Library website.